FISSION OF SWIFT HEAVY IONS AND PARTICLE EVAPORATION IN NUCLEAR TRACK DETECTORS

Jolly Raju

A thesis submitted in partial fulfilment of the requirements

for the degree of

DOCTOR OF PHILOSOPHY

in

Chemistry

Department of Chemistry

NOTRH-EASTERN HILL UNIVERSITY

Shillong- 793 003 (India)

1994

DEDICATED

TO

MY PARENTS

STATEMENT

I hereby declare that the work presented in this thesis entitled **"FISSION OF SWIFT HEAVY IONS AND PARTICLE EVAPORATION IN NUCLEAR TRACK DETECTORS"** *is result of investigations carried out by me in the Department of Chemistry, North-Eastern Hill University, Shillong, India under the supervision of* **Dr. K.K. Dwivedi.** *In keeping with the general practice of reporting scientific observations, due reference has been made wherever the work described is based on the findings of other investigators.*

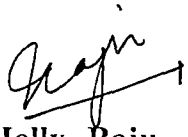

Jolly Raju

North-Eastern Hill University

Bijni Complex, Bhagyakul
Shillong - 793 003 (Meghalaya), India.

Dr. K.K.Dwivedi,
Reader in Chemistry.

CERTIFICATE I

This is to certify that the thesis entitled **"FISSION OF SWIFT HEAVY IONS AND PARTICLE EVAPORATION IN NUCLEAR TRACK DETECTORS"** *submitted by Mr. Jolly Raju for the Degree of Doctor of Philosophy of the North-Eastern Hill University, Shillong, INDIA, embodies the records of original investigations carried out by him under my supervision. He has been duly registered and the thesis presented is worthy of being considered for the award of Ph.D. This work has not been submitted elsewhere for a degree.*

K. K. Dwivedi

Thesis Supervisor

North-Eastern Hill University

Bijni Complex, Bhagyakul
Shillong - 793 003 (Meghalaya), India.

Prof. S. N. Bhat
Head,
Department of Chemistry.

CERTIFICATE II

This is is to certify that Mr. Jolly Raju has satisfactorily completed the following Pre-Ph.D. courses.

	Courses	Grades
1.	Basic German Language	O
2.	Numerical Methods with applications to computer programming.	O
3.	Applications of Nuclear and Radiochemistry.	A
4.	Solid State Chemistry.	A

Prof. S.N. Bhat.
HEAD
Department of Chemistry
North Eastern Hill University
Shillong-793 003

ACKNOWLEDGEMENTS

I express my gratitude to my guide (sir) **Dr. K.K. Dwivedi**, who has not only guided me all along the course of this work, but also was a constant source of inspiration. It was he who had introduced me to this field of "interaction of energetic heavy ions with solids" and its branching area of the fascinating "fork-like events".

I extend my thanks to **Dr. G. Fiedler** and **E. Reichwein** (Justus - Liebig Universität, Giessen, Germany) for certain result oriented discussions at the initial stages of this work.

Also **Prof. R. Brandt** and **Dr. P. Vater** (Kernchemie, Philipps - Universität, Marburg, Germany) for fruitful discussions and **Prof. S.S. Kapoor** (Director, Physics, electronics and instrumentation group, BARC, Bombay, India) for certain effective suggestions during the course of the work.

Thanks are due to **Dr. B. Patro** and **Mr. Nobin Terang** for their help and companionship during the later stages of this work, which helped me to give the present look to the manuscript. Also **the faculty members,** Department of Mathematics, NEHU for allowing me to use their computer for the same.

I thank **Drs. R. Spohr, J. Vetter and C. Trautmann** of GSI, Darmstadt for their help in heavy ion irradiations at UNILAC.

A financial assistance in the form of NEHU (UGC) fellowship (under UGC/CSIR, (NET)) is gratefully acknowledged. Another financial assistance in the form of travel grant by CSIR, New-Delhi, India, to attend the 16th International Conference on Nuclear Tracks in Solids", at Beijing, China, held during Sept. 7-11, '92 is also acknowledged.

I thank **Dr. D.W. Fink** of Hahn-Meitner Institute, Berlin and **Prof. L.T. Chadderton** of Australian National University, Canberra for productive discussions during my stay at Beijing.

I also thank **Mr. Shivaprakashan** and **Mr. Vijayan** for typing of the manuscript.

I thank my teachers for their inspirations.

Also my friends **Vimal, Vidya, Rajesh, Ashraf, Donga, Mazami** for their help.

My thanks also are due to **Mrs. Rekha Dwivedi, Tinu, and Vinni** for their love and care.

My parents for always encouraging me to take up new challenges, my sisters (Manju and Anju) for the care and my brother (Manoj) who offered me a helping hand in every possible way, he could.

Jolly Raju

CONTENTS

Page

LIST OF TABLES

LIST OF FIGURES

CHAPTER I

INTRODUCTION

CHAPTER I

INTRODUCTION

Solid State Nuclear Track Detectors commonly abbreviated as SSNTDs have been applied **[1,2,3]** in a wide spectrum of scientific and technical fields. The utility of this versatile technique ranges from nuclear science and engineering to cosmic ray astrophysics and from geology, archeology and sub-oceanic geophysics to lunar science and meteorites **[4,5,6]**. Right from the development of this track technique, its versatility has been exploited in anthropology **[7]**, geochronology **[8]**, environmental sciences **[9]**, space research **[10]**, superfluidity **[11,12]**, lithography **[13]**, dosimetry **[14]**, medical research **[15]**, study of heavy ion nuclear reactions **[16-19]**, multifragmentation of the projectile **[20, 21, 22]**, particle identification **[23, 24]**, search for magnetic monopoles **[25, 26]**, discovery of super heavy elements **[27]**, exotic decay modes of heavy nuclei **[28,29]**.

This has been possible due to certain advantageous features of these track detectors such as the easy availability, inexpensive and a large choice of detectors ranging from organic polymers to inorganic crystals. At times the detectors are available naturally at the site of interest. The inherent characteristics of these detectors are that they have excellent resolution for mass, charge and energy **[30]** within the boundaries of experimental errors.

The technique too does not require heavy budget equipments. Besides these, the detectors carry a permanent record of the radiation damage to which they were exposed. Moreover the detectors can withstand a large dose of lighter particles and low ionizing radiation.

During the past few years measurement of energy-loss of heavy ions in different elemental and complex media using nuclear track technique has been carried out **[31,32]**. The involvement was also in the characterisation and calibration **[33,34]** of different track detectors for a purposeful utility of these detectors in different fields. Different studies to explore more on the track formation mechanism were also carried out **[35,36,37]**. For the mentioned studies confinement was to the linear tracks i.e the enlarged damage trails of the trajectories of energetic heavy ions in the detector matrix created by chemical processing.

Fig. I.1 is a photomicrograph of a fork-like event in CR-39 irradiated to ^{238}U ions of 15.2 MeV/u. In 1988 Dwivedi et.al. **[38]** reported the observation of fork – like events in CR-39 irradiated to ^{238}U ions of 1.6 GeV. A photomicrograph of two events from their report is shown in **Fig. I.2**. As the different experiments in CR-39, Makrofol-E, Cellulose Nitrate and Mica irradiated to ^{208}Pb, ^{209}Bi and ^{238}U were in progress, similar fork like events were encountered. Fork-like events with a third prong of comparatively shorter length have been observed at the point of bifurcation (fission) for ^{238}U in CR-39 (**Fig. I.3**). Having observed such fork like events a few fundamental querries, which needed explanations were : (i) Definitely the scission of the projectile takes place in the forward hemisphere but is there a possibilty of fusion with the nuclei of the atoms constituting the detector matrix, (ii) A suitable reason for the existence of the third prong. The probable answers to these querries can be sought after determining the masses in the exit channels, the angular distributions of the fragments, Q-Value of the reactions, the relative velocity of fragments and total opening angle in the laboratory and center of mass systems.

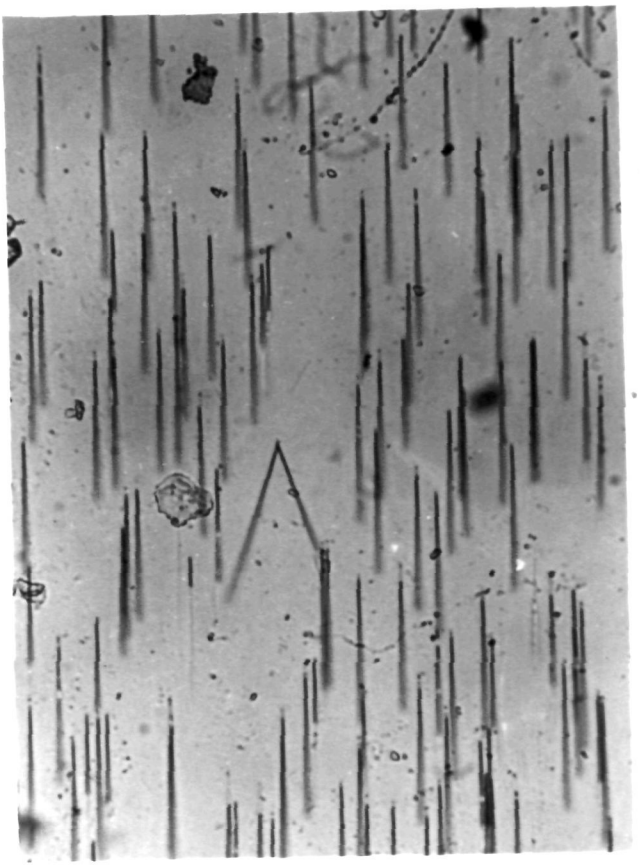

Fig. I.1 A photomicrograph of a fork-like event in CR-39 irradiated to 15.2 MeV/u ^{238}U.

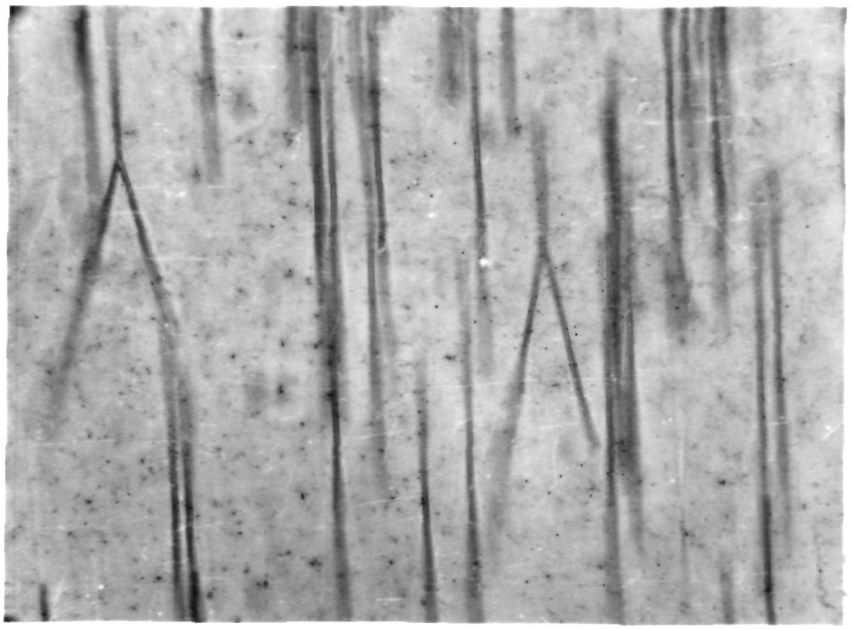

Fig. I.2 A photomicrograph: two events from Dwivedi and Fiedler **[38]** in CR-39 irradiated to 16.3 MeV/u ^{238}U ions.

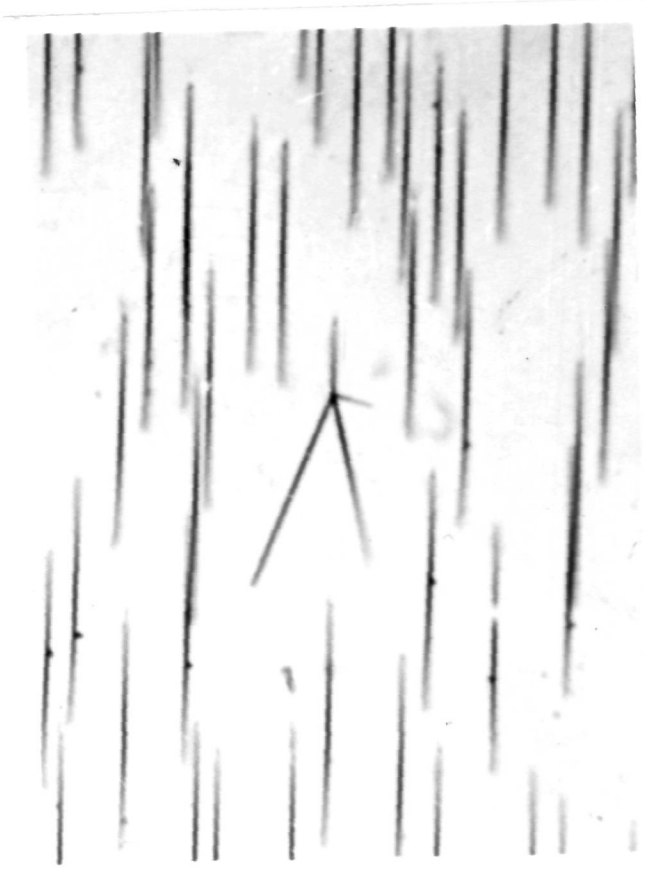

Fig. I.3 A photomicrograph of a fork−like event with the third prong at the point of scission in CR-39. The CR-39 was irradiated to 16.4 MeV/u ^{238}U ions.

On the way to seek the answers to the querries by determining different kinematic variables of the events few barriers too were encounterd. They are: (i) Deriving the real values of different parameters of the prongs from the microscopically observed projected images. The different parameters of the events to be derived are the real lengths of the prongs, the real opening angles with respect to the beam direction and the energy of the projectile at the scission point.

(ii) Analysing each event in terms of the masses of the fragments in the exit channels and other kinematic variables such as the Q-value of the reaction, relative velocity of the fragments, opening angle in the laboratory and centre of mass systems.

(iii) Developing a systematic approach to study the third prongs in terms their actual track lengths and distribution around the axis considered along the trajectory of the projectile.

In an attempt to search the solutions for the above querries along with overcoming the barriers, a 4π geometry technique has been developed for the analysis of these fork-like events. It consists of a geometrical approach followed by computational analysis. The geometrical part takes care of the first barrier while the computational part tackles the second. A systematic approach has been developed to analyze the third prongs in terms of their true track lengths, direction of existence and also the angle with respect to the beam direction. This technique is advantageous over other techniques of radiation measurement as each individual event is registered as a permanent record in the detector matrix. Hence multiple measurements of the same event can be carried out even after few years of its occurence. It also offers the recording of spatially distributed particles in 4π geometry unlike any other conventional 2π detection system.

A description of the subsequent chapters are as follows:

(i) **Chapter II** deals with the theoretical aspects of analysis of the events: geometrical approach followed by computational. In section II.1 the geometrical aspect of the event is discussed where the derivations of different real parameters of an event from the projected parameters have been accomplished. Section II.2 deals with the methods to construct range-energy calibrations needed to calculate pre-fission energy of the projectiles. In section II.3, the logic and the functions of the program 'TRANSCORD' developed for the first step of analysis are described. The second step of analysis done with the help of the application program 'HIFISS' is explained in section II.4 along with the logic used. The trivialities involved in the computation of different kinematical variables along with the mathematical equations used for the purpose are discussed in this chapter. The systematic steps undertaken to study the third prongs have also been explained.

(ii) **Chapter III** contains an account on the systematic procedure undertaken to study these events. At the very beginning the criteria of selecting the detctors to carry out the present kind of study is discussed. Thereafter, preparation of detectors and their irradiations to specific projectiles are described in detail. In section III.3 the chemical processing of the detectors in suitable chemical reagents have been dealt with and in the next section an account on the observation and scanning of the processed detectors is given where the measurement of different parameters of an event are discussed along with the determination of energy of the projectile, the track density and detector calibrations. This chapter is concluded by a detail account on the error analysis.

(iii) **Chapter IV** contains a systematic account of the experimental results and related discussions under the following sub-heads: statistics of events, differential and total cross-sections, total mass of fragments, the Q-Values of the nuclear reactions, relative velocity of fragments, the opening angle in the laboratory and centre of mass systems and the results obtained from the

systematic analysis carried out on the third prongs.

(iv) and finally in **chapter V** the significant results of the present investigation are highlighted. A brief description on the potentialities and scopes of this track technique is presented for some future applications.

(v) The source codes of the programs 'TRANSCORD' and 'HIFISS' are given in the appendices A and B respectively.

CHAPTER II

THEORETICAL ASPECTS

CHAPTER II

THEORETICAL ASPECTS

The barriers encountered to study these events are:

(i) Determination of the real values of different parameters of the events.

(ii) Analysis of each event in terms of different kinematical variables of the events.

(iii) Analysis of the third prong at the pre-scission point, created by the third particle emitted from the pre- scission system.

In the photomicrographs in the previous chapter it is apparent that the observed events are the projected images of the events on the observation plane. Thus tackling the very first problem of determining the values of different parameters of the events, geometrical aspect of the event is considered at first.

II.1 GEOMETRICAL ASPECT OF AN EVENT

The geometrical aspect of an event is the foremost part of the present study as the microscopically observed events are the projected images of the real events on the (x,y) plane i.e. the plane of observation (**Fig. II.1, II.2 a**). The heavy ion enters the detector matrix at the point P (**Fig. II.1, II.2 b**) at an incident angle of α to the surface (plane of observation). The scission occurs at the point O after traversing a distance of L_{pf} μm in the detector matrix. The fragment 'A' traverses a distance of L_A μm while the fragment 'B' traverses a distance L_B μm before coming to rest. θ_A and θ_B (**Fig. II.2 b**) are the angles made by the track length vectors with the axis considered along the trajectory of the projectile. When the event is observed under a microscope the projected image is observed as shown in **Fig. II.2 c**. The various parameters of the event measured are l_{pf}, l_A, l_B, Φ_A and Φ_B (**Fig. II.2 c**). These are the projections of L_{pf}, L_A, L_B, θ_A and θ_B respectively on the observation plane. Another parameter measured is the depth of the end of the trajectories of fragments 'A' and 'B' form the point of scission (bifurcation) i.e. Z_A and Z_B (**Fig. II.3**) respectively. The correction for refractive index has been done by multiplying Z_A and Z_B by the refractive index of the material.

II.1.1 DETERMINATION OF REAL LENGTHS (L_A AND L_B) OF THE PRONGS

In order to determine the actual lengths of the prongs 'A' and 'B' a reference to the **Fig. II.3** is made where attention has been focussed at the point where scission has taken place.

If l_A and l_B are projected lengths of the prongs 'A' and 'B' respectively and Z_A, Z_B are the depths of the track tips 'A' and 'B' from the point of scission, then the dip angles β_A and β_B are:

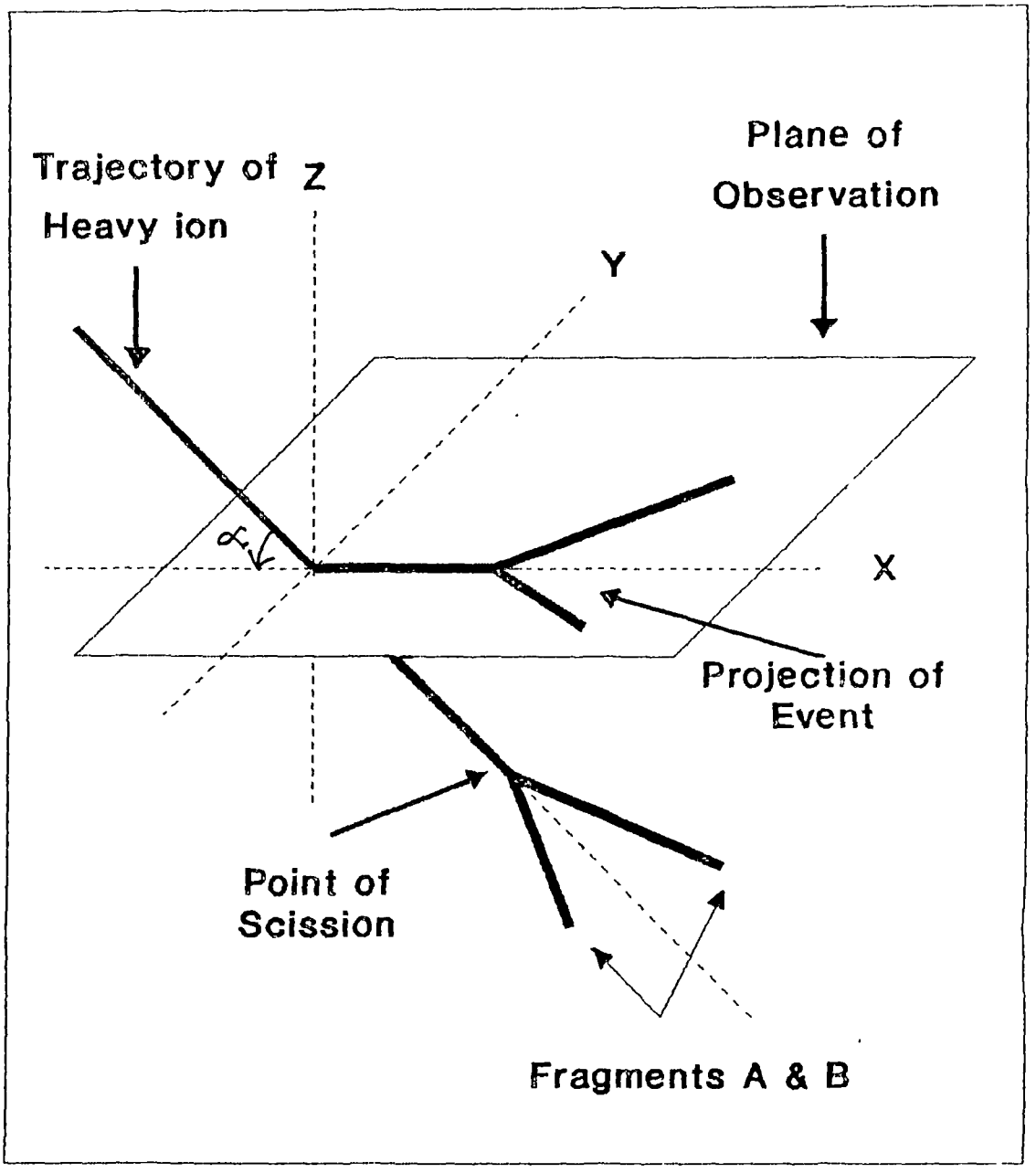

Fig. II.1 Representation of a fork like event and its projection on observation (x,y) plane.

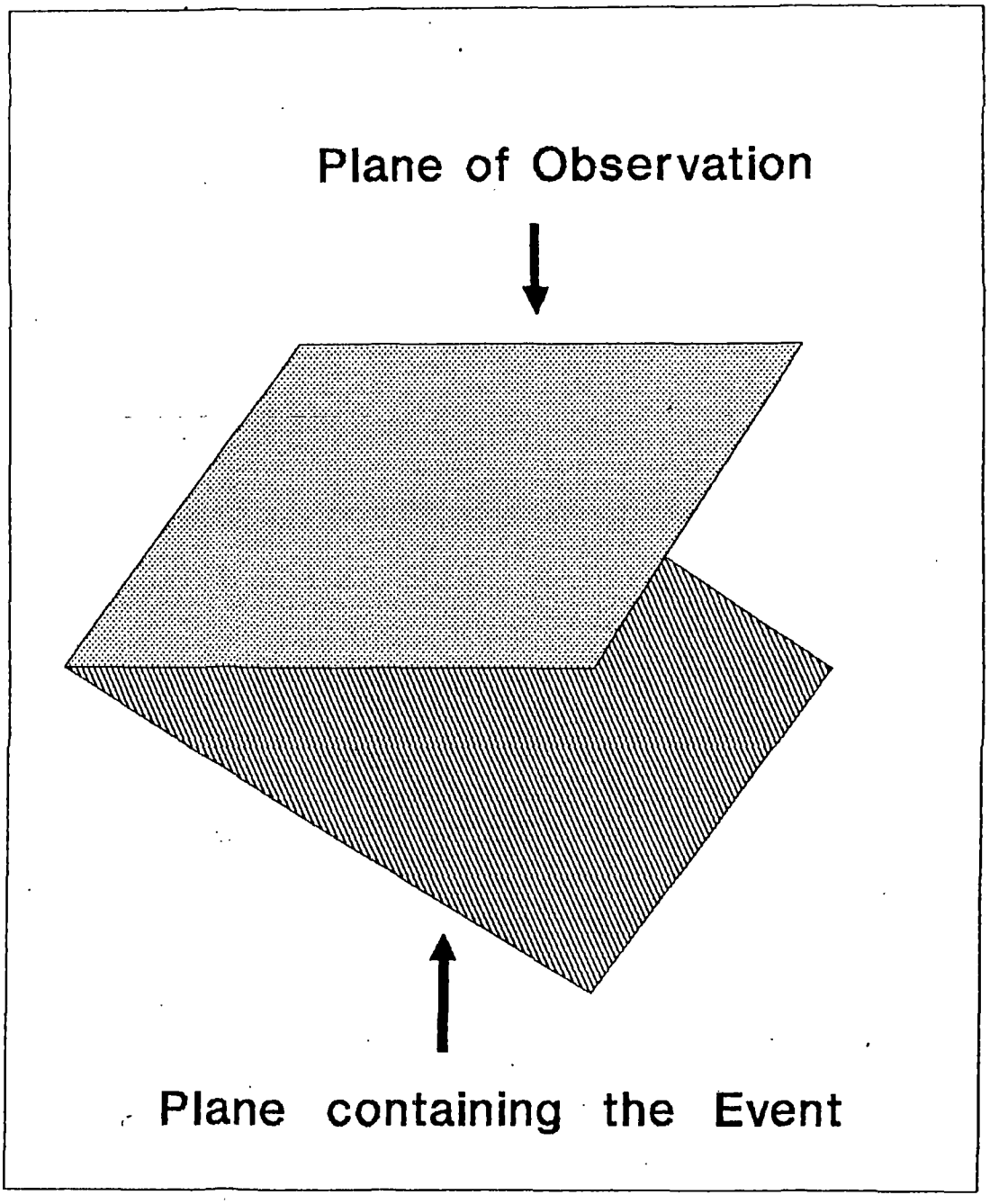

Fig. II.2 (a) A typical view of the two planes: plane of the event and plane of observation.

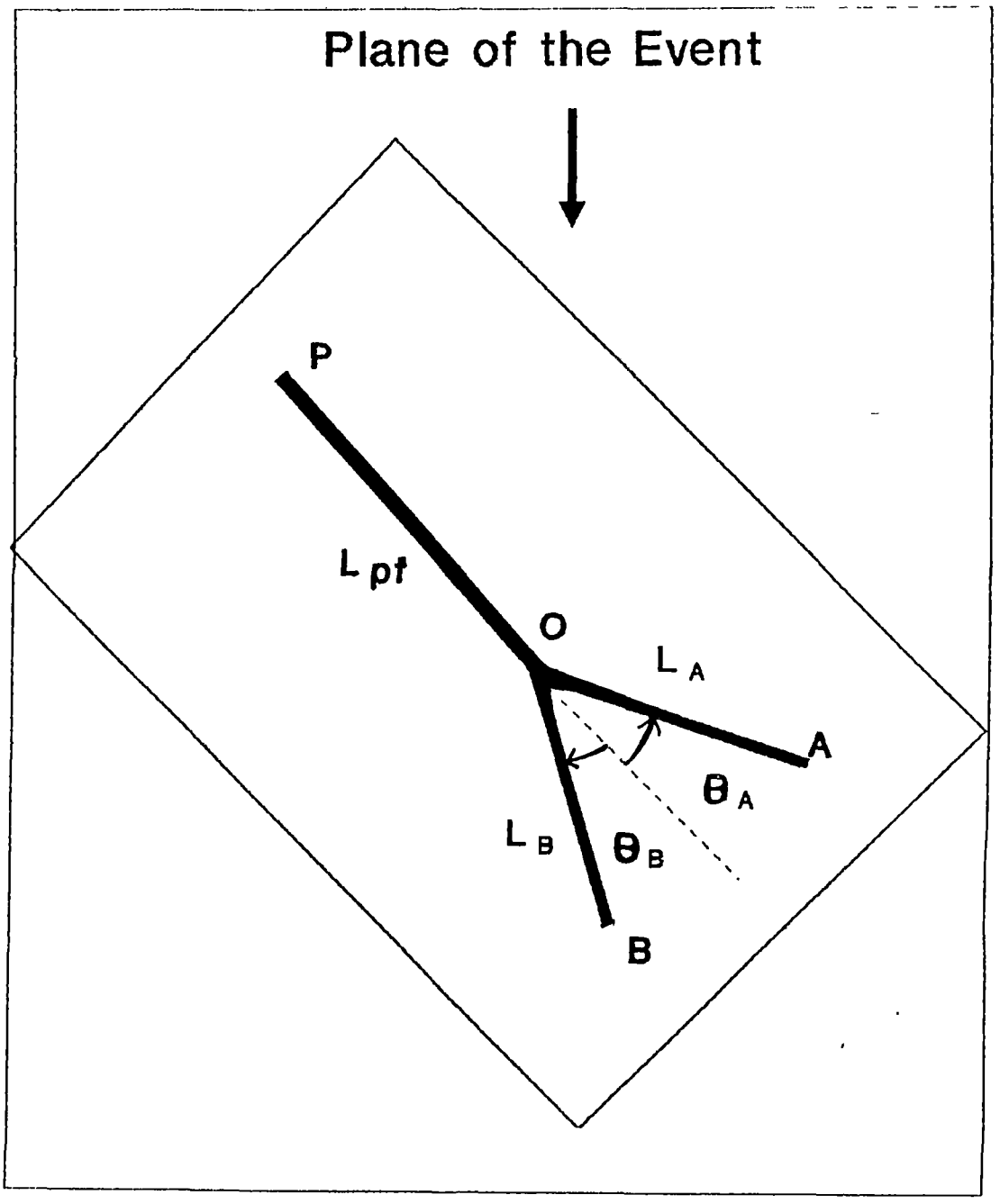

Fig. II.2 (b) A view of an event showing different parameters in its own plane.

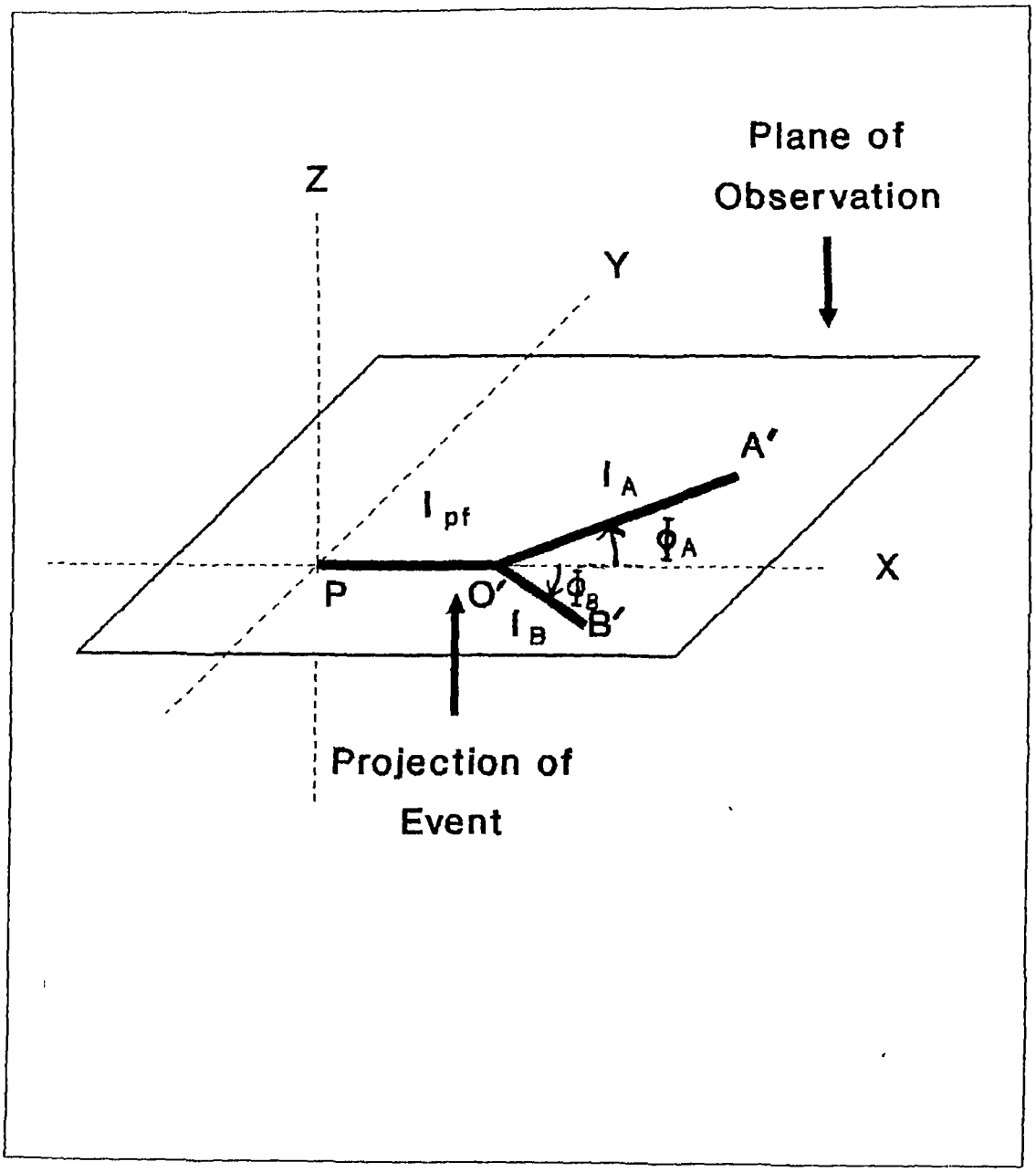

Fig. II.2(c) Projection of an event on the observation plane (x,y) showing different projected parameters.

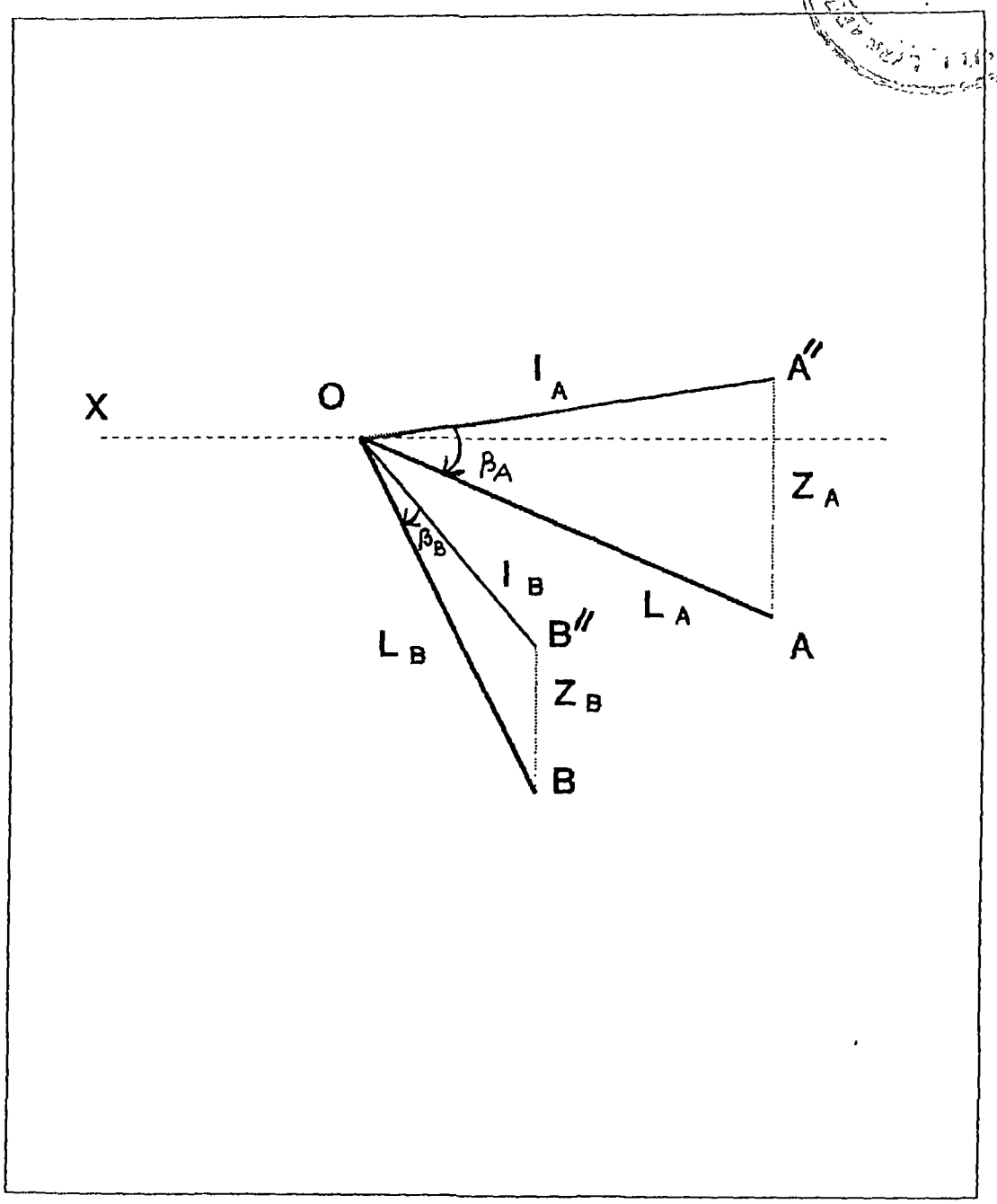

Fig. II.3 A line diagram showing the dip angles and depth of the prong tips with respect to a reference plane parallel to the observation plane containing the scission point O.

$$\beta_A = \tan^{-1} (l_A / Z_A) \quad (2.1)$$

and $$\beta_B = \tan^{-1} (l_B / Z_B) \quad (2.2)$$

(Z_A and Z_B represent real values of the depths after incorporating the correction for refractive index of the material).

Therefore, from **Fig. II.3** the real lengths of the prongs 'A' and 'B' are obtained in the form of following equations

$$L_A = Z_A / \sin \beta_A \quad (2.3)$$

$$L_B = Z_B / \sin \beta_B \quad (2.4)$$

II.1.2 DETERMINATION OF REAL OPENING ANGLES θ_A AND θ_B

After scissioning the fragments move in forward direction along the plane (plane 1 in **Fig. II.4**). But this may not happen as the basic physics of scission would lead to a presumption that after scission the fragments have a possibility to move in the forward hemisphere isotropically around the axis considered along the direction of motion of the pre-scissioning nuclei. Thus the prongs 'A' and 'B' may be tilted from the plane 1 (**Fig. II.4**) by angles δ_A and δ_B as shown in **Fig. II.4**. This phenomenon of tilting of prongs generates two **co-axial syn-apical** cones as shown in **Fig. II.5** where the bases of the cones are two circles with coaxial centres as shown in **Fig. II.6**. These cones with co-axial circular bases are the loci of the track length vectors due to tilting by $\pm 90°$. These circular bases are viewed as concentric from an end-on-position (**Fig. II.6**). The prongs also lie in two different planes (**2 and 3 in Fig. II.4**). This kind of tilting results in to the bending of the plane 1 (**Fig. II.4**).

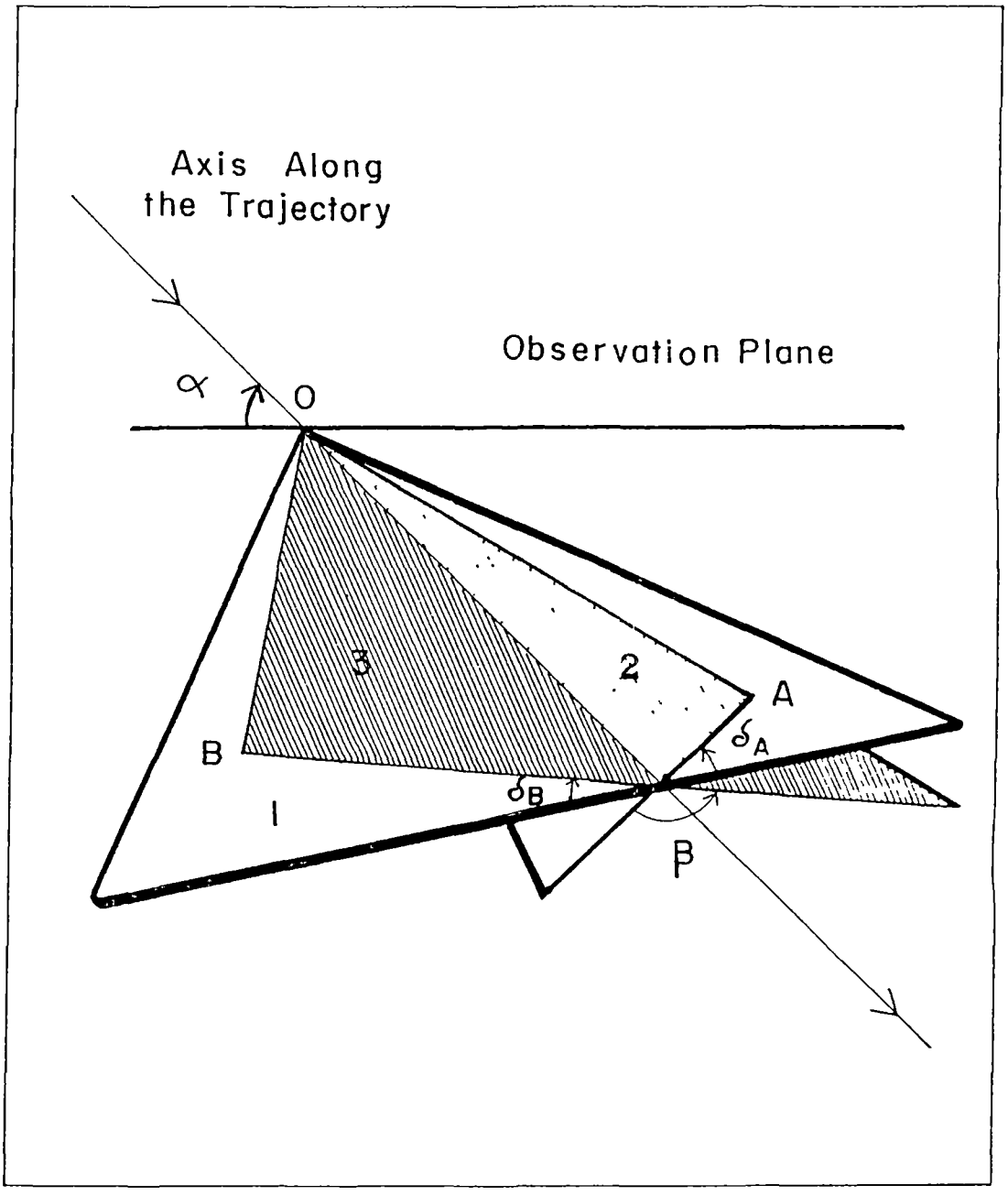

Fig. II.4 Diagram showing the two planes containing the prongs 'A' and 'B' as a result of tilting from the plane 1 by angles δ_A and δ_B respectively and the bending angle ß between these planes.

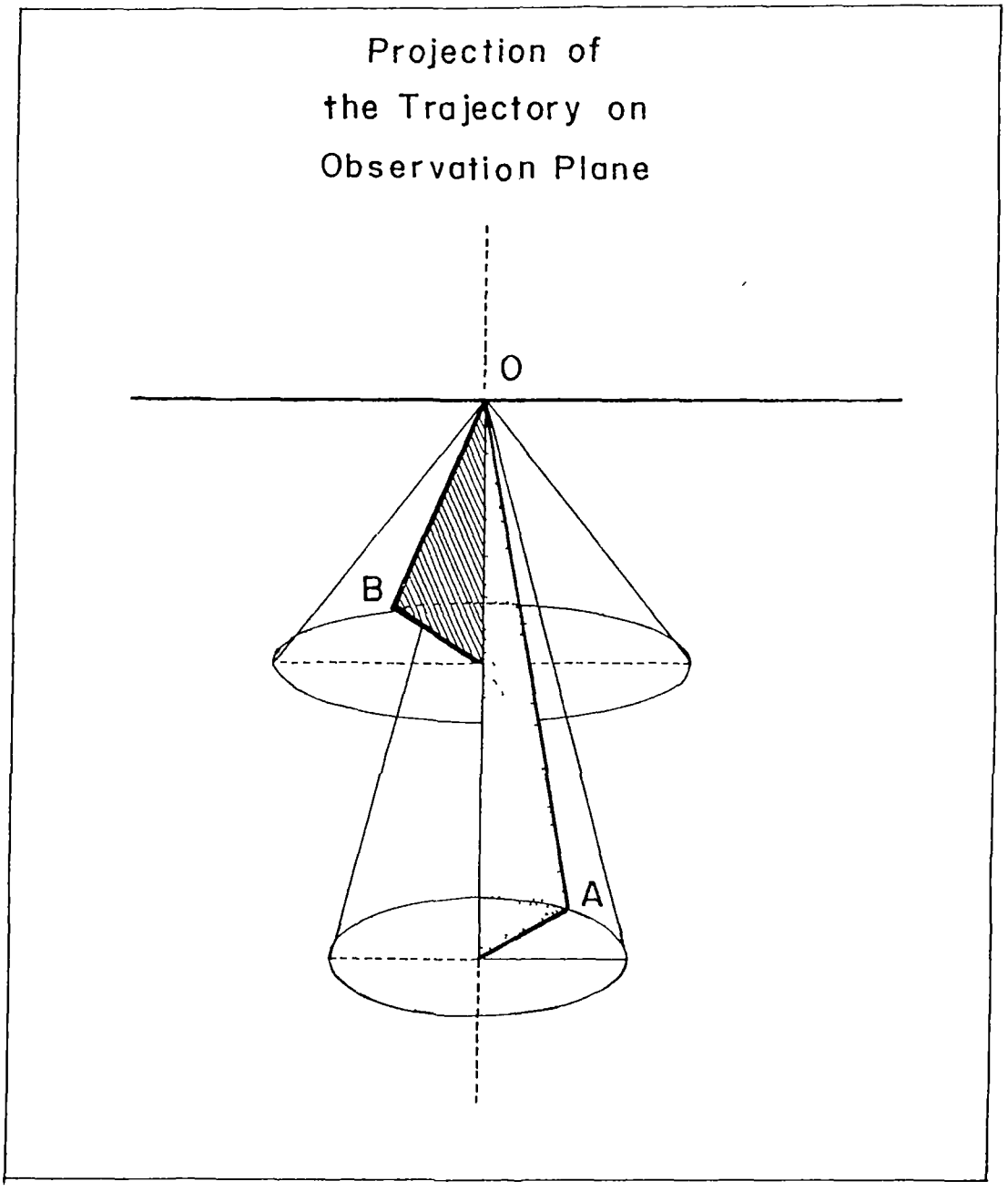

Fig. II.5 A diagram to illustrate the tilting of prongs, resulting in to the formation of two co-axial syn-apical cones.

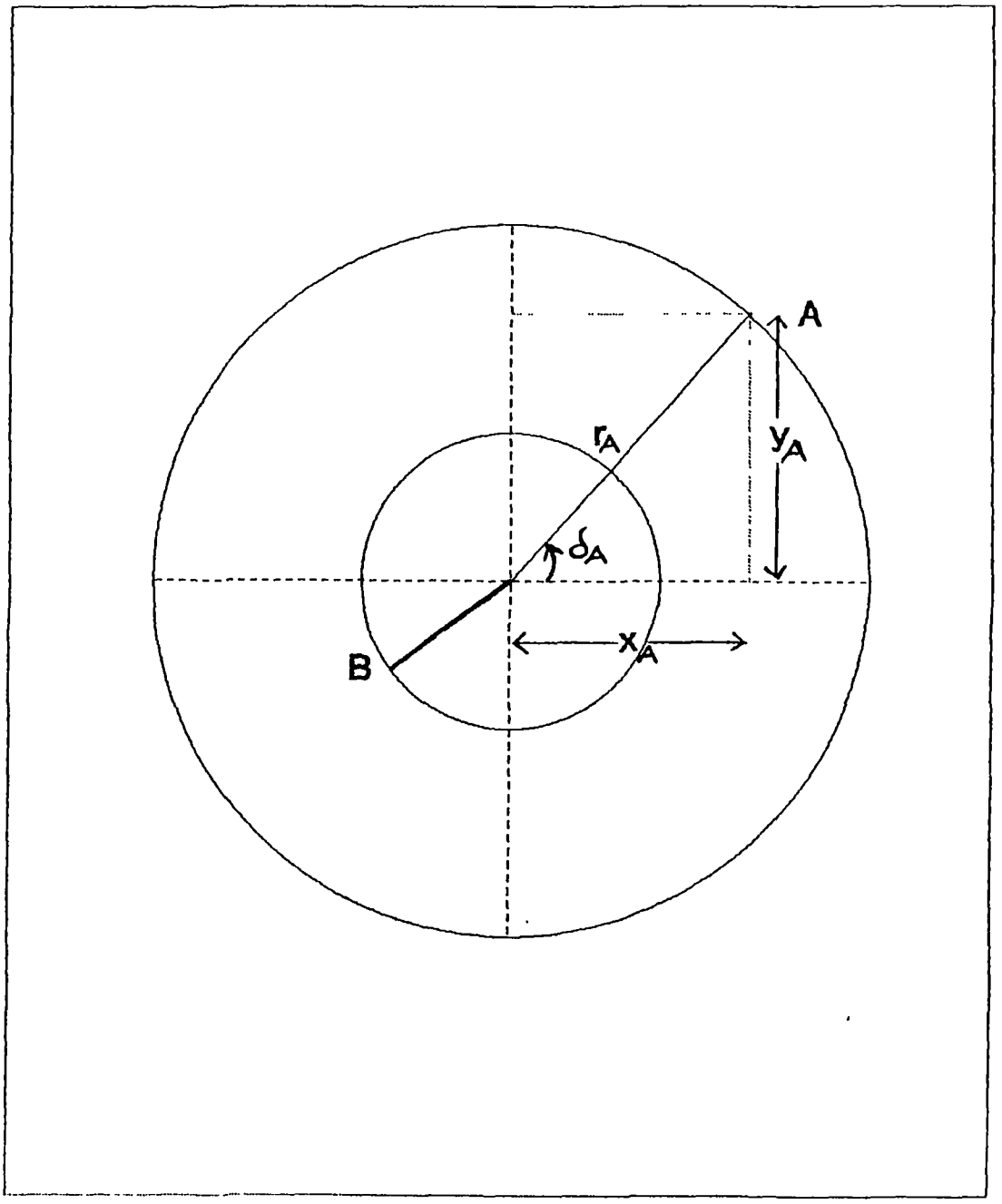

Fig. II.6 End-on-view showing loci of prong tips in the form of two concentric circles. The parameters shown here are used for the determination of the real opening angles θ_A and θ_B.

Considering the base of the cone for prong 'A'in **Fig. II.6**

$$x_A = l_A \sin \Phi_A \quad (2.5)$$

$$y_A = l_A \sin \Phi_A \tan \delta_A \quad (2.6)$$

$$r_A = L_A \sin \theta_A \quad (2.7)$$

and $(r_A)^2 = (x_A)^2 + (y_A)^2$ (2.8)

Substituting the values in equation (2.8)

$$\theta_A = \sin^{-1} (l_A \sin \Phi_A / L_A \cos \delta_A) \quad (2.9)$$

With the help of similar set of arguments for prong 'B'

$$\theta_B = \sin^{-1} (l_B \sin \Phi_B / L_B \cos \delta_B) \quad (2.10)$$

In the equations derived above the values of the δ_A and δ_B are yet undetermined. Determination of the values of δ_A and δ_B are discussed in the next section.

II.1.3 DETERMINATION OF TILTING ANGLES δ_A AND δ_B

Moving on to the next figure i.e. **Fig. II.7**, where a line diagram has been drawn for the prongs with tilting angles of δ_A and δ_B.

Considering the prong 'A':

If Z_A is the depth of the prong 'A'and Z_{Ao} is the depth of the prong had there been no tilting of the prong 'A' by an angle δ_A then

$$Z_{Ao} = Z_A \pm \Delta Z_A \quad (2.11)$$

where ΔZ_A is the difference in the vertical distance (DA_o) as shown in **Fig. II.7** .

(Conventions for δ_A : when the prong lies above the plane 1 then δ_A is positive and below the plane δ_A is negative).

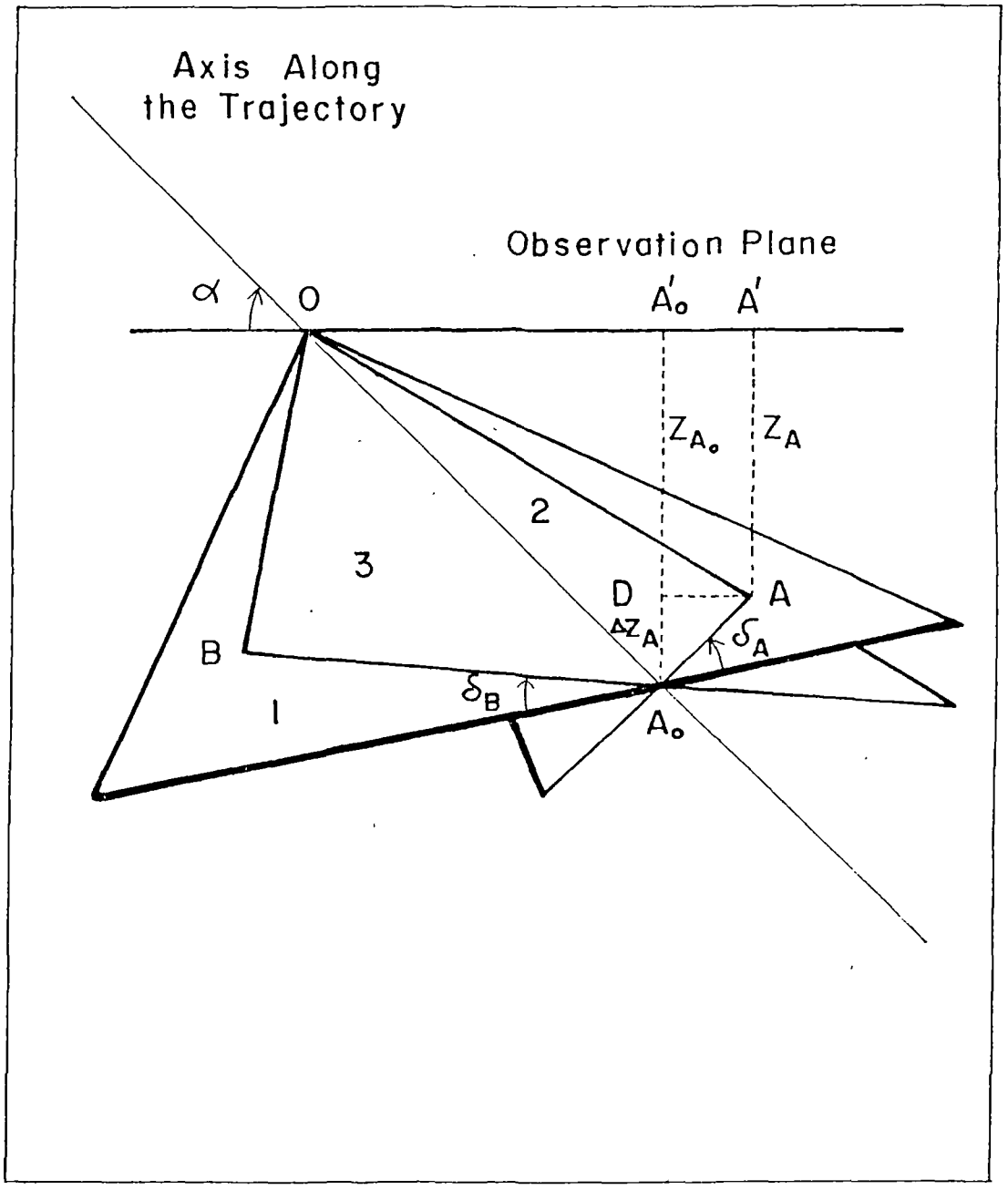

Fig.II.7 A line diagram of the planes due to the tilting of the prongs in order to derive the tilting angles (δ_A and δ_B).

$Z_{Ao} = l_A \cos \Phi_A \tan \alpha$ (when there is no tilting) (2.12)

and from **Fig. II.6 and Fig. II.7**

$\Delta Z_A = l_A \sin \Phi_A \tan \delta_A \cos \alpha$ (2.13)

Substituting the values of Z_A and ΔZ_A into the equation (2.11)

$Z_{Ao} = Z_A \pm l_A \sin \Phi_A \tan \delta_A \cos \alpha$ (2.14)

Evaluation of Z_{Ao} is done by considering two specific cases-

CASE 1 When δ_A is negative:

In this case the prong 'A' lies below the plane 1 (**Fig. II.7**)

$Z_{Ao} = (OA'_o + A'_o A') \tan \alpha = Z_A - \Delta Z_A$ as $Z_{Ao} < Z_A$

$= (l_A \cos \Phi_A + \Delta Z_A \tan \alpha) \tan \alpha$

$= l_A \cos \Phi_A \tan \alpha + \Delta Z_A \tan^2 \alpha$

$\Rightarrow Z_A - \Delta Z_A = l_A \cos \Phi_A \tan \alpha + \Delta Z_A \tan^2 \alpha$

$\Rightarrow l_A \cos \Phi_A \tan \alpha - Z_A = -\Delta Z_A \sec^2 \alpha$ (2.15)

Considering only the numerical value and substituting the value of $\Delta Z_A = l_A \sin \Phi_A \tan \delta_A \cos \alpha$ in the above equation (2.15)

$$\tan \delta_A = \frac{l_A \cos \Phi_A \tan \alpha - Z_A}{l_A \sin \Phi_A \sec \alpha} \quad (2.16)$$

CASE 2: When δ_A is positive:

For this case the prong lies above the plane 1 in **Fig. II.7**

$Z_{Ao} = Z_A + \Delta Z_A$ (2.17)

$= (OA') \tan \alpha$

$= (OA' - A'A'_o) \tan \alpha$ as tilting of the prong above the plane 1 increases the projected length of the prong.

$= (l_A \cos \Phi_A - \Delta Z_A \tan \alpha) \tan \alpha$

$l_A \cos \Phi_A \tan \alpha - \Delta Z_A \tan^2 \alpha = Z_A + \Delta Z_A$

Again substituting the value of ΔZ_A we have

$$\tan \delta_A = \frac{l_A \cos \Phi_A \tan \alpha - Z_A}{l_A \sin \Phi_A \sec \alpha} \qquad (2.18)$$

With the help of similar set of arguments for the prong 'B'

$$\tan \delta_B = \frac{l_B \cos \Phi_B \tan \alpha - Z_B}{l_B \sin \Phi_B \sec \alpha} \qquad (2.19)$$

The equations (2.1) to (2.19) have been used for the purpose of determining the actual values of the parameters of an event from the measured (projected) values.

II.1.4 CROSSCHECK FOR THE DERIVED EQUATIONS

In order to prove the validity of the equations (2.18) and (2.19) three specific known cases are considered.

CASE 1 : When $\delta_A = 0°$

$=>$ $\tan \delta_A = 0$ and for this case

Z_{Ao} should be equal to Z_A

Substituting the values of δ_A in equation 2.18

$$\tan \delta_A = \left[\frac{l_A \cos \Phi_A \tan \alpha - Z_A}{l_A \sin \Phi_A \sec \alpha}\right] = 0$$

$=>$ $l_A \cos \Phi_A \tan \alpha = Z_A$

Again from equation (2.12) $l_A \cos \Phi_A \tan \alpha = Z_{Ao}$

Therefore, $Z_A = Z_{Ao}$ which is the expected condition.

Similar set of arguments holds good when $\delta_B = 0°$.

CASE 2: When $\delta_A = 90°$

$\tan \delta_A$ = indeterminant and tends to infinity

Substituting once again in Equation 2.18

$l_A \sin \Phi_A \sec \alpha = 0$

$\sin \Phi_A = 0$ as (l_A and $\sec \alpha$) $= 0$

$\Rightarrow \Phi_A = 0$ i.e. the projected opening angle $= 0$.

This condition holds good for the situation when the prong is tilted by an angle 90° from the original plane, the projected opening angle is zero.

Finally an intermediate situation considered.

CASE 3: When the tilting takes place by an angle 45°

$\delta_A = 45°$

$\tan \delta_A = 1$

Referring to the **Fig. II.6** i.e the base of the cones where two co-axial circles are shown. If $\delta_A = 45°$ then $\tan \delta_A = 1$ and

thus from the equation (2.18) of δ_A we have

$$l_A \cos \Phi_A \tan \alpha - Z_A = l_A \sin \Phi_A \sec \alpha$$

$$\Rightarrow l_A \cos \Phi_A \sin \alpha - Z_A \cos \alpha = l_A \sin \Phi_A$$

$$\Rightarrow \{(OA'_o + A'_o A') Z_{Ao} / OA_o\} - \{ Z_A (OA'_o) / (OA_o)\} = x_A$$

$$\Rightarrow \{(OA'_o + y_A \sin \alpha) Z_{Ao} / OA_o\} - \{Z_A (OA'_o)/(OA_o)\} = x_A$$

$$\Rightarrow \{OA'_o (Z_{Ao} - Z_A) / OA_o\} - \{y_A \sin \alpha Z_{Ao} / OA_o\} = x_A$$

$$\Rightarrow \Delta Z_A \cos \alpha + y_A \sin^2 \alpha = x_A$$

Again $\Delta Z_A = y_A \cos \alpha$; Substituting the value

$$y_A \cos^2 \alpha + y_A \sin^2 \alpha = x_A,$$

$\therefore y_A = x_A$, which is the expected situation evident from **Fig. II.6** when the tilting is 45°; $y_A = x_A$.

Thus by counterchecking the validity of equations (2.18) and (2.19) has been established. In **Table II.1** the equations used for determination of various parameters of an event have been summarized.

Table II. 1

SUMMARY OF EQUATIONS DERIVED IN ORDER TO DETERMINE DIFFERENT PARAMETERS OF AN EVENT

$$L_A = Z_A / \sin \beta_A \qquad (2.3)$$

$$L_B = Z_B / \sin \beta_B \qquad (2.4)$$

$$\Theta_A = \sin^{-1} (l_A \sin \Phi_A / L_A \cos \delta_A) \qquad (2.9)$$

$$\Theta_B = \sin^{-1} (l_B \sin \Phi_B / L_B \cos \delta_B) \qquad (2.10)$$

$$\delta_A = \tan^{-1} \left(\frac{l_A \cos \Phi_A \tan \alpha - Z_A}{l_A \sin \Phi_A \sec \alpha} \right) \qquad (2.18)$$

$$\delta_B = \tan^{-1} \left(\frac{l_B \cos \Phi_B \tan \alpha - Z_B}{l_B \sin \Phi_B \sec \alpha} \right) \qquad (2.19)$$

II.2 RANGE ENERGY CALIBRATIONS

As will be discussed in the second part of the analysis that the energy at which the scission has taken place is to be determined from the pre-fission track length in order to determine the incident momentum. This has been accomplished by the energy E vs. track length(L) calibration for a specific energetic ion in a detector medium. The energy E (in MeV) of a heavy ion is a non-linear function of the track length which can be expressed by the equation of the form

$$E\ (MeV) = \sum_{\mu=0}^{n} a_\mu L^\mu \qquad (2.20)$$

where n is the order of the polynomial and a_μ are the coefficients determined with the help of the application program 'TRAPOL1' **[39]** and 'TRACAL1' **[39-41]**. For different initial energies of an ion in a detector medium the best sets of coefficients are to be determined by considering the least mean square root deviation. Determination of best sets of coefficients for ^{238}U and ^{209}Bi in CR-39 and Makrofol-E has been done as explained in the next chapter in order to determine the energy at the pre-fission point with the help of subroutine PXY used in the program 'TRANSCORD'.

II.3 THE PROGRAM 'TRANSCORD'

The program **'TRANSCORD'** is an application program developed in high level language 'FORTRAN' to carry out the first step of the analysis. **Fig. II.8** is a flow chart for the program 'TRANSCORD'. This program consists of two subroutines PXY and ACTCAL to perform desired jobs . PXY is used for the computation of energy of the projectile from the track length at the scission point while ACTCAL performs the calculation of the real parameters

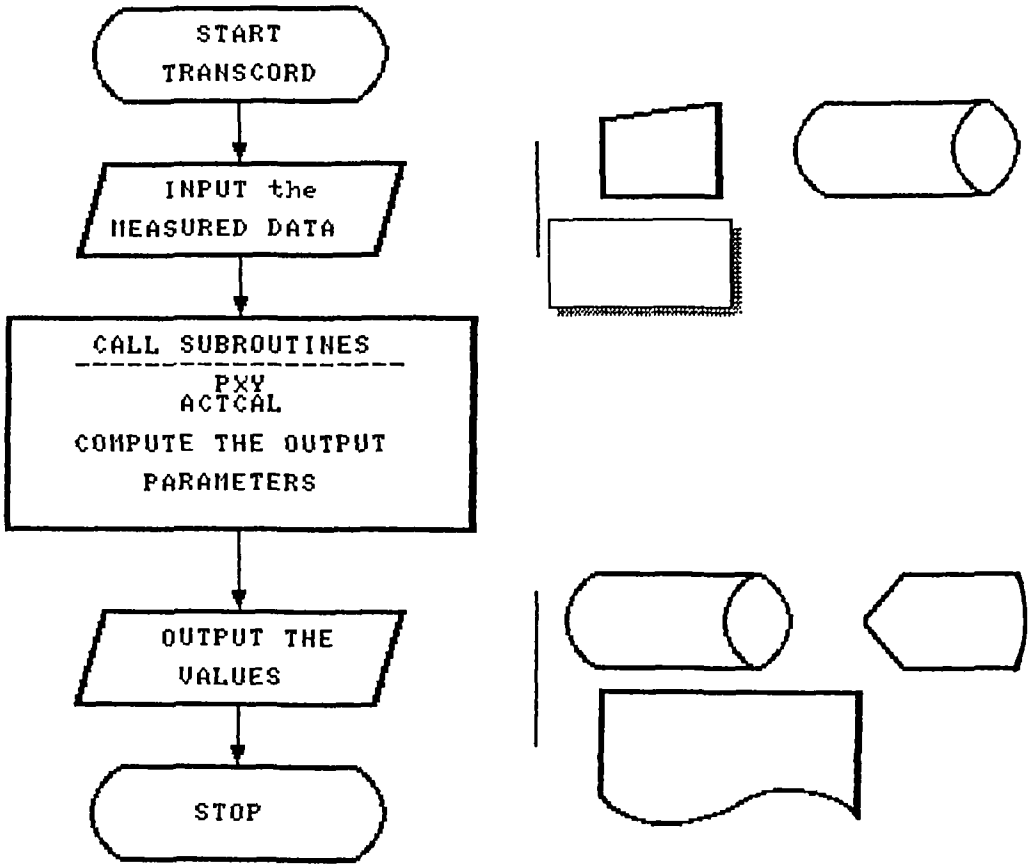

INPUT PARAMETERS: l_{PF}, l_A, l_B, ϕ_A, ϕ_B, Z_A, Z_B, ϕ, fac, μ, Coefficients.

OUTPUT PARAMETERS: L_A, Θ_A, L_A, Θ_B, E_{PF} (Input values for HIFISS)

L_{PF}, L_A, Θ_A, L_B, Θ_B, δ_A, δ_B, β, β_A, β_B (Detail Parameters)

Fig. II.8 A flow chart of the program 'TRANSCORD'. The input and output variables also stated.

of an event with the help of the derived equations of section II.1 from the projected parameters of an event. Input and output variables of the program are explained in the flow chart. The program generates two output files. One contains the input data to be fed to the analysing program 'HIFISS' for the next step of analysis while the other contains different output variables in detail.

II.4 THE PROGRAM 'HIFISS' (Heavy Ion FISSion)

Second part of the analysis begins with the determination of the masses of the fragments in the two different exit channels. Once the masses are found, various other kinematical parameters are being determined. In order to carry out this part of analysis one more application program **'HIFISS'** (Heavy Ion FISSion) has been developed in FORTRAN. Computation of the masses is being done by the 'BINARY' search **[42-45]** algorithm in the 'DYNAMIC MODE' with the consideration that the momentum is being conserved for the fragments in the two different exit channels. 'BINARY' search is an algorithm used for the purpose of picking up a number from an array of few numbers. **Fig. II.9** is a representation of 'BINARY' search algorithm in the tree form. Here each node has two leaves called the right child and the left child. Normal binary search is for an existing mode of data structure. But in the present case the data nodes to be searched do not exist as the masses to be determined are unknown and hence each node to be searched in the succeeding step has to be created in the previous step (logic behind 'DYNAMIC' mode).

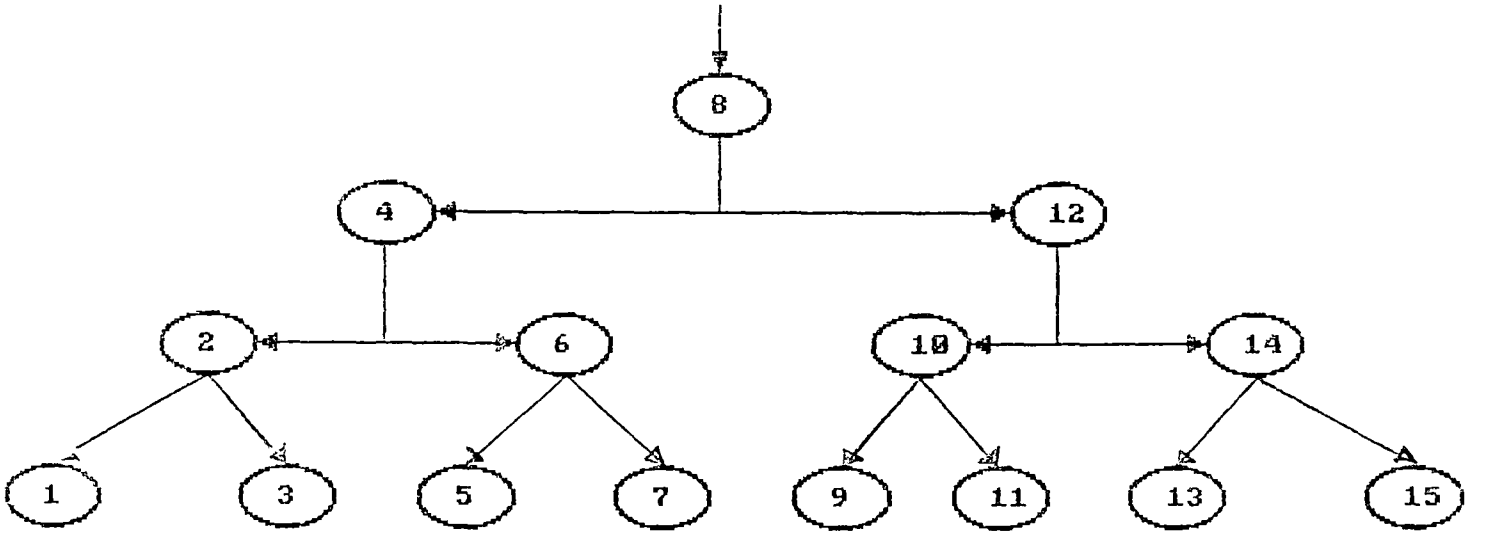

Fig. II.9 Representation of a 'BINARY TREE' in the binary search algorithm.

Thus the scission of the projectile with mass M_P at energy 'ELAB' MeV is associated with incident momentum

$$P_{in} = 2\ M_P\ ELAB \qquad (2.21)$$

From the dynamics of fission process **(Fig. II.10)** the momentum for fragments 'A' and 'B' are

$$P_A = M_A\ V_A \qquad (2.22)$$

$$P_B = M_B\ V_B \qquad (2.23)$$

Considering the vertical components (along the trajectory of the projectile) of the momentum for each fragment

$$P_{in} = M_A\ V_A \cos\theta_A + M_B\ V_B \cos\theta_B \qquad (2.24)$$

while the horizontal components (perpendicular to the trajectory of the projectile) are

$$M_A\ V_A \sin\theta_A = M_B\ V_B \sin\theta_B \qquad (2.25)$$

By substitution

$$P_A = P_{IN} / (\sin\theta_A (\cot\theta_A + \cot\theta_B)) \qquad (2.26)$$

and

$$P_B = P_{IN} / (\sin\theta_B (\cot\theta_A + \cot\theta_B)) \qquad (2.27)$$

An example would be more explanatory for this purpose. For the fragment 'A' whose track length is L_A μm the mass considered is 10 amu for the lower extreme while for the other extreme the mass considered is 228 amu, if the projectile is ^{238}U. It is well known that the velocity V is a non-linear function **[16-18]** of mass and track length which may be expressed by the following equation

$$V = \sum_{\mu=0}^{m} \sum_{\nu=0}^{n} C_{\mu\nu} M^{\mu} L^{\nu} \qquad (2.28)$$

where m and n are the order of the polynomial and $C_{\mu\nu}$ are the best set of coefficients generated.

Thus for a particular mass the velocity can be evaluated and thereby the momentum. By applying the 'BINARY' search algorithm in the 'DYNAMIC' mode if the momentum is conserved by applying the equations (2.21 - 2.27),

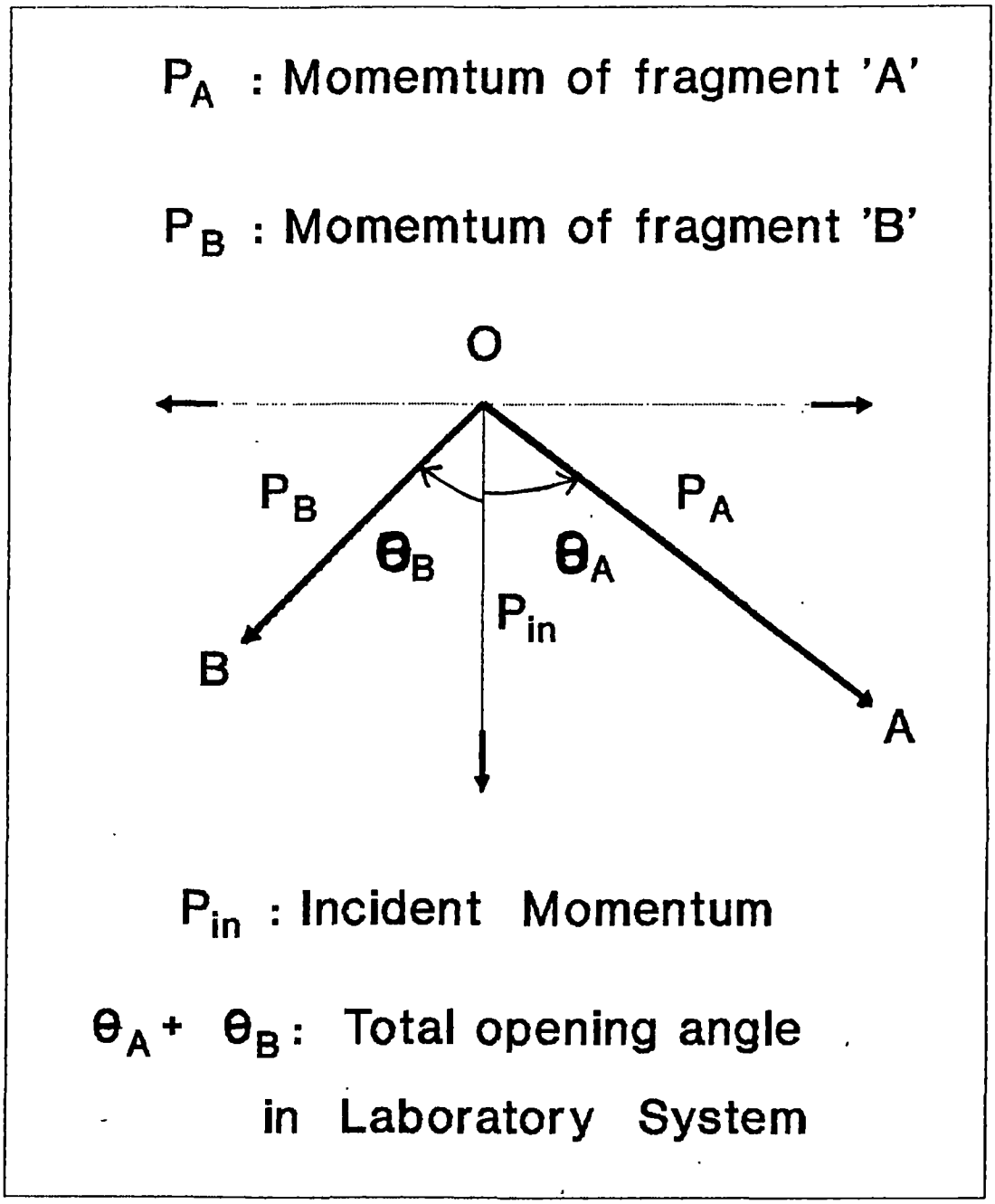

Fig.II.10 A diagram to explain the dynamics of fission process in terms of different momentum components.

masses are found for the two exit channels else in an iterative manner new masses are considered by the logic of 'BINARY TREE' and again similar process is repeated. If at the end of the 'BINARY TREE' iteration, the masses are not found then the particular event is said to have not passed through the analysis.

From the masses searched, the velocity of the fragments is calculated by using the equation (2.28) with the help of pre - determined coefficients and in turn the kinetic energy.

The total kinetic energy

ETOT = K. E. of fragment 'A' + K.E.of fragment 'B' (2.29)

The subroutine 'MASS' along with 'RTNE', 'FV1', 'FV2', 'VELF1' and 'VELF2'in 'HIFISS' is used to find masses of each fragment in the exit channels. The other subroutines used are 'CARTES','SKALAR'and 'ANGL12'. **Fig. II.11** is a flow chart for the program 'HIFISS' where the input and output variables are indicated. **Fig. II.12** is another flow chart for the program 'HIFISS' where the different interactive functions and subroutines used are shown.

II. 4. 1 TOTAL MASS OF FRAGMENTS

The masses in the two exit channels for an event are searched by the program 'HIFISS' as explained above. The total mass abbreviated as 'MTOT' is equal to the sum of the masses of the fragments in the two exit channels. Mathematically

$$MTOT = M_A + M_B \qquad (2.30)$$

MTOT may also be called as pre-fission mass. From the values of total mass of fragments, it is possible to find the reasons for the occurence of fork-like events. If the value of total mass of fragment is found to be near the value of projectile mass than the compound nucleus formation as a phenomenon for

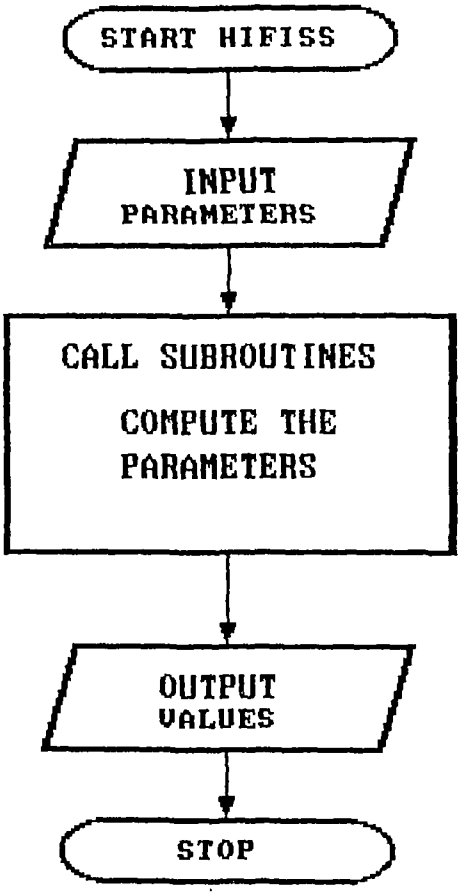

INPUT PARAMETERS

NUMBER OF EVENTS,

MASS OF THE PROJECTILE,

MASSES OF THE ELEMENTS IN THE DETECTOR,

FISSION IS SYMMETRIC OR ASYMMETRIC
(Only for Simulation),

MASS DEPENDENT VELOCITY RANGE COEFFICIENTS,

INPUT DATA FILE ($L_A, \theta_A, L_B, \theta_B, E_{pf}$)

OUTPUT PARAMETERS

M_A , M_B , E_A , E_B, ETOT, Q-VAL, V-REL, ASSY. PARA,

ETA12, CM (SCATT. ANGL.).

Fig. II.11 A flow chart of the program 'HIFISS'. The input and output variables are also stated.

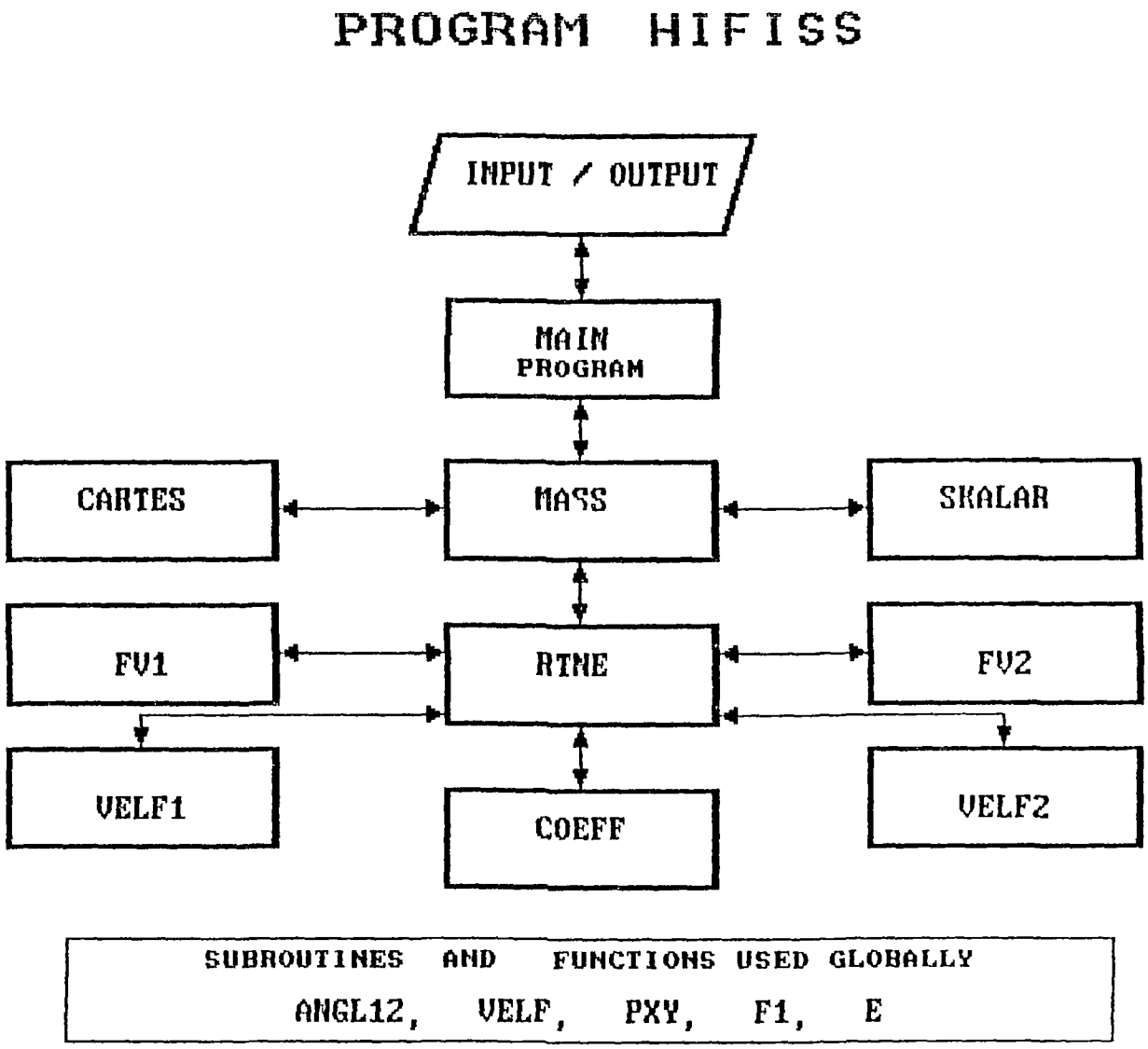

Fig. II.12 A flow chart of the program 'HIFISS' showing the different interactive subroutines and functions.

the occurence of these events can be ruled out. The conclusions derived from the total mass distributions for each system in the present study are discussed in chapter IV.

II.4.2 THE Q-VALUE

The Q-Value of fission is defined as the excess of energy released in the process of fragmentation of the nuclei by the difference in the value of the 'BINDING ENERGY'. It is one of the significant signatures of the fission process. For the fission of heavy ions and also the compound systems, the energy released has a particular value associated with it as explained by the systematics of Viola **[46]**. Difference of energy between 'ETOT' and 'ELAB" is the 'Q-Value' for each event i.e. the total kinetic energy released during scission.

From Viola systematics, **[46]** the total kinetic energy released in fission was computed as

$$E_K = 0.1071\, Z^2/A^{1/3} + 22.2\ \text{MeV} \qquad (2.31)$$

where Z is the charge of the compound nuclei and A is the mass. With the availability of data on light fissioning systems with precision and accuracy and by minimizing the contributions from competing processes the present modification **[47]** of the equation is

$$E_K = (0.1189 \pm 0.0011)\, Z^2/A^{1/3} + 7.3\ (\pm 1.5)\ \text{MeV} \qquad (2.32)$$

For the present investigation two projectiles i.e. ^{209}Bi and ^{238}U in CR-39 and Makrofol-E detectors have been selected. Both these detectors contain H, C and O atoms in different stoichiometric ratios. The calculated Q-Values using Viola systematics for fission of the projectiles and the probable compound nuclei have been tabulated in **Table II.2**. The evaluation of Q-Value is necessary as it is expected to indicate the kind of nuclear phenomenon associated with these fork like events.

Table II.2

Q-VALUES CALCULATED FROM THE VIOLA SYSTEMATICS FOR THE MENTIONED COMPOUND NUCLEI

COMPOUND NUCLEI	Q-Value (MeV)
^{238}U	169.7
$^{238}U + {}^{1}H \rightarrow {}^{239}Np$	173.0
$^{238}U + {}^{12}C \rightarrow {}^{250}Cf$	188.6
$^{238}U + {}^{16}O \rightarrow {}^{254}Fm$	195.1
^{209}Bi	145.3
$^{209}Bi + {}^{1}H \rightarrow {}^{210}Po$	148.5
$^{209}Bi + {}^{12}C \rightarrow {}^{221}Ac$	163.1
$^{209}Bi + {}^{16}O \rightarrow {}^{225}Pa$	169.2

II.4.3 RELATIVE VELOCITY OF THE FRAGMENTS

Relative velocity of a fragment with respect to the other is another important evidence for the kind of phenomenon taking place in these two pronged events. It is well known that for fission relative velocity of the fragments is 2.4 cm/ns **[46- 48]**. If V_A and V_B are the velocities of the fragments 'A' and 'B' respectively then the x and y component of relative velocity are:

$$V_{Rx} = V_{Ax} - V_{Bx} \quad \text{(the x component)} \quad \text{while} \qquad (2.33)$$

$$V_{Ry} = V_{Ay} - V_{By} \quad \text{(the y component)} \qquad (2.34)$$

And therefore the relative velocity (V_R) is

$$V_R = [\, V^2_{Rx} + V^2_{Ry} \,]^{1/2} \qquad (2.35)$$

In the program 'HIFISS' the subroutines 'COEFF' and 'SKALAR' are used for the calculation of relative velocity.

II.4.4 TOTAL OPENING ANGLE IN LABORATORY AND CENTRE OF MASS SYSTEM

Total opening angle in the laboratory and in the centre of mass system between the fragments are some of the other evidences for the nature of phenomenon taking place in these events. The scattering angle in the laboratory is the total opening angle ($\theta_A + \theta_B$) between the fragments and in the centre of mass it is defined as the angle between the direction of the incident momentum and the direction of relative velocity (**Fig. II. 13**). In the program 'HIFISS' the subroutine 'ANGL12' is introduced for the calculation of scattering angle in the centre of mass system. Logic used for the determination of total opening angle in the centre of mass system is calculation of the dot product of two vectors (incident momentum and relative velocity).

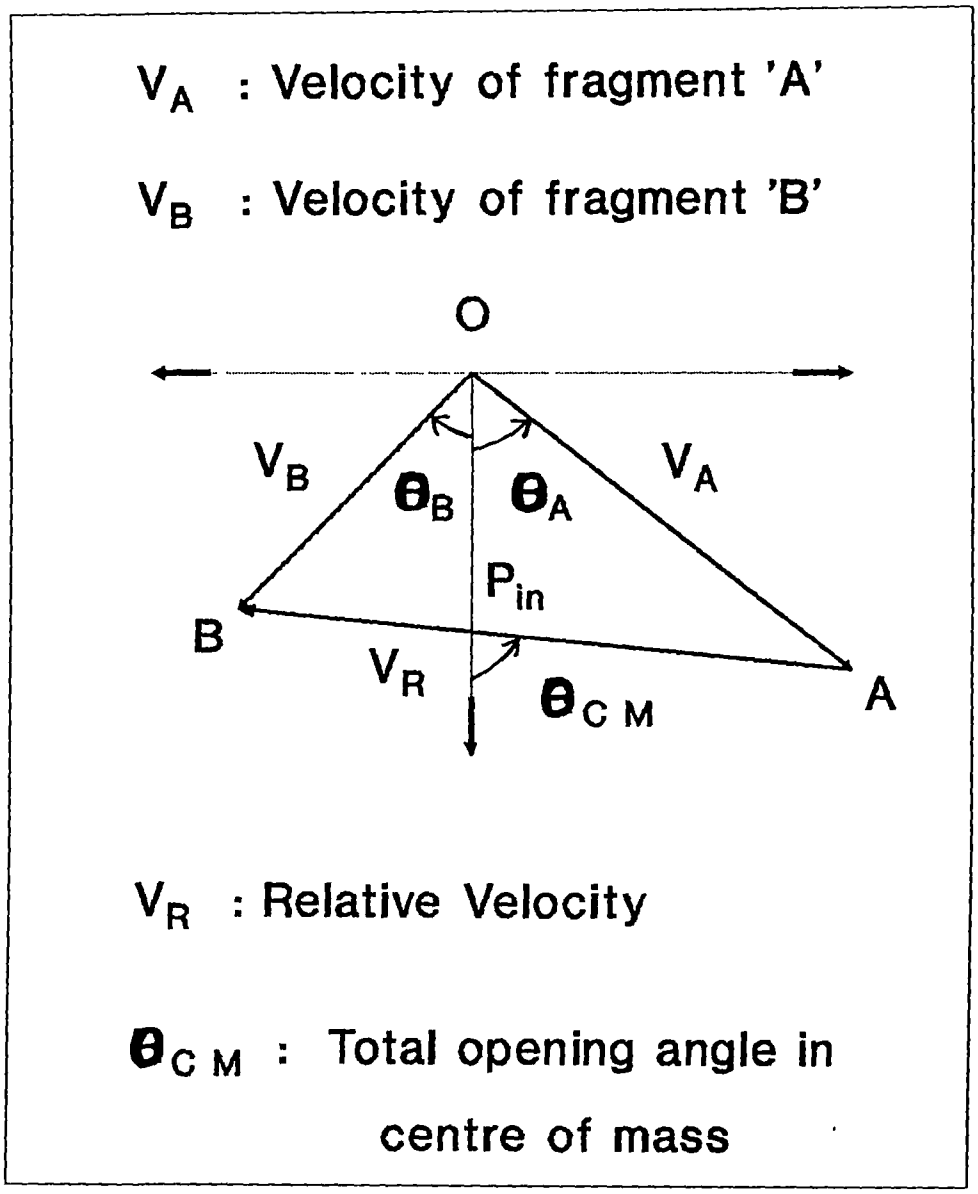

Fig. II.13 A diagram to explain the different velocity vectors for the determination of relative velocity and the total opening angle in the centre of mass system.

II.4.5 DATA TEST FOR THE PROGRAM 'HIFISS'

The validity of the program 'HIFISS' is checked by considering certain artificially created symmetric and asymmetric events. In fact 'SIMULATIONS' with artificially created events were being carried out.

(i) For the event due to the symmetric fission of ^{238}U in CR- 39 the following input data were considered. Let the fission take place at energy 2570.0 MeV. Track lengths of each track (L_A and L_B) of 150.9 μm each and opening angles (θ_A and θ_B) of 15° each.

E_{pf} = 2570.0 MeV; L_A = 150.9μm = L_B; θ_A = 15° = θ_B

The values computed by the program 'HIFISS' are tabulated in **Table II.4**

(ii) Similarly for an asymmetric fission of ^{238}U in CR-39 the input values of the artificially created events are tabulated in **Table II.3** while the output values are listed in **Table II.4**

The output values computed by the program 'HIFISS' are in agreement with the expected values. This proves the soundness of the logic used for developing the program 'HIFISS'.

II. 5 DIFFERENTIAL AND TOTAL CROSS-SECTION

Cross-section is defined as the probability of occurence for a particular kind of nuclear process. Hence the cross-section for the occurence of fork like events can be defined as the number of interactions per unit flux of the projectile per unit number of atoms present in the detector matrix. The flux for the present case is considered as the number of projectiles per unit cross-sectional area. Therefore the total cross-section can be expressed in the mathematical form as

$$\sigma_e = \frac{N_e}{n \Phi a x} \qquad (2.36)$$

Table II.3

VALUES OF DIFFERENT PARAMETERS OF THE ARTIFICIALLY CREATED EVENTS FOR TESTING THE PROGRAM 'HIFISS'

Symmetric and Asymmetric fission of ^{238}U in CR-39

	E_{pf}(MeV)	L_A(μm)	Θ_A	L_B(μm)	Θ_B
Symmetric M_A = 119.0 M_B = 119.0	2570.0	150.9	15.0°	150.9	15.0°
Asymmetric M_A = 94.0 M_B = 144.0	3190.0	404.0	17.8°	124.5	11.2°

Table II.4

VALUES OBTAINED FROM 'HIFISS' FOR THE ARTIFICIALLY CREATED EVENTS

Symmetric and Asymmetric fission of ^{238}U in CR-39

	M_A (Mass unit)	M_B (Mass unit)	MTOT (Mass unit)	Q-Value (MeV)	V-REL cm/ns	Scatt. angle(CM)
Symmetric Fission	119.8	119.8	239.6	165.2	2.4	90°
Asymmetric Fission	93.5	143.5	237.0	156.2	2.4	53.5°

where

σ_e : Cross-section in barns for the occurence of these events,

N_e : Total number of events,

n : Number of target atoms per unit volume of the detector matrix,

Φ : Number of projectiles per unit area (Flux),

a : Total surface area of the detector.

x : Detector thickness considered.

For total cross-section calculation, N_e is the total number of events which passed through the analyzing program 'HIFISS'. The thickness considered is the range of the projectile down to 6 MeV/u (threshold limit observed for these events).

As few resonance peaks have been observed in the plots of number events vs. the pre-fission energy, it is worth-while to discuss the calculation of differential cross-sections corresponding to these peaks. The number of events under each resonance peak are considered as N_e and the differential target thickness is obtained from the FWTM value of the resonance peak. The values of 'Φ' and 'a' are invariant, while the value of n has been calculated for each individual peak considering number of atoms of the particular element present in the detector matrix on the basis of coulomb barrier. For example at energies above 11 MeV/u of the projectiles number of 'H' atoms are also considered for differential cross-section calculation while below 11 MeV/u, only the number of C and O atoms are considered.

II.6 ANALYSIS OF THE THIRD PRONG

Fork-like events with a third prong at the point of scission were observed for ^{238}U in CR-39. It has been assumed that this third prong must have been created by the prefission emission (evaporation) of particle from the excited

compound system. The reasons for such an assumption has been explained along with the observations in chapter IV. Being the first study on this interesting aspect of the phenomenon, attempt has been to determine the actual length of the third prongs and also the directional behaviour of ejection either in the forward or backward hemisphere. The studies related to the identification of the particles which create these prongs in terms of mass and energy are deferred due to the poor statistics. Once again a geometrical approach is undertaken. In **Fig. II.14 (a and b)** the top and side view of an event with the third prong is shown. The measured parameters of the third prong are the projected track length (l_p), the projected angle (Φ_p) and depth (Z_p) of the prong from the point of scission.

Let β_p be the angle by which it is inclined then

$$\tan \beta_p = Z_p / l_p \qquad (2.37)$$

where Z_p is the depth of the third prong from the point of scission and l_p is the projected length of the third prong.

Thus the actual length of the third prong is

$$L_p = Z_p / \sin \beta_p \qquad (2.38)$$

where Z_p contains the correction for the refractive index of the detector matrix (CR-39).

The directional behaviour of emission of these particles in backward and forward hemisphere is derived by considering a plane which is perpendicular to the direction of the incoming beam. The variable δ_p is calculated for the simplicity of derivation and it is the angle of tilting of the plane containing the third particle from the observation plane. One more equation has been derived to calculate δ_p which is expressed as

$$\delta_p = \tan^{-1} \frac{Z_p}{l_p \sin \Phi_p} \qquad (2.39)$$

The equations derived for the third prong are tabulated in **Table II.5.**

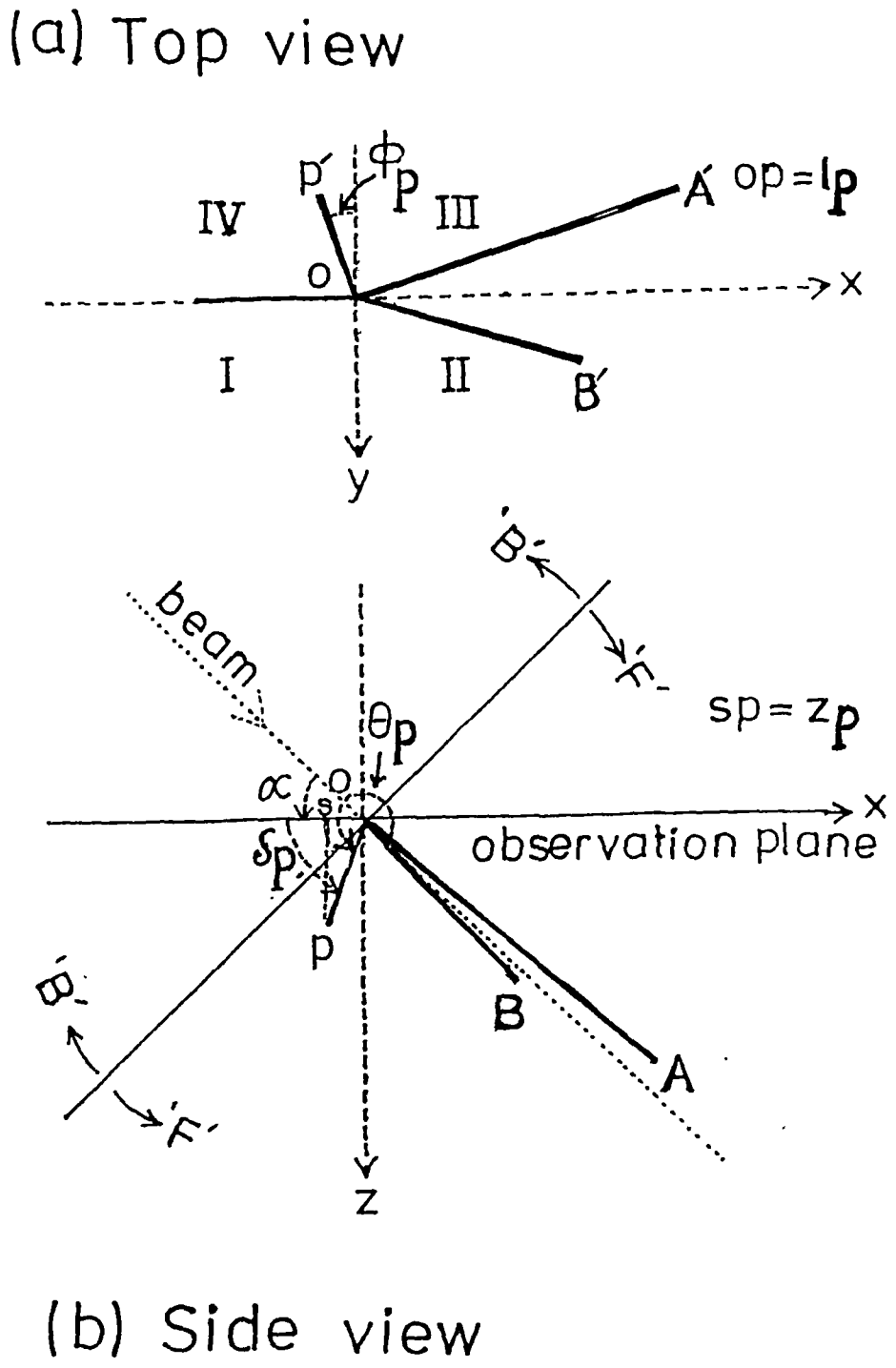

Fig.II.14 Line diagrams showing an event with the third prong. (a) Top view (xy -plane). (b) Side view (xz-plane) . Different parameters are also indicated.

Table II.5

DERIVED EQUATIONS TO DETERMINE THE PARAMETERS OF THE THIRD PRONG

$$L_P = Z_P \; / \; \sin \beta_P \qquad (2.38)$$

$$\delta_P = \tan^{-1} (Z_P \; / \; l_P \sin \Phi_P) \qquad (2.39)$$

Θ_P : as described in the Table II.6

The systematic approach undertaken to derive the directional behaviour (Backward 'B' and Forward 'F') of the third prong along with the angle (θ_p) with respect to the direction of the incoming projectile is explained in **Table II.6.**

Table II.6

DETERMINATION OF PARTICLE DIRECTION (Θ_P) WITH RESPECT TO BEAM DIRECTION

Θ_P (MEASURED IN A COUNTER CLOCKWISE DIRECTION)

QUADRANT	Z_P	δ_P	DIRECTION	Θ_P in degrees
I	-	$>\alpha$ $<\alpha$	BACKWARD	$180+\alpha-\delta_P$
	0	0	BACKWARD	$180+\alpha$
IV	+	$>90-\alpha$ $<90-\alpha$	FORWARD BACKWARD	$180+\alpha+\delta_P$
II	+	$>\alpha$ $<\alpha$	FORWARD	$360+\alpha-\delta_P$ $\alpha-\delta_P$
	0	0	FORWARD	α
III	-	$>90-\alpha$ $<90-\alpha$	BACKWARD FORWARD	$\alpha+\delta_P$

CHAPTER III

EXPERIMENTAL PROCEDURE

CHAPTER III

EXPERIMENTAL PROCEDURE

III.1 SELECTION OF DETECTORS

The fascinating fork-like events were observed initially for ^{238}U in CR-39 [38]. Later on such events were observed for ^{238}U in Makrofol-E, Cellulose Nitrate and Mica detectors. As the work on different experiments were in progress they were observed in similar detectors irradiated to ^{209}Bi and ^{208}Pb. Since then the inquisitiveness grew about the selection of detectors to carry out systematic heavy ion fission studies in a 4π geometry in order to find possible explanations for the occurence of these events. The choice of detectors for such experiments is very important as the occurence of such phenomenon in a detector is found to be comparatively low, and therefore the registration efficiency of a detector must be high with a low energy threshold for registration, so that the entire gamut of particles from lower to higher masses are recorded. Moreover the damage trails created by the fragments in the different exit channels should be completely etchable too. Though etching efficiency of a detector is purely a geometrical requirement of irradiation, few simple properties have been considered in selecting the detectors - such as the detector composition, registration efficiency and registration threshold to record the etchable tracks of particles with wider spectrum of masses.

For the present investigation two sensitive polymeric track detectors were selected. These are: (a) Allyl-diglycol polycarbonate and (b) Bisphenol-A polycarbonate, which have commercial names **CR-39** and **Makrofol-E** respectively. Selection of these two detectors has been mainly due to the initial observation of events were in CR-39 and also because CR-39 has an inherent property of its own for detection of various low energetic particles with a high registration efficiency. It also has low value of registration threshold energy for a wide spectrum of masses. It has already been reported that CR-39 can efficiently register low (60-727 KeV) **[49]** as well as high energetic (upto 10 MeV) protons **[50,51]**. CR-39 has also been used for the detection of anomalous fragments produced in the reactions of energetic heavy ion collisions **[52]**. Its application has also been exploited for the determination of projectile fragmentation cross-sections in the relativistic heavy ion collisions **[20,53,54]**. The application has also been in search for projectile fragments with fractional charges in relativistic heavy ion collisions **[21]**. Besides CR-39 is excellent in optical standards **[55]** as the optical trasperancy is not degraded even after subjecting to high radiation doses and prolonged etching.

Makrofol-E - a sensitive polycarbonate track detector with capability of recording α-particles of energy as low as 1 MeV **[56,57,58]**. Makrofol-E has been used as an ion discriminator ($Z < 5$) for the detection of exotic radioactive decay mode of ^{222}Ra and ^{224}Ra by ^{14}C emission. Both CR-39 and Makrofol-E contain C,H and O in different stoichiometric ratios per *monomer. Important properties of these two detector materials are tabulated* in **Table III.1.**

III.2 PREPARATION OF DETECTORS AND IRRADIATIONS

CR-39 and Makrofol-E were cut from commercially available sheets in to square pieces of size 2x2 cm^2. After removal of surface protective layers, they

Table III.1

IMPORTANT PROPERTIES OF CR-39 AND MAKROFOL-E

Properties	CR-39	Makrofol-E
Commercially available as	CR-39	Makrofol-E
Monomeric composition	$C_{12}H_{18}O_7$	$C_{16}H_{14}O_3$
Chemically identified as	Allyl-Diglycol Carbonate	Bisphenol-A Polycarbonate
Molecular Weight	274.0	254.0
Density (g/ml)	1.32	1.14
Refractive Index	1.5	1.63
Thickness (μm)	1500	300
Uniformity	Good	Good
Surface View	Optical Grade	Optical Grade
Optical Behaviour	Transparent	Transparent
$(dE/dx)_c$	5.0 MeV*	5.0 MeV**
Minimum detectable mass (particle)	α	p
Manufactured by	Homalite Corp. Wilmington, Del. U S A.	Bayer (AG) Leverkusen, Germany.

* Ref. [36] ; ** Ref. [35]

were washed properly in order to remove surface contaminations. The detectors were irradiated to a well collimated beams of ^{209}Bi and ^{238}U at the XO port of UNILAC, GSI, Darmstadt. An account on the irradiations carried out are in **Table III.2.** Variations in the energy have been done in order to find the cut-off (threshold) value of energy for the occurence of fork like events in the detectors. The degraded energies were obtained by using aluminium foils of uniform thickness.

III.3 CHEMICAL PROCESSING

Revealation of tracks by chemical treatment is more of an art than science, nevertheless it remains an important aspect of nuclear track technique, as a suitable etchant under an optimum condition would be helpful in developing the well defined tracks with good contrast leading to measurement of various parameters of an event without much deviation. To find a suitable etchant and its proper thermal condition for CR-39 and Makrofol-E few test experiments were undertaken. Selection of a suitable chemical reagent under an optimum condition is based on few important factors such as - the complete etching of the prongs of an event and also the time. The time required to etch the prongs of an event should not be too large so that a major portion of the detector thickness remains unetched. Last but not the least the detector surface must not be degraded in optical standards after etching as this would cause an optical interference of the transmitted light of the microscope during the measurement of different parameters of an event. This leads to a large deviation in the values of calculated parameters. **Table III.3** is an account on the suitable etchants for the two detectors used for the present investigation along with the thermal conditions. Thus the chemical processing of the irradiated samples in the mentioned chemical reagents were carried out under optimum conditions to reveal the fork-like events as well as the linear tracks of the projectiles.

Table III. 2

SPECIFICATIONS OF IRRADIATIONS CARRIED OUT

PROJECTILES		^{209}Bi		^{238}U
DETECTOR	CR-39	MAKROFOL-E	CR-39	MAKROFOL-E
INCIDENT ANGLE	45°	45°	30° , 45°	45°
ENERGY (MeV/u)	13.0	13.0	16.4 , 15.2 14.0 , 13.0 11.3 , 8.0 8.0	17.2 , 16.0 14.3 , 12.4 10.0
FLUENCE (cm^{-2})	10^5	10^5	3×10^4 & 10^4	10^4

Table III. 3

AN ACCOUNT ON THE SUITABLE ETCHING CONDITIONS FOR THE TWO DETECTORS USED

	CR-39	Makrofol-E
Chemical Reagent	NaOH	NaOH
Concentration	6N	5N
Temperature (°C)	55.0 ± 0.5	45.0 ± 0.5
Duration	2 - 6 Hrs.	2 - 5 Hrs.

III.4 OBSERVATION AND SCANNING

Completely developed track detectors were scanned under an optical microscope (Leitz, Laborlux D) at a low magnification (156x) in order to locate the positions of the events. The location of an event is helpful in doing multiple measurements of various parameters of the event. The positions of the events were recorded as the coordinates (x,y) of the scanning plane. Once an event was located after recording its location the various parameters of the event were measured. Thus two kinds of protocols were generated. One for recording the positions along with the shapes of the events while the other to record the various measured parameters.

III.4.1 MEASUREMENT OF VARIOUS PARAMETERS

a. OF A FORK-LIKE EVENT

As mentioned in the previous chapter measurement of various linear dimensions of the projected image of each event such as the pre-fission track length (l_{pf}) and the lengths of the prongs 'A' and 'B' (l_A and l_B respectively) were measured with the help of pre-calibrated micrometer placed in the eye-piece at 625x magnification. The minor axis of the elliptical face of each event was measured at 1526x magnification to find the bulk etch rate, in order to incorporate the surface etching corrections to the pre- fission track length. The angles Φ_A and Φ_B (**Fig. III.1**) were measured with the help of a specially designed and fabricated goniometer placed in the eye-piece of the microscope. An enlarged view of the goniometer disc is shown **Fig. III.2** through which microscopic angles can be measured with an accuracy of $\pm 2°$.

The depths of the prongs (Z_A and Z_B) from the point scission were measured with the help of 'HEIDENHAIN' depth measuring device. Procedure for the measurement of depths with the help of 'HEIDENHAIN' depth measuring

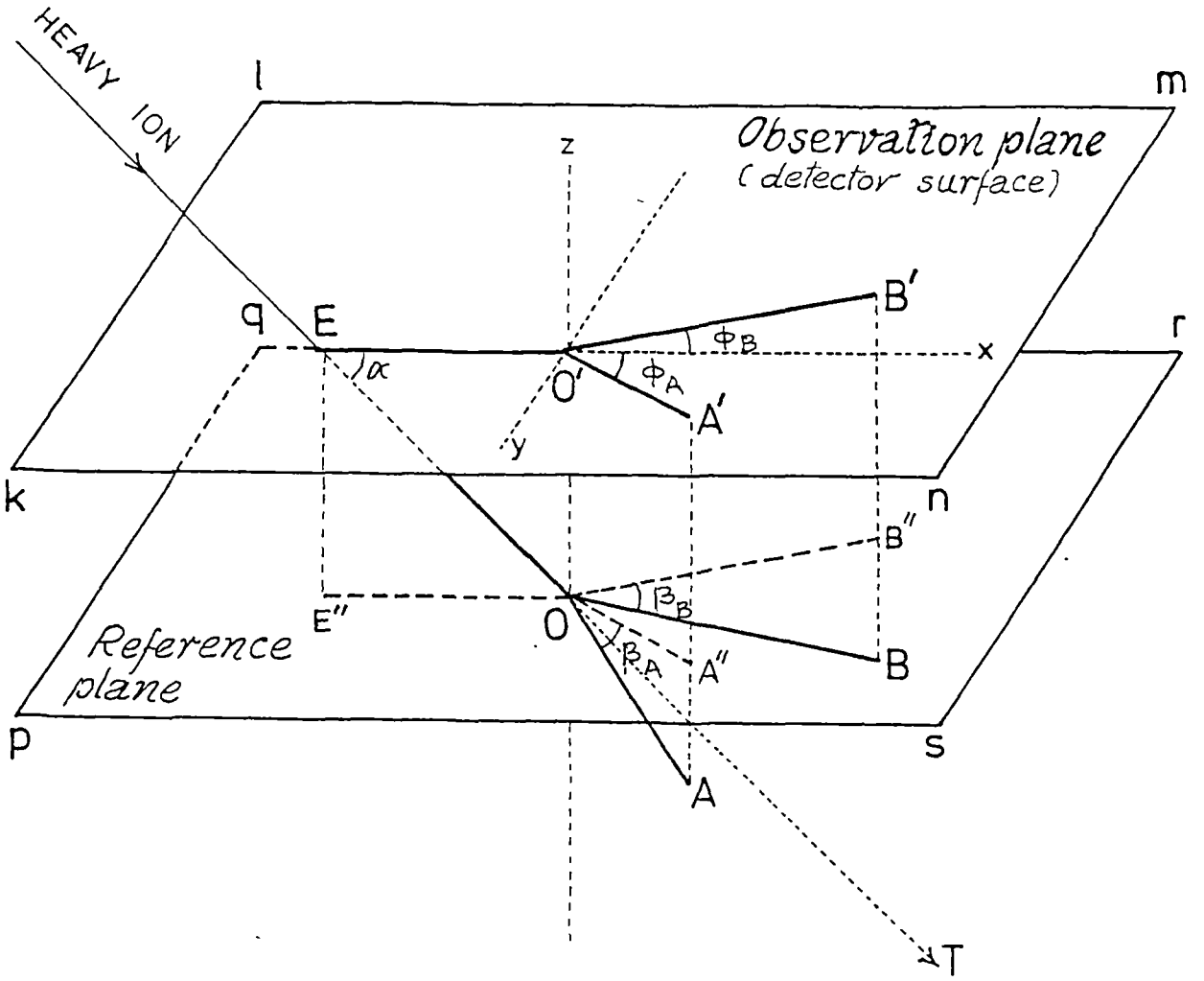

Fig. III.1 A line diagram of an event with different projected and real parameters.

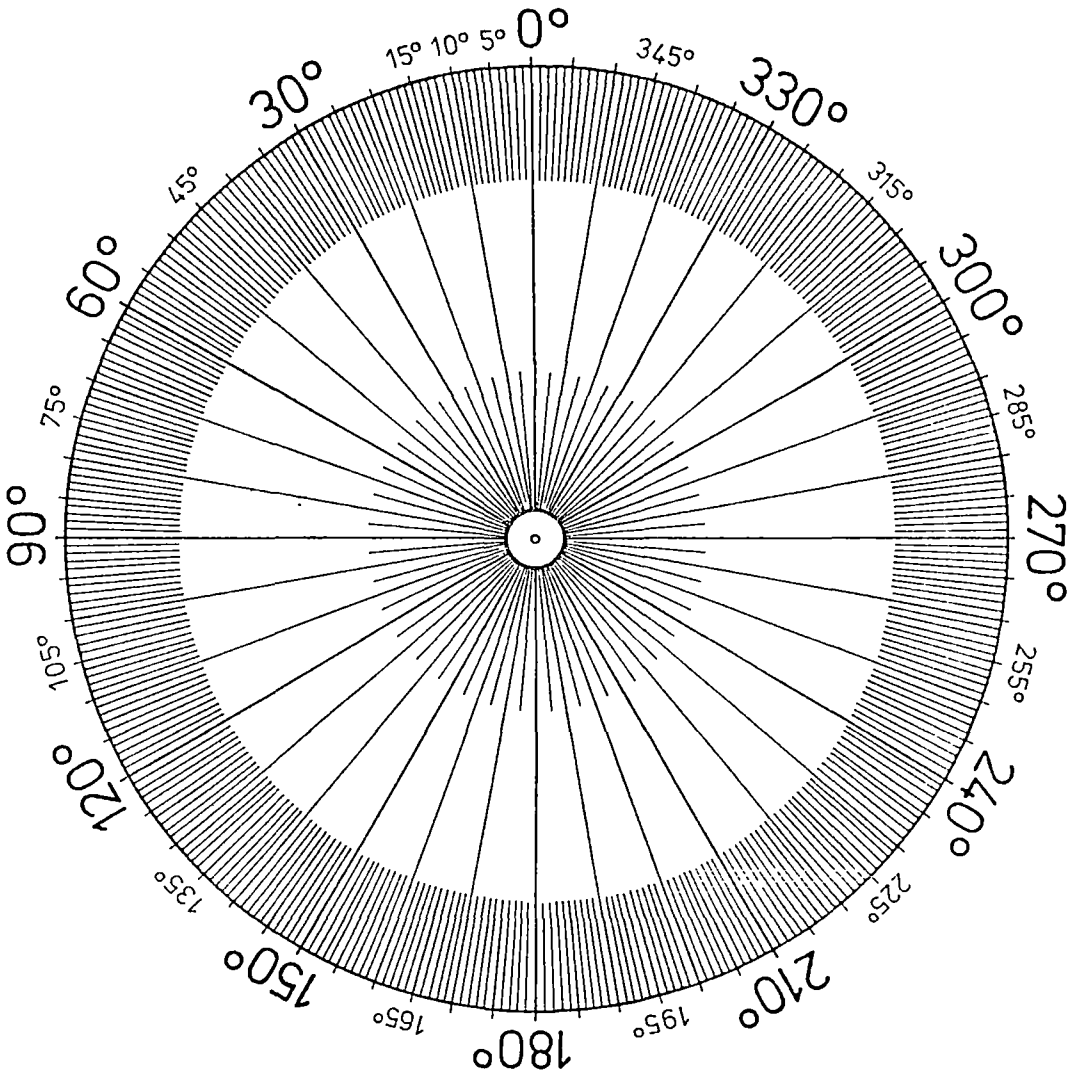

Fig. III.2 An enlarged view of the angle measuring device.

device has already been reported [59] in detail. In brief it consists of a measuring gauze (CT-60) with a plunger, a remote control for the plunger movement and a display unit (VRZ 210). The measuring length of the gauze (CT-60) has a glass scale with a DIADUR- line grating (pitch 10 μm). The scale grating is photoelectrically scanned. The output signals of the gauze head are interpolated and digitised in the (VRZ 210) display unit. This device has a claimed accuracy of $\pm 0.1\ \mu$m for any kind of thickness measurement. For measuring the depths of the prongs 'Z_A' and 'Z_B' the head of the plunger is kept in contact with the stage of the microscope. The depths of the prongs from the pre-fission point are measured by first focussing the microscope at the point of bifurcation and resetting the display to zero and then by moving the stage downward to focus the prong tips and recording the values from the dispaly unit.

b. OF A FORK-LIKE EVENT WITH THE THIRD PRONG

Similar measurements have been carried out for the events with the third prong too. The two longer prongs were measured exactly in a similar fashion as mentioned above. For the third prong the projected length (l_p) was measured. The angle Φ_p **(Fig. II.14)** was measured with the help of the goniometer placed in the eyepiece of the microscope while Z_p was measured with the help of 'HEIDENHAIN' depth measuring device. The measured parameters of the third prong were also recorded in the protocols.

III.4.2 DETERMINATION OF TRACK DENSITY

The number of tracks under a graticule placed in the eye – piece of the microscope were counted at 625 magnification. An average of 100 such fields of view for each piece of detector were considered to determine the average track density. This value of track density has been used for cross-section calculation (differential as well as total) as discussed in the previous chapter (Section. II.5).

III.4.3 DETERMINATION OF ENERGY OF THE PROJECTILES

The degraded energies of the projectiles were obtained by placing uniform aluminium degrader foils of known thickness on the surface of the detectors at the time of irradiation. Even though the energy-loss in the degrader foils can be determined from the range-energy calibrations of the degrader but for the present case a different approach is undertaken. In this a track length distribution is generated to find the most probable track length for a given energy in a detector. The most probable track lengths were found from gaussian fittings to the track length distributions, generated with the help of the application program 'TRADIS'[39]. After this the most probable energy is found from the pre-calibrated energy-track length curves of the particular projectile in the specific detector matrix. By this method any possible sources of errors in the variation of energy and non—uniformity of degrader foils are taken care of.

III.5 CALIBRATION OF DETECTORS

Calibration of detectors is a primary requirement for the present study. As explained in the previous chapter, two different kinds of calibrations for any detector is essential. The first kind of calibration for the detectors is energy 'E' in MeV as a non-linear function of track length 'L' in μm which can be expressed as

$$E\ (MeV) = \sum_{\mu=0}^{m} a_\mu L^\mu \qquad (3.1)$$

where m is the order of the polynomial, a_μ are the best set of coefficients. It has been observed for the present systems that the best set of coefficients could be obtained by using third or fourth order of polynomials.

Determination of the best set coefficients involve two steps of computation. First the coefficients are calculated for different orders of the function with the help of an application program 'TRAPOL1' **[39]**. Next is to determine the values of mean square root deviation for each set of coefficients with the help of another program 'TRACAL1'**[39]**. The set of coefficients with least mean square root deviation is considered as the best set.

This kind of calibration is required to find the energy of the projectile at the point of scission from the pre-fission track length as explained in the previous chapter to calculate the incident momentum.

For the present investigation the best set of coefficients were determined for each initial energy of ^{209}Bi and ^{238}U in CR-39 and Makrofol-E by the above mentioned method. In **Table III.4, III.5, III.6** the best set of coefficients for ^{238}U and ^{209}Bi of different energies in the two detectors have been tabulated along with the values of mean square root deviations.

The other calibration is the polynomial interdependence between the velocity, the range and the mass of the penetrating nuclei **[16 - 18]**. This kind of polynomial may be expressed as a function of the following type

$$V = \sum_{\mu=0}^{m} \sum_{\nu=0}^{n} C_{\mu\nu} M^{\mu} L^{\nu} \qquad (3.2)$$

where m and n are the orders, V is the velocity in cm/10^{-10}s, L is the track length in μm, M is the mass in amu and $C_{\mu\nu}$ are the best set of coefficients. Here too the best set of coefficients are determined with the help of a two step computation as explained above but the application programs used are 'TRAPOL2' **[39]** and 'TRACAL2' **[39]**.

Table III.4

BEST SETS OF COEFFICIENTS (a_μ) FOR TRACK LENGTH ENERGY CALIBRATIONS FOR ^{238}U AT DIFFERENT ENERGIES IN CR-39 ALONGWITH MEAN SQUARE ROOT DEVIATIONS (MSRD)

ENERGY (MeV/u)	$\mu=0$	$\mu=1$	$\mu=2$	$\mu=3$	$\mu=4$	MSRD (MeV)
16.4	0.3882263 E+04	-0.1193808 E+02	-0.1071845 E+00	0.3455083 E-03	0.3985019 E-05	16.37
15.2	0.3643977 E+04	-0.2288587 E+02	0.1257750 E+00	-0.1638164 E-02	0.5732740 E-05	8.53
14.0	0.3414577 E+04	-0.1659282 E+02	0.6050715 E-01	-0.7194827 E-03	0.2157124 E-03	7.71
13.0	0.2925585 E+04	-0.1192741 E+02	-0.1841945 E+00	0.9016395 E-05	-	13.26
11.3	0.2639809 E+04	-0.1441646 E+02	-0.1834477 E+00	0.1093903 E-02	-	7.31

Table III.5

BEST SETS OF COEFFICIENTS (a_μ) FOR TRACK LENGTH ENERGY CALIBRATIONS FOR ^{238}U AT DIFFERENT ENERGIES IN MAKROFOL-E ALONGWITH MEAN SQUARE ROOT DEVIATIONS (MSRD)

ENERGY (MeV/u)	μ=0	μ=1	μ=2	μ=3	μ=4	MSRD (MeV)
17.2	0.4017941 E+04	-0.1187016 E+02	-0.5901808 E-01	0.1575082 E-03	-	10.1
16.0	0.2851142 E+04	-0.9657531 E-01	0.5832607 E-03	-0.4979835 E-05	0.1256037 E-07	12.1
14.3	0.3580150 E+04	-0.1137500 E+02	-0.7609643 E-01	0.2329216 E-03	-	12.2
12.4	0.2851142 E+04	-0.9668364 E+01	-0.1409166 E+00	0.5918434 E-03	-	14.8

Table III.6

BEST SETS OF COEFFICIENTS (a_μ) FOR TRACK LENGTH ENERGY CALIBRATIONS FOR ^{209}Bi OF 13.0 MeV/u IN CR-39 AND MAKOROFOL-E

DETECTOR						MSRD
	$\mu = 0$	$\mu = 1$	$\mu = 2$	$\mu = 3$	$\mu = 4$	(MeV)
CR-39	0.2706201 E+04	-0.1741950 E+02	0.2763704 E-01	-0.1034439 E-02	0.5517039 E-05	11.0
MAKROFOL-E	0.2713070 E+04	-0.1594110 E+02	0.5438349 E-01	-0.8641609 E-03	0.3285227 E-05	12.0

With the help of the available experimental as well as theoretical data on ranges of various ions in these detectors (CR-39 and Makrofol-E), calibrations were done by finding the most appropriate sets of coefficients. The values of the best sets of coefficients for ^{238}U and ^{209}Bi in CR-39 and Makrofol-E are tabulated in **Tables III.7, III.8, III.9, III.10.**

III.6 ERROR ANALYSIS

Error is the difference between a calculated or observed value and the true value. Systematic error arises due to the calibration of the instrument or from bias on the part of observer. Such kind of errors are to be incorporated in the analyzed data to arrive at any meaningful result.

In the present study while measuring the linear dimensions of any parameter of an event, it is impossible to measure half a division of the micrometer in the eye-piece with accuracy. Hence the measurement inaccuracy for linear dimension measurement is considered to be half a division at any magnification. Similarly while measuring the depth (Z) by focussing downward an error of $\pm 2\ \mu m$ was observed. Again during the measurement of polar dimensions i.e the angles, an inaccuracy of $\pm 2°$ was seen. Thus error analysis in the present study is of no less importance as every stage of analysis is associated with certain amount of experimental and its resultant inaccuracies. To determine these inaccuracies 'SIMULATION' on an artificially created event was carried out by varying the values of different parameters of the ideal event within the limits of encountered inaccuracies.

III.6.1 EXPERIMENTAL ERRORS

Error in the measurement of track length was determined to be $\pm 1.2\ \mu m$ while the diameters were measured with an accuracy of $\pm 0.5\ \mu m$. In the measurement of depth (Z) a maximum error of $\pm 2.0\ \mu m$ was observed. The measurement inaccuracy for the angles were $\pm 2.0°$.

Table III.7

BEST SET OF COEFFICIENTS ($C_{\mu\nu}$) FOR MASS DEPENDENT RANGE VELOCITY. CALIBRATION OF ^{238}U IN CR-39

ν	$\mu = 0$	$\mu = 1$	$\mu = 2$
0	0.1213506 E+00	-0.1554904 E-06	0.1528530 E-08
1	-0.1314036 E-02	-0.6019131 E-05	-0.5684072 E-11
2	0.3470264 E-05	-0.3999806 E-06	0.2862580 E-10
3	0.2908217 E-02	0.1504498 E-08	-0.1901278 E-11
4	0.4550553 E-04	0.8295458 E-08	0.6770951 E-14

Table III.8

BEST SET OF COEFFICIENTS ($C_{\mu\nu}$) FOR MASS DEPENDENT RANGE VELOCITY CALIBRATION OF ^{238}U IN MAKROFOL-E

ν	$\mu = 0$	$\mu = 1$	$\mu = 2$
0	0.9925967 E+01	-0.4311017 E-07	0.3266701 E-09
1	-0.7602514 E-03	-0.9190254 E-05	-0.5277252 E-12
2	0.9363168 E-06	-0.1098678 E-06	-0.4101623 E-11
3	0.2986263 E-02	0.2437144 E-09	-0.3022643 E-12
4	0.1903410 E-04	0.1166270 E-07	0.1098474 E-15

Table III.9

BEST SET OF COEFFICIENTS ($C_{\mu\nu}$) FOR MASS DEPENDENT RANGE VELOCITY CALIBRATION FOR ^{209}Bi IN CR-39

ν	$\mu = 0$	$\mu = 1$	$\mu = 2$
0	0.1106475 E-00	-0.1166413 E-06	0.1251213 E-08
1	-0.1064560 E-02	-0.8775751 E-05	-0.3651106 E-11
2	0.2295874 E-05	-0.3293366 E-06	0.1591273 E-10
3	0.3222633 E-02	0.1074325 E-08	-0.1478611 E-11
4.	0.3799670 E-04	0.1295213 E-08	0.3204593 E-14

Table III.10

BEST SET OF COEFFICIENTS ($C_{\mu\nu}$) FOR MASS DEPENDENT RANGE VELOCITY CALIBRATION FOR ^{209}Bi IN MAKROFOL-E

ν	$\mu = 0$	$\mu = 1$	$\mu = 2$
0	0.1246483 E+00	-0.1611997 E-07	0.1283036 E-09
1	-0.4998273 E-03	-0.3115168 E-05	0.2381801 E-12
2	-0.8352487 E-06	-0.7619823 E-07	0.1952578 E-12
3	0.2061127 E-02	0.8357435 E-11	0.5024913 E-13
4	0.1788410 E-04	0.1084376 E-08	-0.4599233 E-15

The other errors during experimentation were the maintenance of temperature during chemical processing and the time recorded for etching. They introduce a negligible errors in the present investigation and hence were not taken into account for a detail analysis.

III.6.2 ERRORS IN THE DERIVED QUANTITIES

Table III.11 gives an account on the errors involved in the derived parameters of an event due to the measurement inaccuracies. To arrive at these values at first an ideal event was created. Then measurement inaccuracies were incorporated to the values of the projected parameters of the event. Finally these values were fed to the program 'TRANSCORD' in the first step of analysis. The deviations from the ideal situation were considered as the errors in the values of real parameters of an event. It may be observed that the measurement inaccuracies lead to a maximum deviations of $\pm 2.3\,\mu$m in the lengths of the prongs, $\pm 1.5°$ in the real opening angles and $\pm 4°$ in the tilting angles.

III.6.3 ERRORS IN THE DIFFERENT KINEMATIC VARIABLES

The final step of analysis is the determination different kinematic variables of an event (fragment masses, relative velocity, Q-Value, asymmetry parameter) as explained in the previous chapter. These values too are determined with certain amount of inaccuracies due to the errors involved in the first step of analysis. Once again the values for an 'ideal' event and the inaccuracies along with them were considered.. Then these values were fed to the program 'HIFISS' in order to evaluate the errors in the second step of analysis. Measurement inaccuracies lead to a maximum error of ± 20 amu in the total mass while an error of ± 30 MeV in the Q-Value. The relative velocity could be determined within an accuracy of ± 0.02 cm/ns.

Table III.11

EFFECT OF MEASUREMENT INACCURACIES ON THE REAL PARAMETERS OF AN EVENT

ERROR PRONE PARAMETERS	ERRORS	L_A	Θ_A	L_B	Θ_B	δ_A	δ_B
l_A, l_B	± 1.22	± 1.0	$\pm 0.05°$	± 1.0	$\pm 0.05°$	$\pm 2.3°$	$\pm 2.3°$
Φ_A, Φ_B	$\pm 2.0°$	---	$\pm 1.5°$	---	$\pm 0.05°$	$\pm 1.6°$	$\pm 1.6°$
l_A, l_B Φ_A, Φ_B	± 1.22 $\pm 2.0°$	± 1.0	$\pm 1.5°$	± 1.0	$\pm 1.5°$	$\pm 1.0°$	$\pm 1.0°$
Z_A, Z_B	± 2.0	± 1.4	$\pm 0.1°$	± 1.4	$\pm 0.1°$	$\pm 4.0°$	$\pm 4.0°$
l_A, l_B Φ_A, Φ_B Z_A, Z_B	± 1.22 $\pm 2.0°$ ± 2.0	± 2.3	$\pm 1.4°$	± 2.3	$\pm 1.4°$	$\pm 3.8°$	$\pm 3.8°$

CHAPTER IV

RESULTS AND DISCUSSION

CHAPTER IV

RESULTS AND DISCUSSION

IV.1 STATISTICS OF EVENTS

In **Table IV.1 (a, b, c, d)** the total number of events observed at each initial energy of ^{238}U and ^{209}Bi in CR-39 and Makrofol-E have been tabulated. It also contains the number of events which pass through the analysing program 'HIFISS' i.e. the events for which the fragment masses in the exit channels could be searched. It is apparent from the statistics that for ^{238}U in CR-39 nearly 90% events could pass through the program as fission events. Similar is the observation for the same projectile in Makrofol-E.

Again for ^{209}Bi of 13.0 MeV/u in CR-39 and Makrofol-E 98% and 96% events respectively could pass through the analysis.

As evident from the above results that majority of events have passed through the analyzing program 'HIFISS', it may be concluded that a similar nuclear phenomenon is responsible for the creation of these events.

Table IV.1.

STATISTICS OF EVENTS

(a) ^{238}U in CR-39

ENERGY (MeV/u)	16.4	15.2	14.0	13.0	11.3	8.0	6.0
Number of Events Observed	577	65	183	122	62	4	nil.
Number of Events Passed. through the analysis	520	59	165	110	56	2	nil.

Table IV.1

STATISTICS OF EVENTS

(b) ^{238}U in MAKROFOL-E

ENERGY (MeV/u)	*17.2*	*16.0*	*14.3*	*12.4*	*10.0*
Number of Events Observed	*300*	*185*	*187*	*70*	*15*
Number of Events passed through the analysis	*280*	*172*	*170*	*64*	*12*

Table IV.1

(c) ^{209}Bi in CR-39

ENERGY (MeV/u)	13.0
Number of Events Observed	351
Number of Events passed through the analysis	347

(d) ^{209}Bi in Makrofol-E

ENERGY (MeV/u)	13.0
Number of Events Observed	654
Number of Events passed through the analysis	628

IV.2 DIFFERENTIAL AND TOTAL CROSS-SECTIONS

Fig. IV.1 to Fig. IV.5 are the plots of number of events as a function of pre-fission energy for ^{238}U projectile of five different (16.4, 15.2, 14.0, 13.0, 11.3 MeV/u) initial energies in CR-39. In these plots it is clearly seen that resonances occur at pre-fission energies 7.0, 9.4, 11.8 and 14.2 MeV/u (marked a, b, c and d). Determination of differential cross-sections at these resonance energies has been done and are tabulated in **Table IV.2.**

Similarly for ^{238}U in Makrofol-E the plots are represented in **Fig. IV.6 to Fig. IV.9.** Again these plots contain distinct resonance peaks (marked a, b, c, d) at 7.0, 9.4, 11.8 and 14.2 MeV/u respectively. For these systems also the differential cross-sections have been determined and are tabulated in **Table IV.3.**

For 13.0 MeV/u ^{209}Bi in CR-39 and Makrofol-E the plots are shown in **Fig. IV.10 and Fig. IV.11** respectively. Here too the resonance peaks are observed at the same pre-fission energies which are separated by 2.4 MeV/u. The differential cross- sections at these energies have been determined and are tabulatd in **Table IV.4.**

From these plots (**Fig. IV.1 - Fig. IV.9**) it is very much apparent that there exists a threshold (cut-off) value of energy for the occurence of these events as below 6 MeV/u for ^{238}U and 5.8 MeV/u for ^{209}Bi no events do occur. This indicates the existence of a coulomb barrier of interaction between the projectile and the atoms constituting the detector matrix. Hence qualitatively it can be said that the projectile has undergone fusion with the atoms of the detector matrix before scissioning. The complete and incomplete component of fusion is not possible to be resolved due to the limitations of this technique.

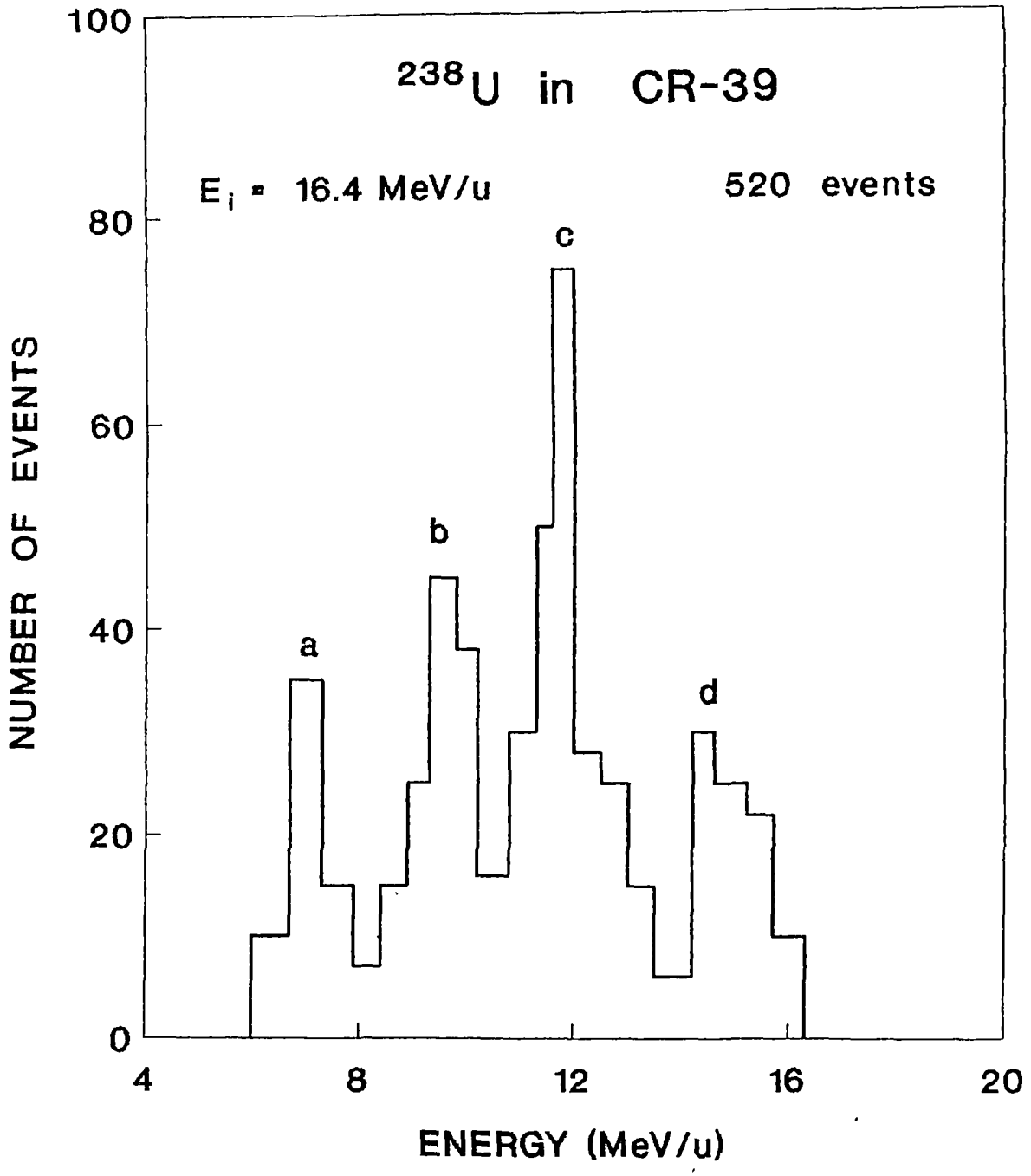

Fig. IV.I Plot of Number of events at different pre-fission energy for 16.4 MeV/u ^{238}U in CR-39. Resonance peaks observed at a) 7.0 Mev/u, b) 9.4 MeV/u, c) 11.8 MeV/u, d) 14.2 MeV/u.

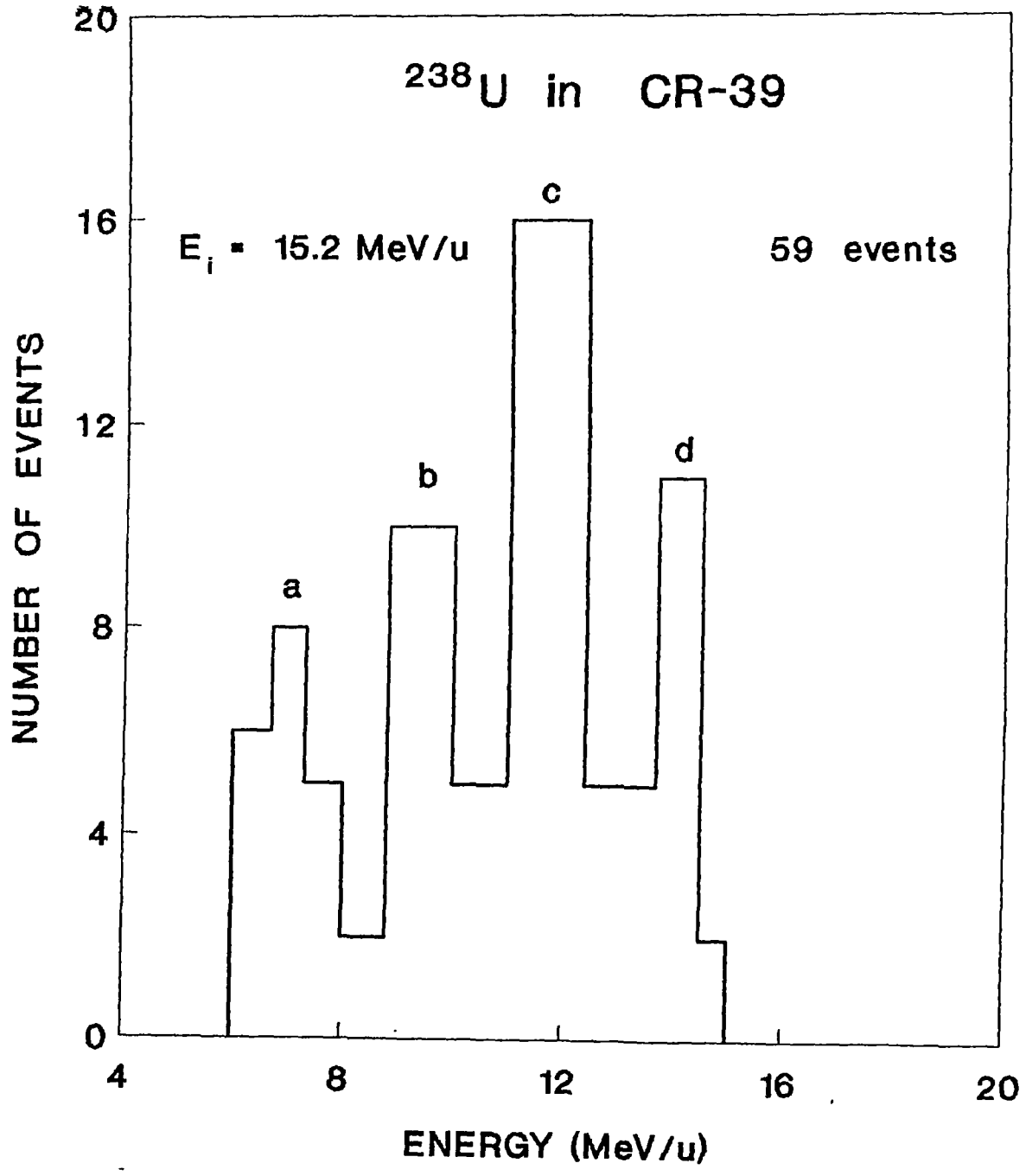

Fig. IV.2 Plot of number of events at different pre-fission energy for 15.2 MeV/u ^{238}U in CR-39. Resonance peaks at a) 7.0 MeV/u; b) 9.4 MeV/u; c) 11.8 MeV/u; d) 14.2 MeV/u are shown.

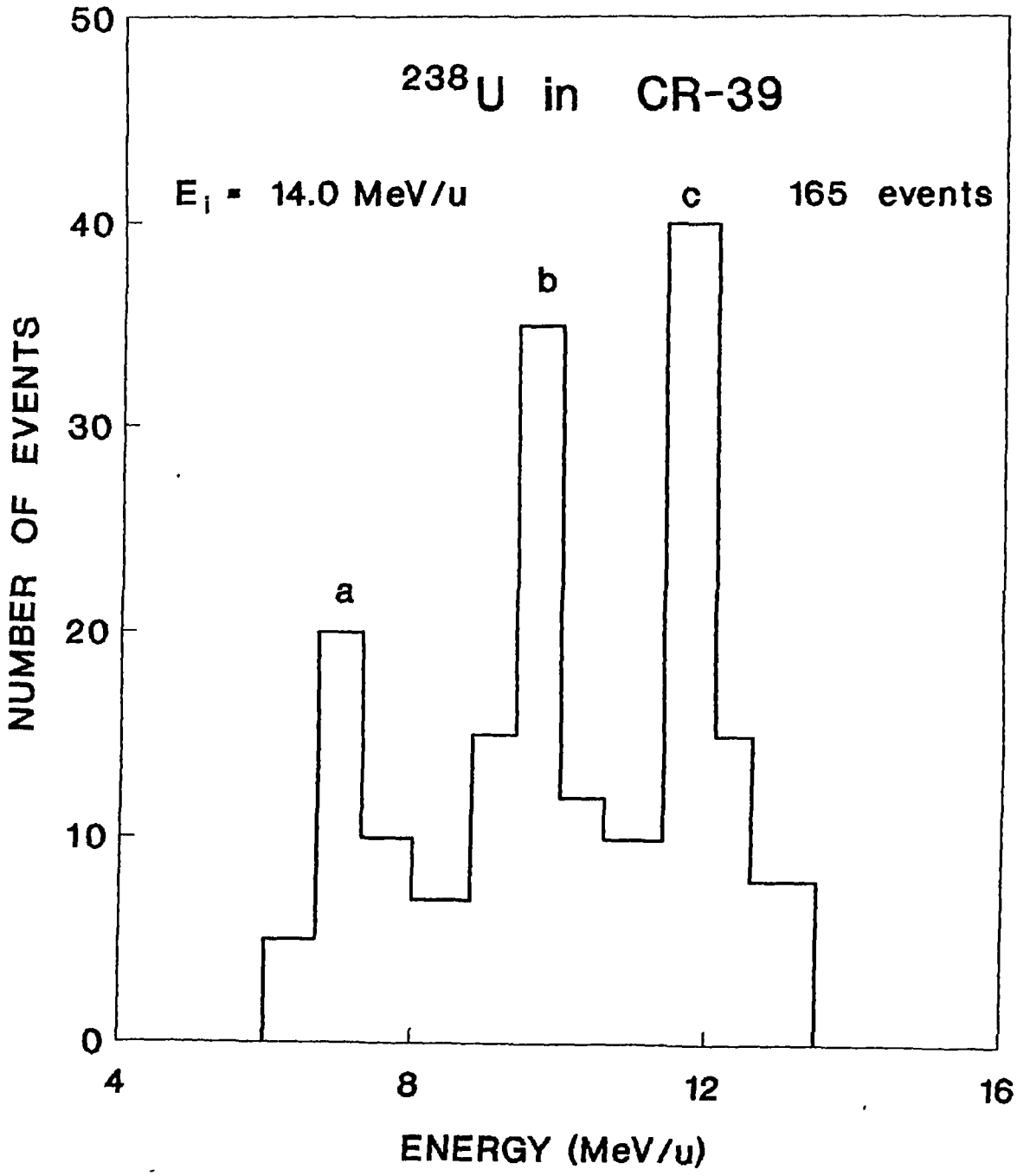

Fig. IV.3 Plot of number of events at different pre-fission energy for 14.0 MeV/u ^{238}U in CR-39. a) 7.0 MeV/u; b) 9.4 MeV/u; c) 11.8 MeV/u are the positions of the resonance peaks.

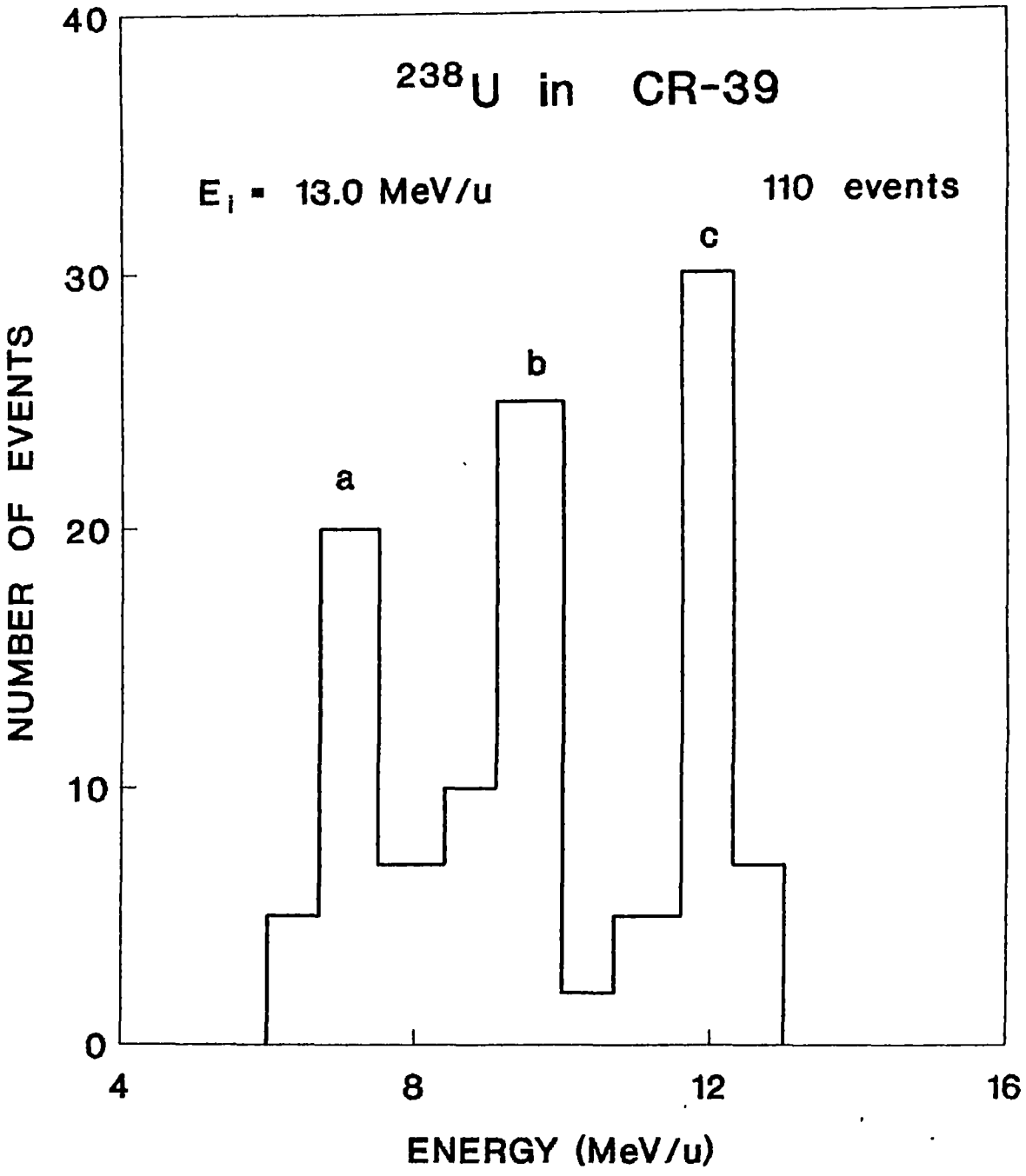

Fig. IV.4 Plot of number of events at different pre-fission energy for 13.0 MeV/u ^{238}U in CR-39. Resonance peaks are observed at a) 7.0 MeV/u; b) 9.4 MeV/u; c) 11.8 MeV/u.

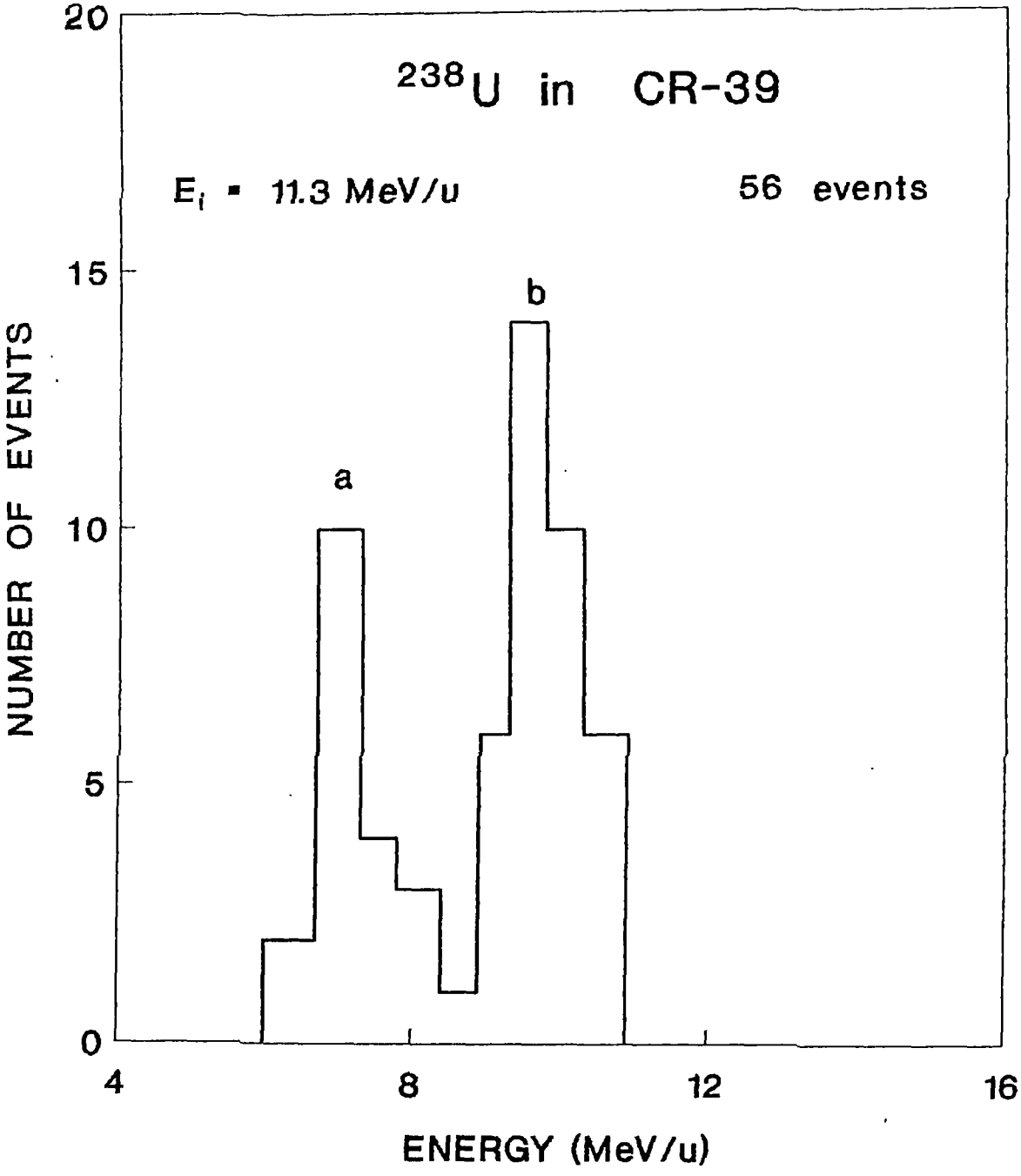

Fig. IV.5 Plot of number of events at different pre-fission energy for 11.3 *MeV/u* ^{238}U *in CR-39. Two resonance peaks shown are at a)* 7.0 MeV/u; b) 9.4 MeV/u.

Table IV.2

DIFFERENTIAL CROSS-SECTIONS CORRESPONDING TO RESONANCE PEAKS FOR ^{238}U IN CR-39

INITIAL ENERGY (MeV/u)	E^{*}_{pf} (MeV/u)	No. of Events**	Effective Thickness(μm)	CROSS-SECTION (mb)
16.4	7.0	60	20	147 ± 10
	9.4	108	19	278 ± 13
	11.8	173	18	471 ± 15
	14.2	61	20	129 ± 10
15.2	7.0	12	20	138 ± 10
	9.4	16	20	186 ± 15
	11.8	21	15	324 ± 20
	14.2	10	25	93 ± 10
14.0	7.0	35	20	135 ± 10
	9.4	50	17	227 ± 15
	11.8	65	20	279 ± 20
13.0	7.0	25	12	131 ± 8
	9.4	37	20	193 ± 12
	11.8	42	20	220 ± 20
11.3	7.0	14	13	125 ± 10
	9.4	28	15	217 ± 20

* Pre-fission Energy

** Events corresponding to resonance peaks

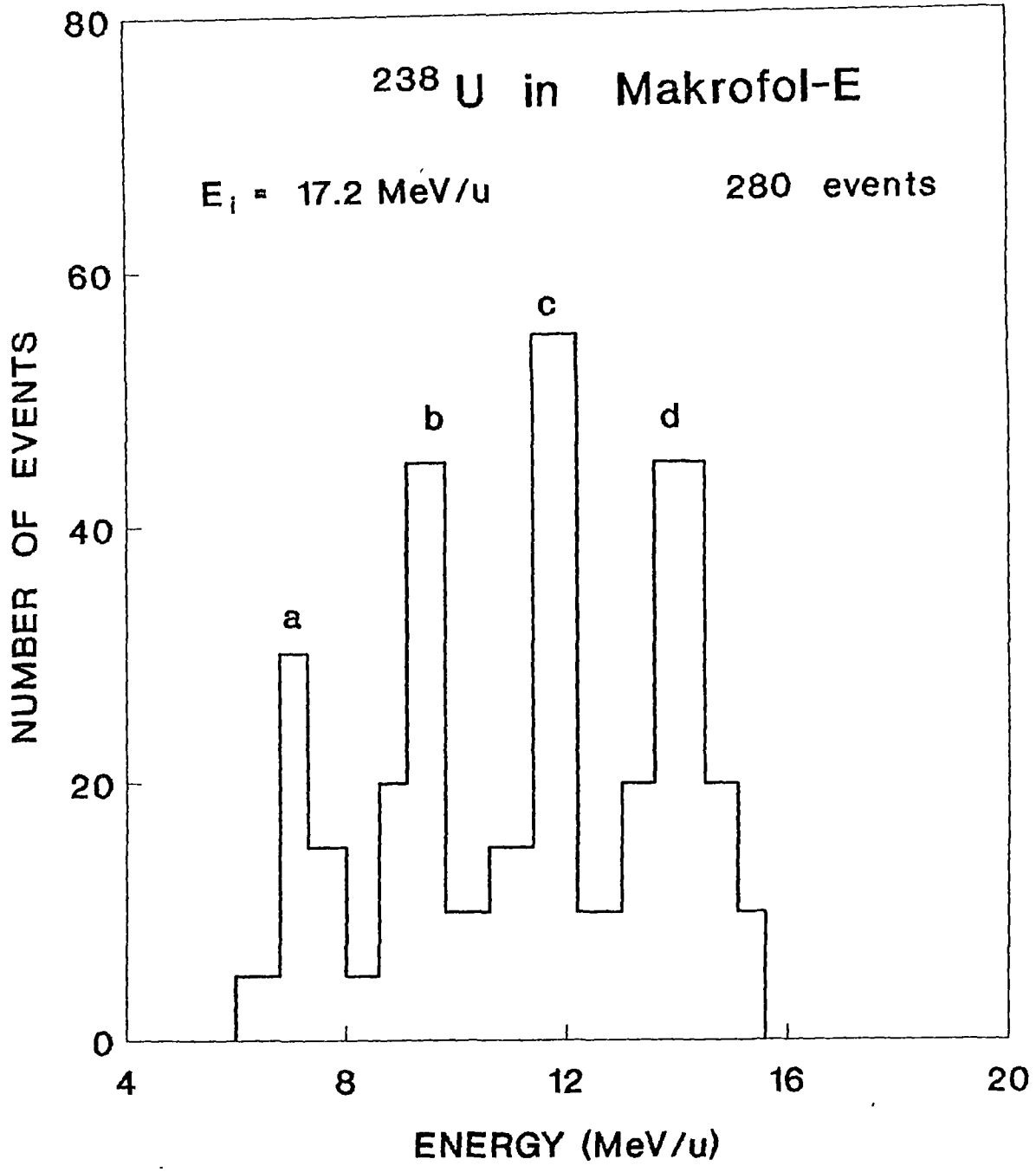

Fig. IV.6 Plot of number of events occurring at different pre-fission energies for 17.2 MeV/u ^{238}U in Makrofol-E. Resonance peaks observed at energies a) 7.0 MeV/u, b) 9.4 MeV/u, c) 11.8 MeV/u, d) 14.2 MeV/u.

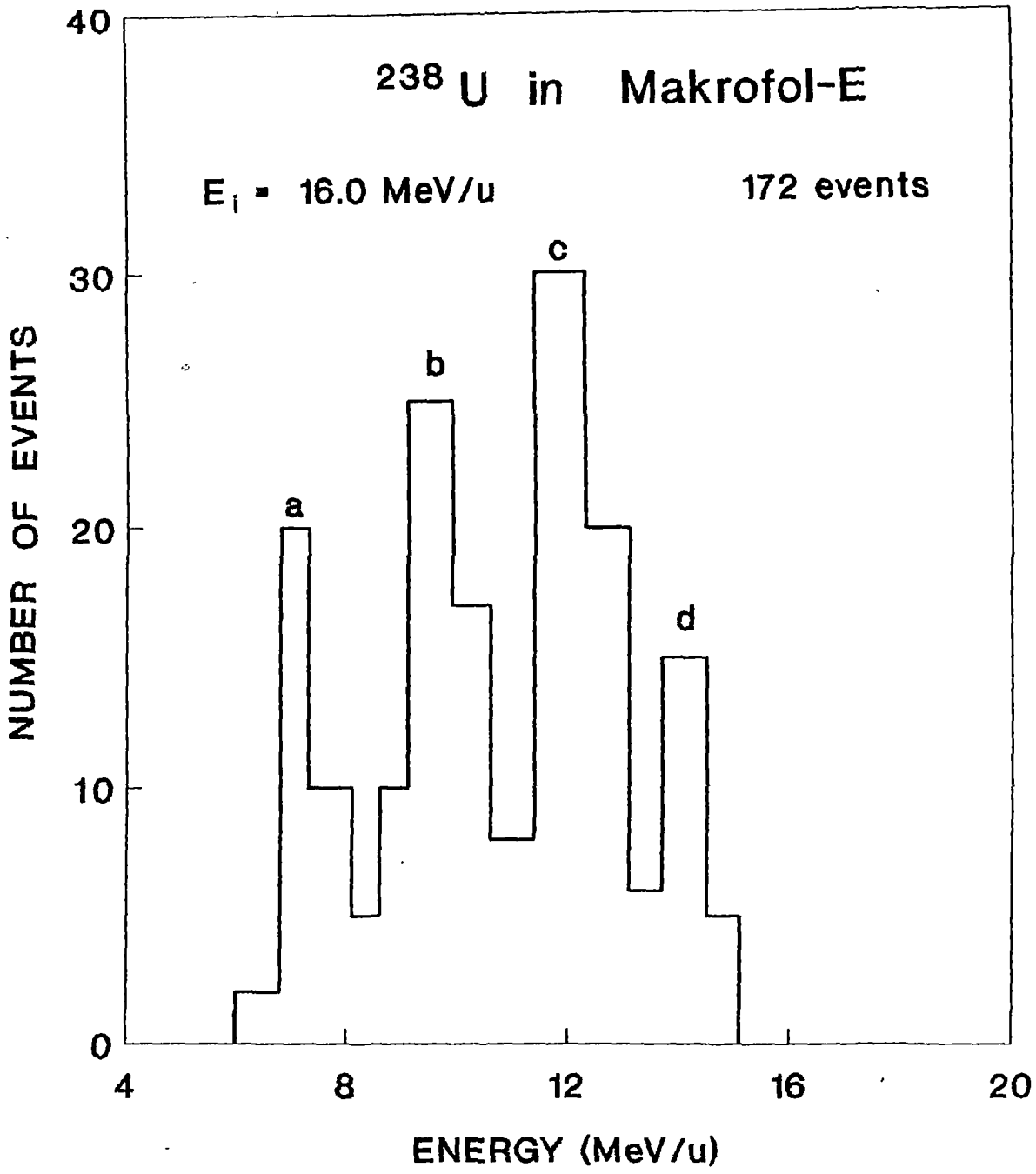

Fig. IV.7 Plot of number of events occurring at different pre-fission energies for 16.0 MeV/u ^{238}U in Makrofol-E. Resonance peaks observed at energies a) 7.0 MeV/u, b) 9.4 MeV/u, c) 11.8 MeV/u, d) 14.2 MeV/u.

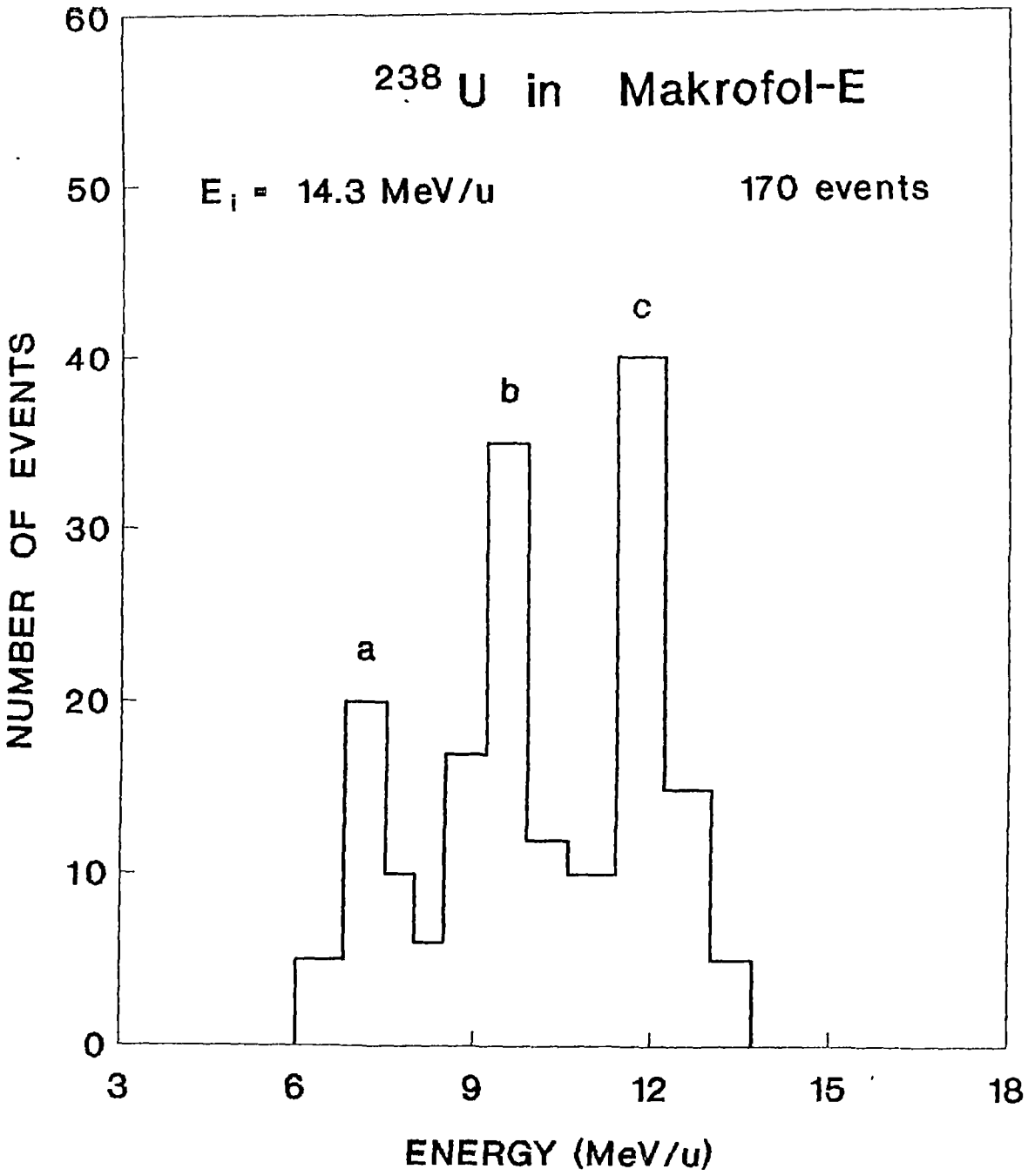

Fig. IV.8 Plot of number of events occurring at different pre-fission energies for 14.3 MeV/u ^{238}U in Makrofol-E. Resonance peaks observed at energies a) 7.0 MeV/u, b) 9.4 MeV/u, c) 11.8 MeV/u.

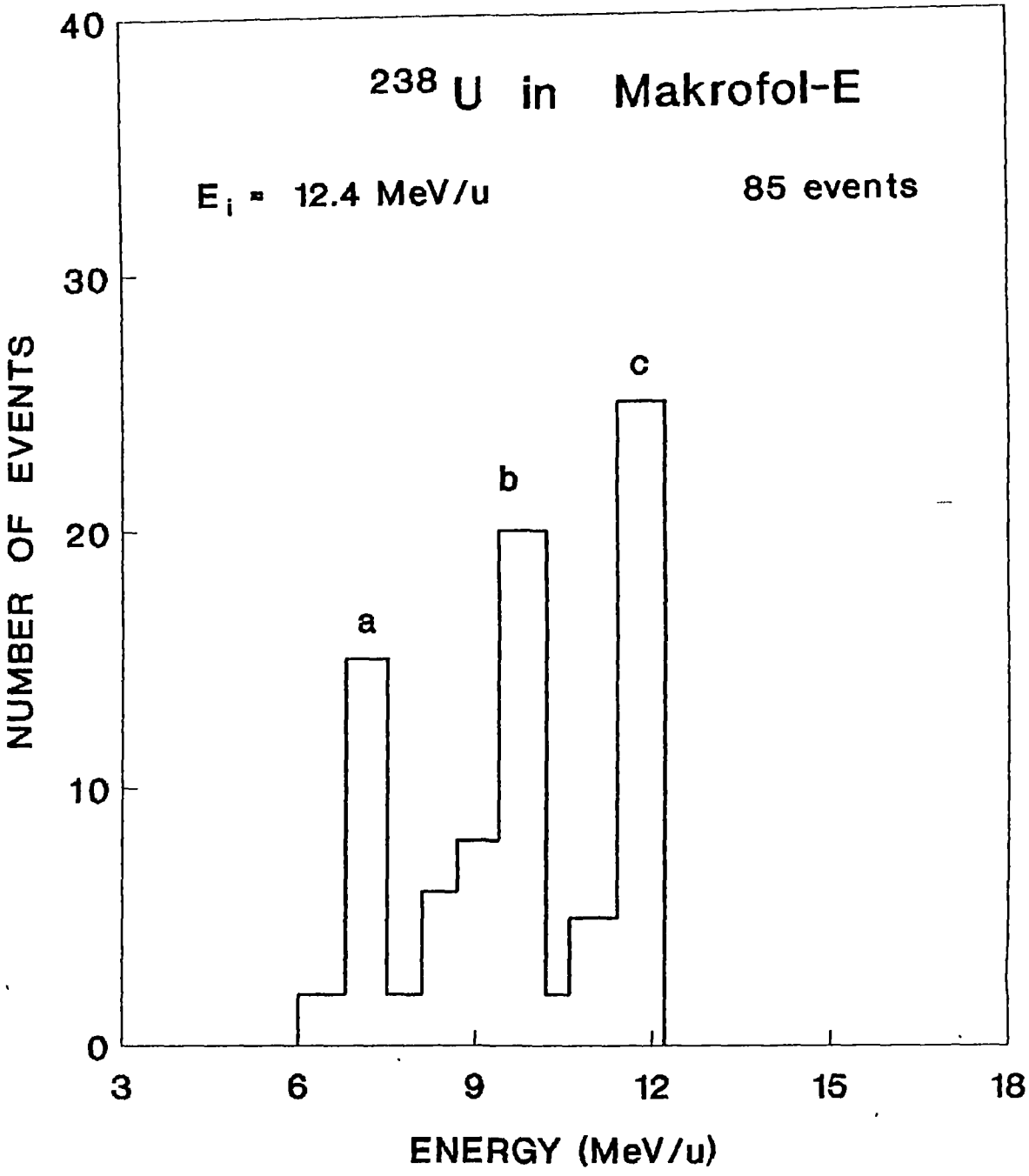

Fig. IV.9 Plot of number of events occurring at different pre-fission energies for 12.4 MeV/u ^{238}U in Makrofol-E. Resonance peaks observed at energies a) 7.0 MeV/u, b) 9.4 MeV/u, c) 11.8 MeV/u.

Table IV.3

DIFFERENTIAL CROSS-SECTIONS CORRESPONDING TO RESONANCE PEAKS FOR ^{238}U IN MAKROFOL-E

INITIAL ENERGY (MeV/u)	E^{*}_{pf}(MeV/u)	No. of Events**	Effective Thickness (μm)	CROSS-SECTION (mb)
17.2	7.0	40	13	172 ± 15
	9.4	65	21	194 ± 13
	11.8	80	22	203 ± 20
	14.2	37	21	102 ± 10
16.0	7.0	20	13	128 ± 10
	9.4	35	15	173 ± 13
	11.8	46	21	183 ± 15
	14.2	25	27	97 ± 10
14.3	7.0	25	13	118 ± 10
	9.4	60	21	170 ± 13
	11.8	65	21	195 ± 15
12.4	7.0	16	12	124 ± 10
	9.4	25	15	158 ± 15
	11.8	32	17	202 ± 20

* Pre-fission Energy

** Events corresponding to resonance peaks

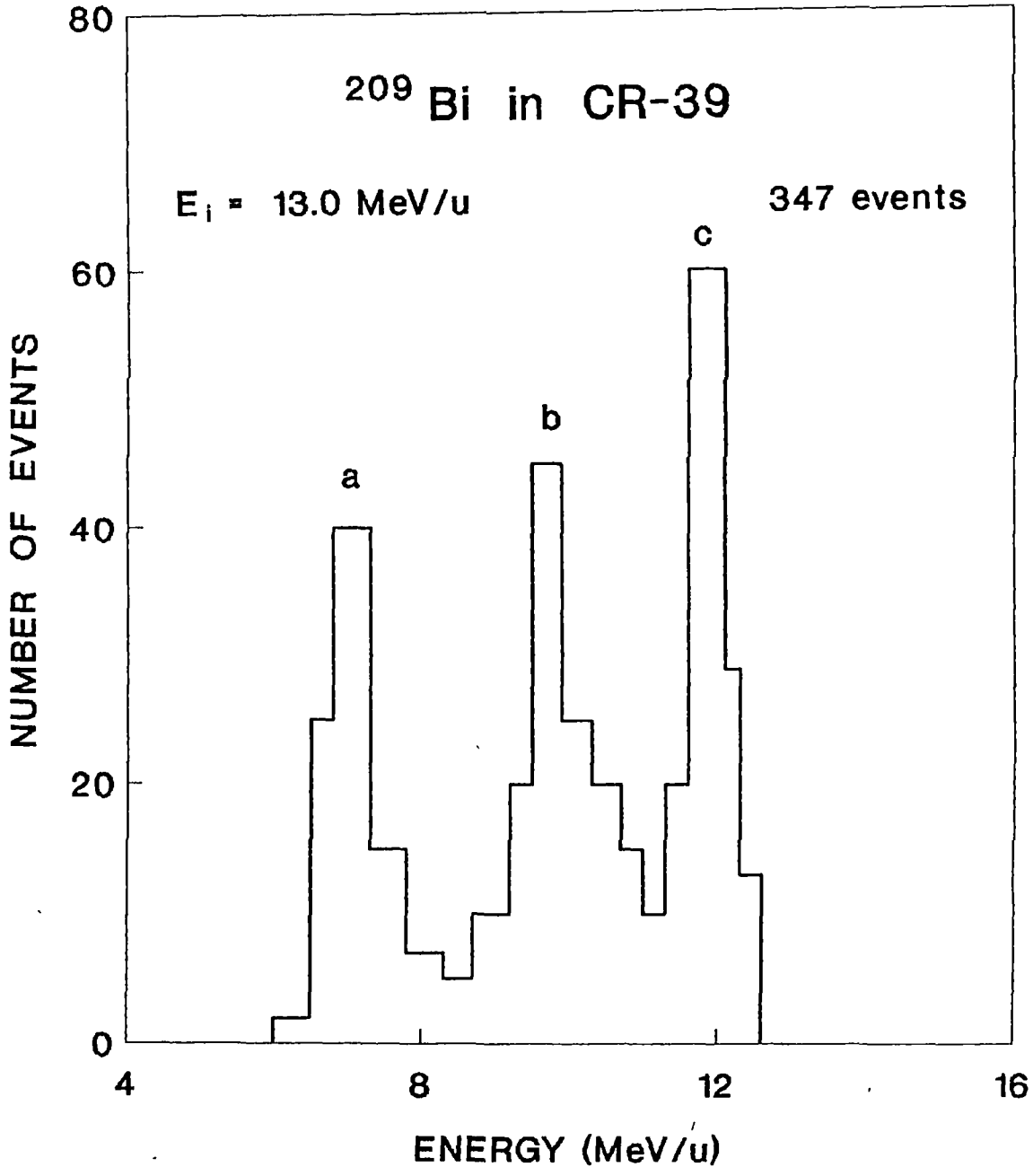

Fig. IV.10 Plot of number of events occurring at different pre-fission energies for 13.0 MeV/u ^{209}Bi in CR-39.

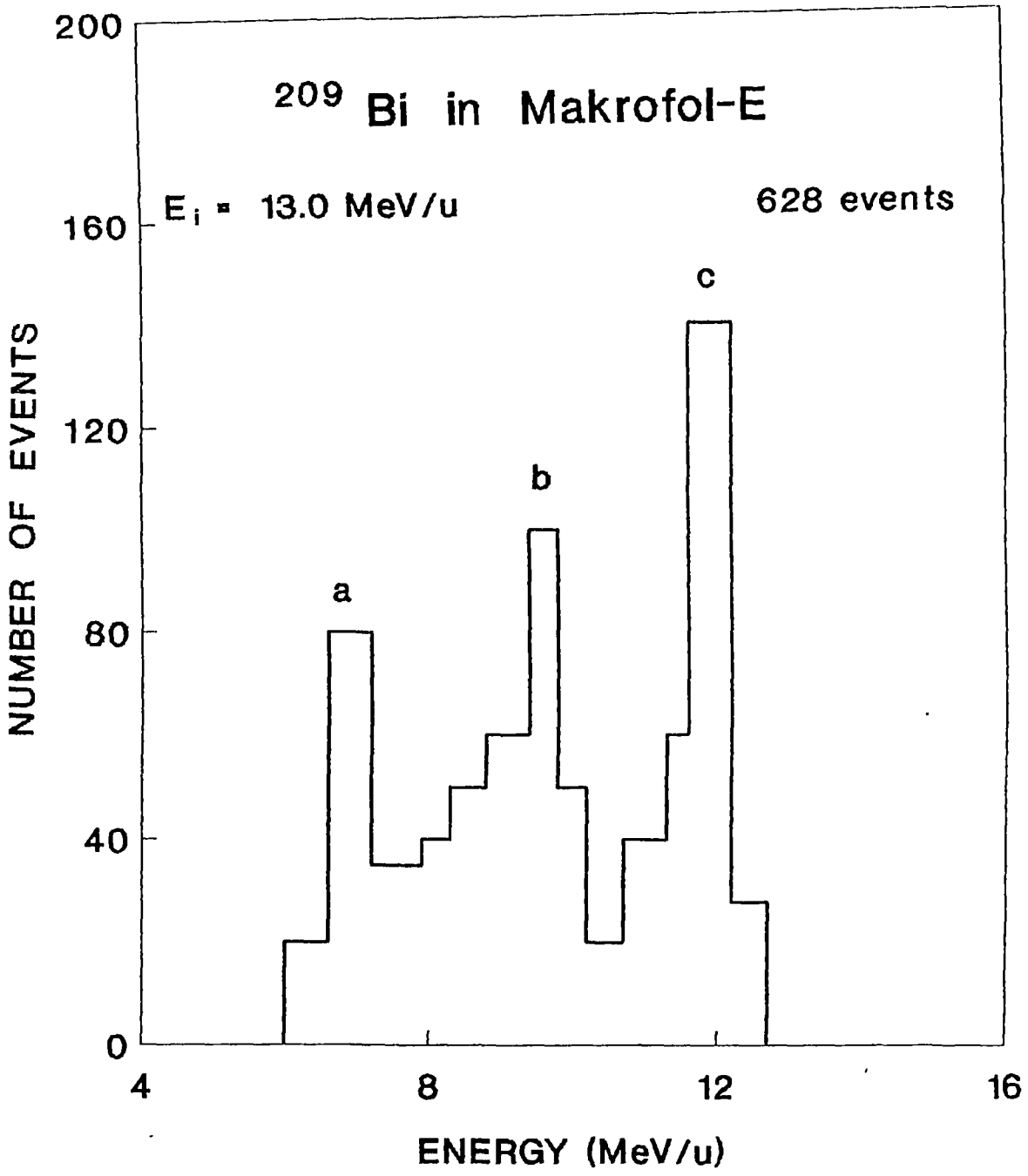

Fig. IV.11 Plot of number of events occurring at different pre-fission energies for 13.0 MeV/u ^{209}Bi in Makrofol-E.

Table IV.4

DIFFERENTIAL CROSS-SECTIONS CORRESPONDING TO RESONANCE PEAKS FOR ^{209}Bi OF 13.0 MeV/u

DETECTOR	E^{*}_{pf}(MeV/u)	No. of Events**	Effective Thickness(μm)	CROSS-SECTION (mb)
CR-39	7.0	80	11.8	164 ± 12
	9.4	100	10	216 ± 13
	11.8	109	10	236 ± 15
Makrofol-E	7.0	105	12	150 ± 10
	9.4	210	14	182 ± 13
	11.8	265	17	220 ± 18

* Pre-fission Energy

** Events corresponding to resonance peaks

The values of differential cross-sections corresponding to the pre-fission energies at 11.8 MeV/u were found to be the maximum for ^{238}U in CR-39 and Makrofol-E. This is very much expected as the number of events observed at this pre-fission energy is maximum. Similarly for ^{209}Bi in CR-39 and Makrofol-E the differential cross-section corresponding to pre-fission energy 11.8 MeV/u is the highest. Further it may be noted that the fusion barrier of projectiles (^{209}Bi and ^{238}U) with H is just surmounted at around 12 MeV. This is the reason for sudden increase in the number of events at 11.8 MeV/u as shown in **Fig. IV.1 to Fig. IV.11** except in **Fig. IV.5**, where the projectile energy is less than 11.8 Mev/u.

The total cross-section for the occurence of these events in the mentioned systems have been determined and are tabulated in **Tables IV.5 - IV.7**. Excitation function plots (total cross-section as a function of energy) for ^{238}U in CR-39 and Makrofol-E have been generated and are in **Fig. IV.12 and Fig. IV.13** respectively. It is apparent from these two plots that total cross-section increases with increase in the energy of the projectile. This leads to the conclusion that inelastic scattering as a cause for the occurence of the events can be ruled out, as the coulomb barrier for O, C and H are gradually surmounted with increase in projectile energy from 6 MeV onwards. Hence fusion-fission should be responsible for creating the fork like events.

IV.3 TOTAL MASS OF FRAGMENTS

The program 'HIFISS' searches the masses of the fragments in the two different exit channels for each event by conserving momentum as explained in chapter II. The values of total mass were found to be randomly distributed in each case. Hence the values in each case were fitted to a gaussian distribution as shown in **Figs. IV.14 to IV.17**. From these kind of distributions the most probable values of total mass were determined corresponding to the

Table IV.5

TOTAL CROSS-SECTIONS FOR ^{238}U IN CR-39 AT DIFFERENT ENERGIES

ENERGY (MeV/u)	TOTAL NO. OF EVENTS*	EFFECTIVE THICKNESS (μm)	CROSS-SECTION (mb)
16.4	520	117 ± 2.0	212 ± 10
15.2	59	104 ± 1.5	183 ± 10
14.0	165	90 ± 1.5	144 ± 10
13.0	110	77 ± 1.5	109 ± 7
11.3	56	60 ± 1.5	71 ± 5

* Number of events which passed through the analysing program 'HIFISS'

Table IV.6

TOTAL CROSS-SECTIONS FOR ^{238}U IN MAKROFOL-E AT DIFFERENT ENERGIES

ENERGY (MeV/u)	TOTAL NO. OF EVENTS*	EFFECTIVE THICKNESS (μm)	CROSS-SECTION (mb)
17.2	280	151 ± 2.0	208 ± 10
16.0	172	130 ± 1.5	170 ± 10
14.3	170	120 ± 1.5	115 ± 8
12.4	64	101 ± 1.0	92 ± 8

*Number of events passed through the analysing program 'HIFISS'

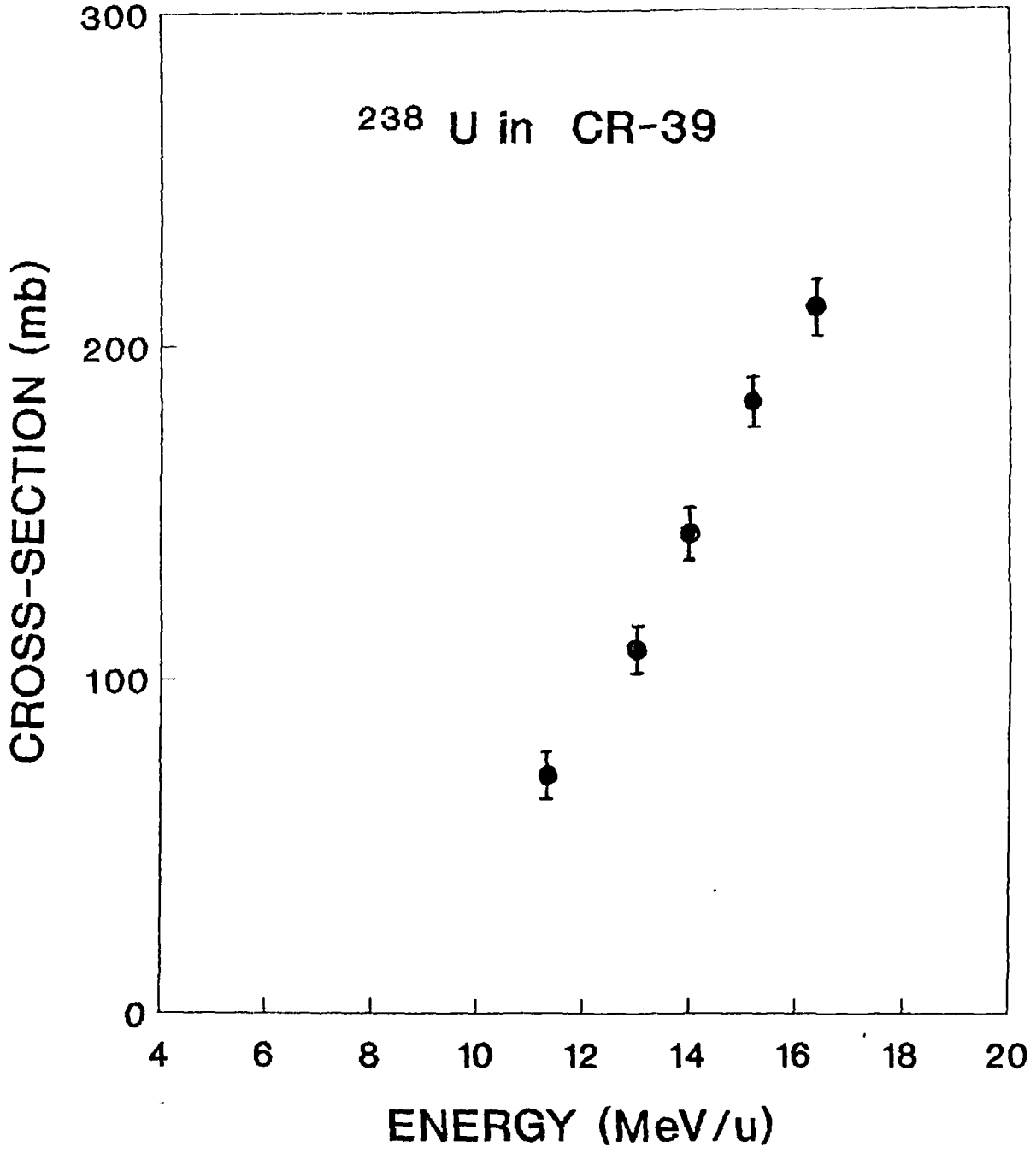

Fig. IV.12 Excitation function plot for ^{238}U in CR-39.

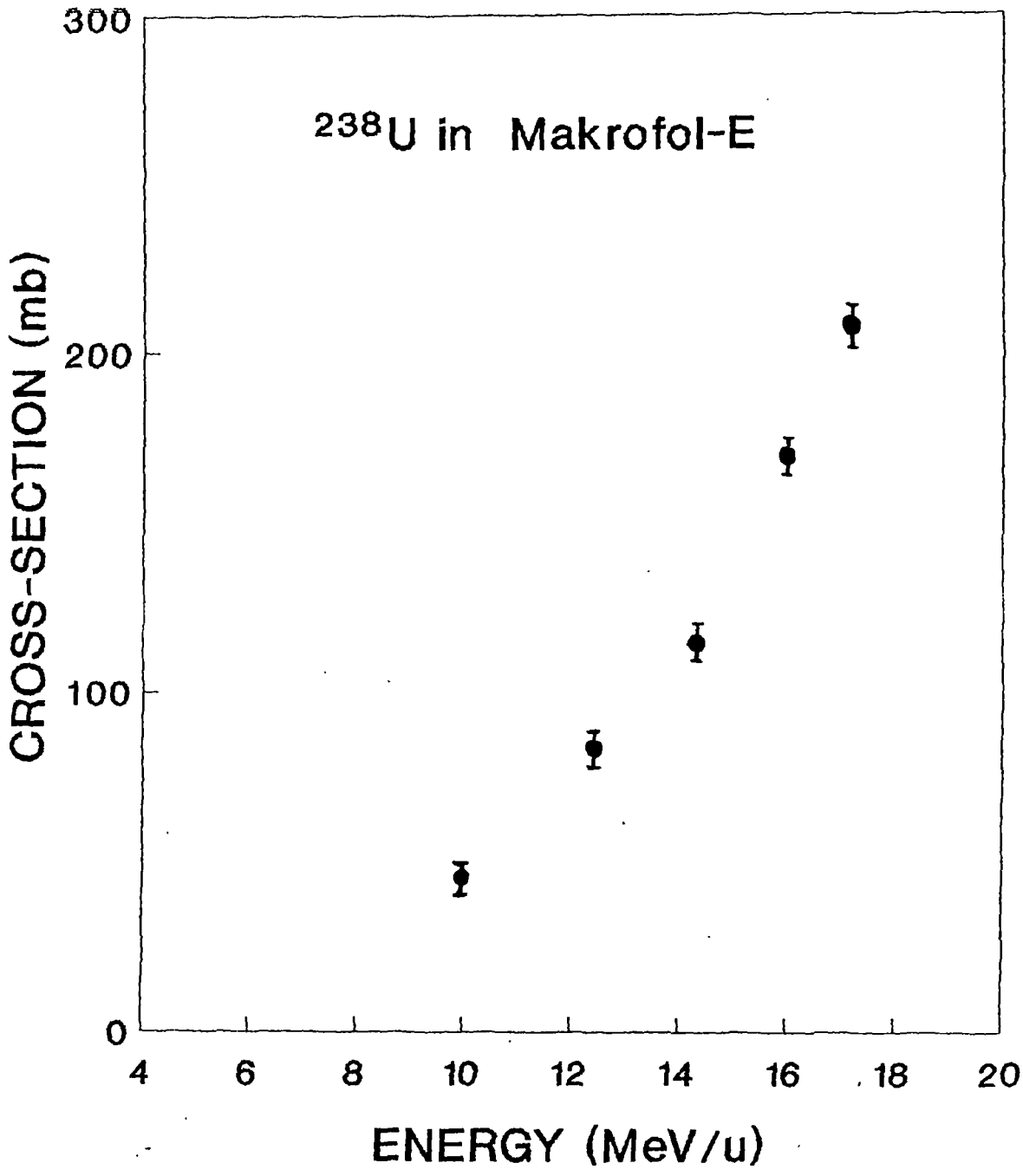

Fig. IV.13 Excitation function plot for ^{238}U in Makrofol-E

Table IV.7

TOTAL CROSS-SECTIONS FOR ^{209}Bi AT 13.0 MeV/u IN CR-39 AND MAKROFOL-E

DETECTOR	TOTAL NO. OF EVENTS*	EFFECTIVE THICKNESS (μm)	CROSS-SECTION (mb)
CR-39	347	80 ± 1.5	99 ± 5
MAKROFOL-E	628	94 ± 1.2	87 ± 5

* Number of Events passed through the analysing program 'HIFISS'

peak positions. **Table IV.8** contains the most probable values of total mass of fragments for ^{238}U in CR-39 at different energies along with the standard deviations. Most probable mass values for ^{238}U in Makrofol-E are in **Table IV.8. Table IV.9** contains similar data for 13.0 MeV/u ^{209}Bi in CR-39 and Makrofol-E.

Most probable values of total mass for ^{238}U in CR-39 and Makrofol-E are found to be about 250 amu with standard deviations ranging from 8 - 12 amu. This clearly indicates that the projectile has undergone fusion with the nuclei of the atoms H, C and O present in the detector matrix. Similarly for ^{209}Bi the most probable value for total mass is 222 amu with standard deviation of about 8 amu. This observation further supports our earlier conclusion. Though the individual peaks for the compound systems ($^{238}U + {}^{1}H$, $^{238}U + {}^{12}C$, $^{238}U + {}^{16}O$, $^{209}Bi + {}^{1}H$, $^{209}Bi + {}^{12}C$, $^{209}Bi + {}^{16}O$) are not possible to be resolved but a cumulative effect may be observed by the use of SSNTDs for studying nuclear reactions.

IV.4 THE Q-VALUES OF THE NUCLEAR REACTIONS

The Q-Values determined for these events are helpful in assigning the phenomenon for the occurence of these events. The Q-Value according to Viola systematics for binary fragmentation due to the random neck scission of the projectile or the compound systems generated in these events have already been tabulated in **Table II.2** . As described in chapter II the Q-Value in each case were computed by the analysing program 'HIFISS'. The values were found to be randomly distributed and hence were fitting well to a gaussian distribution generated by the application program 'TRADIS' **[39]** . **Figs. IV.18 - IV.21** are such plots for different projectile detector systems.

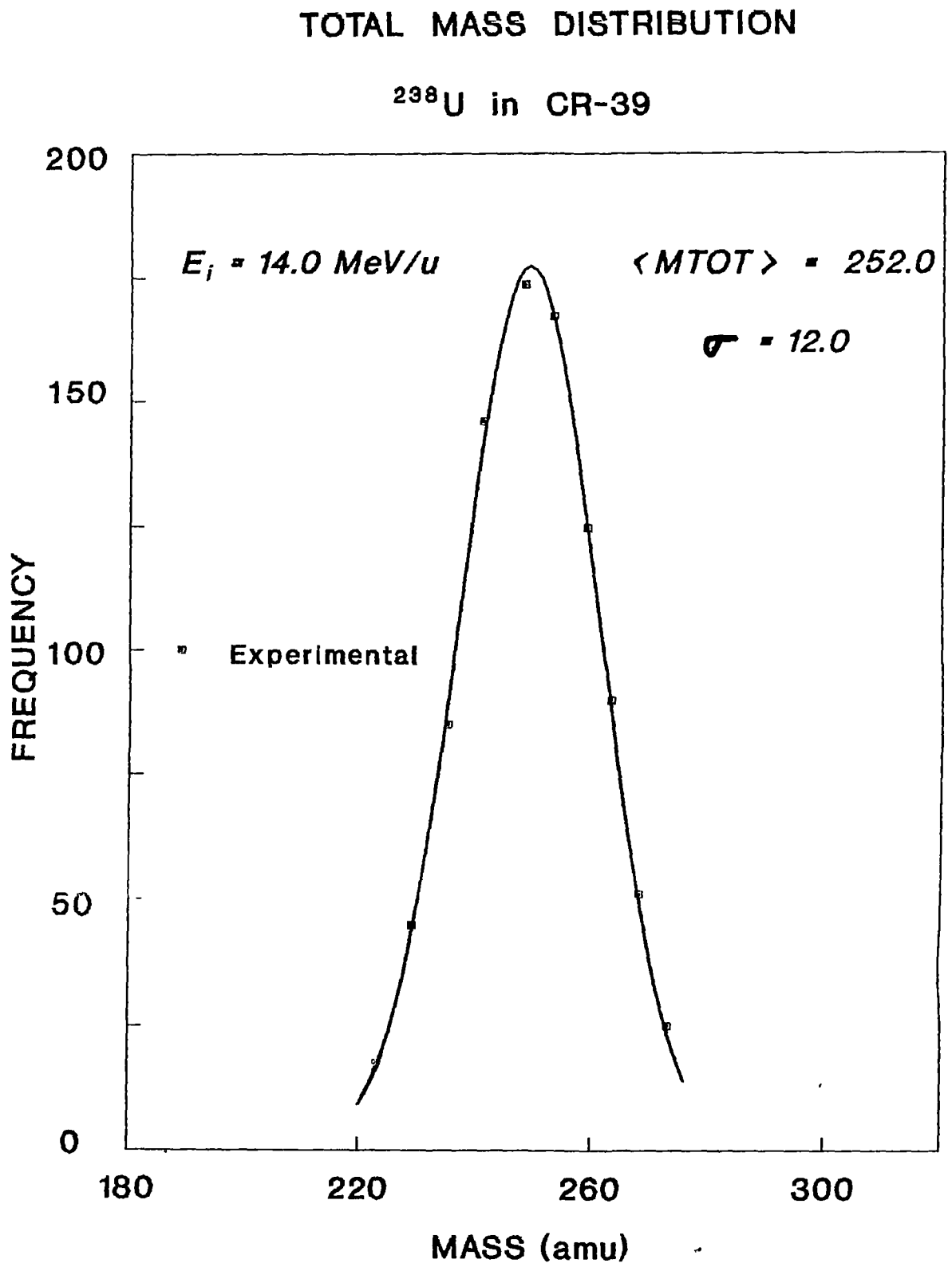

Fig. IV.14 Total mass of fragments distribution for 14.0 MeV/u ^{238}U in CR-39.

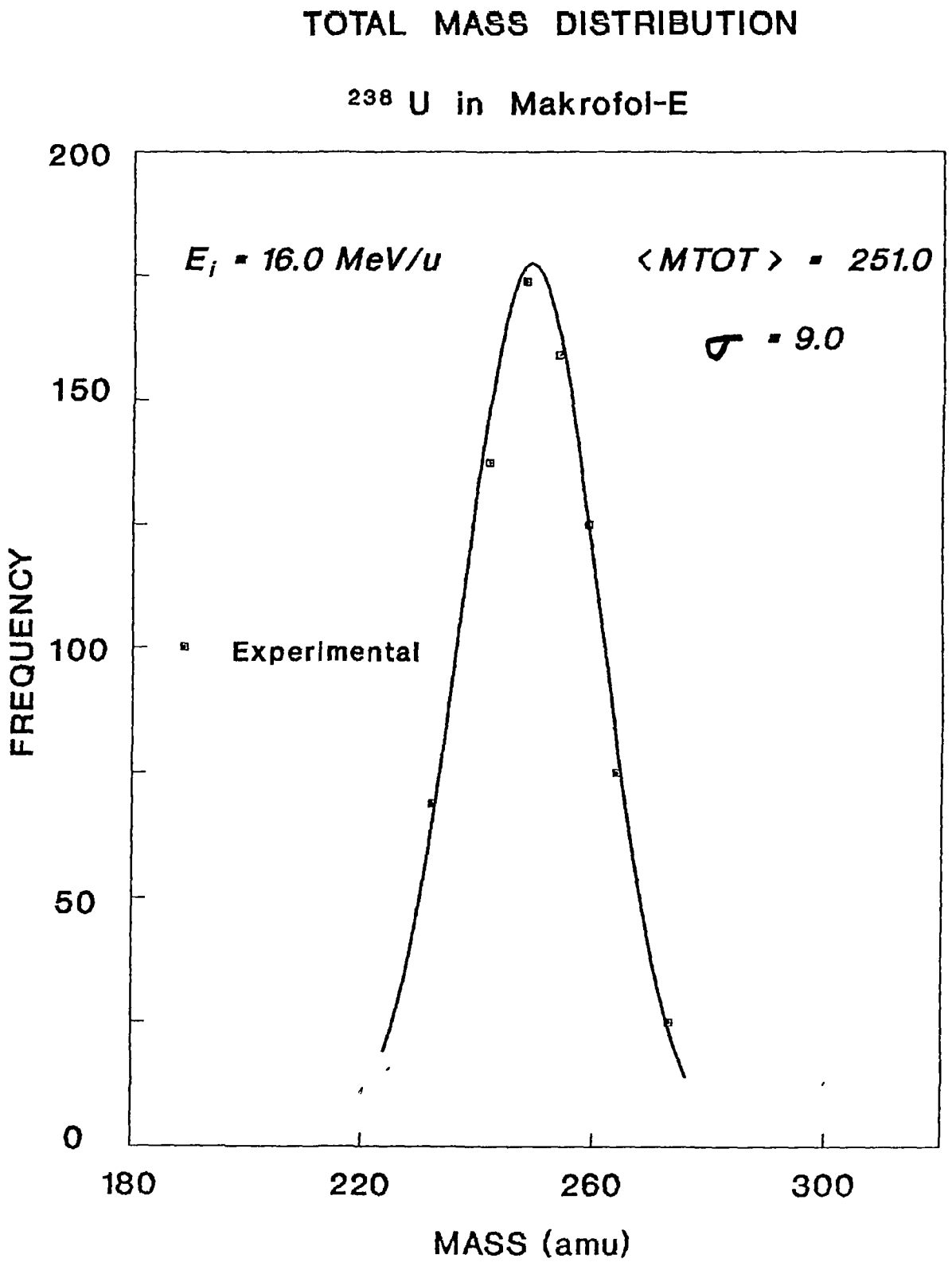

Fig.IV.15 Total mass of fragments distribution for 16.0 MeV/u ^{238}U in CR - 39.

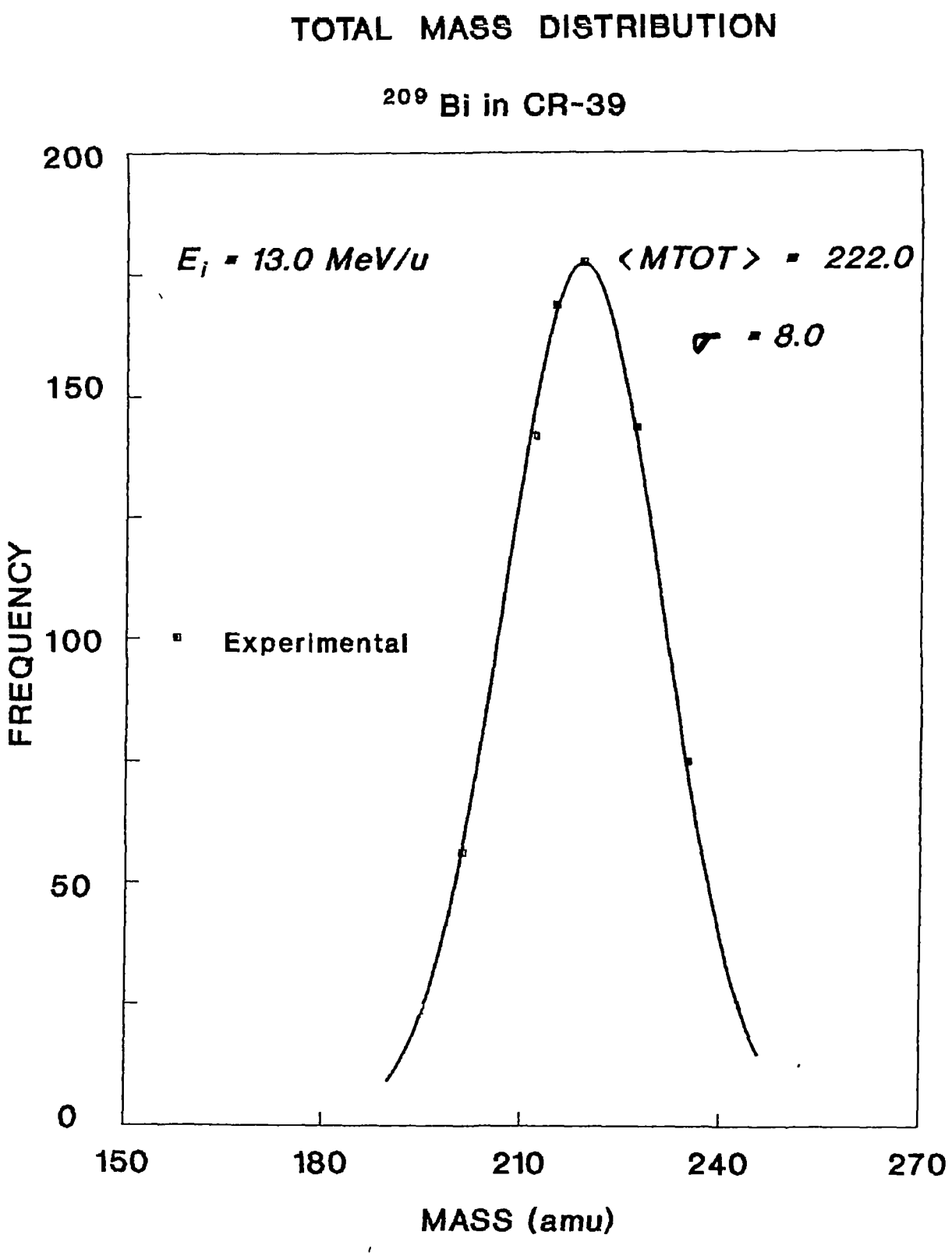

Fig. IV.16 Total mass of fragments distribution for 13.0 MeV/u ^{209}Bi in CR-39.

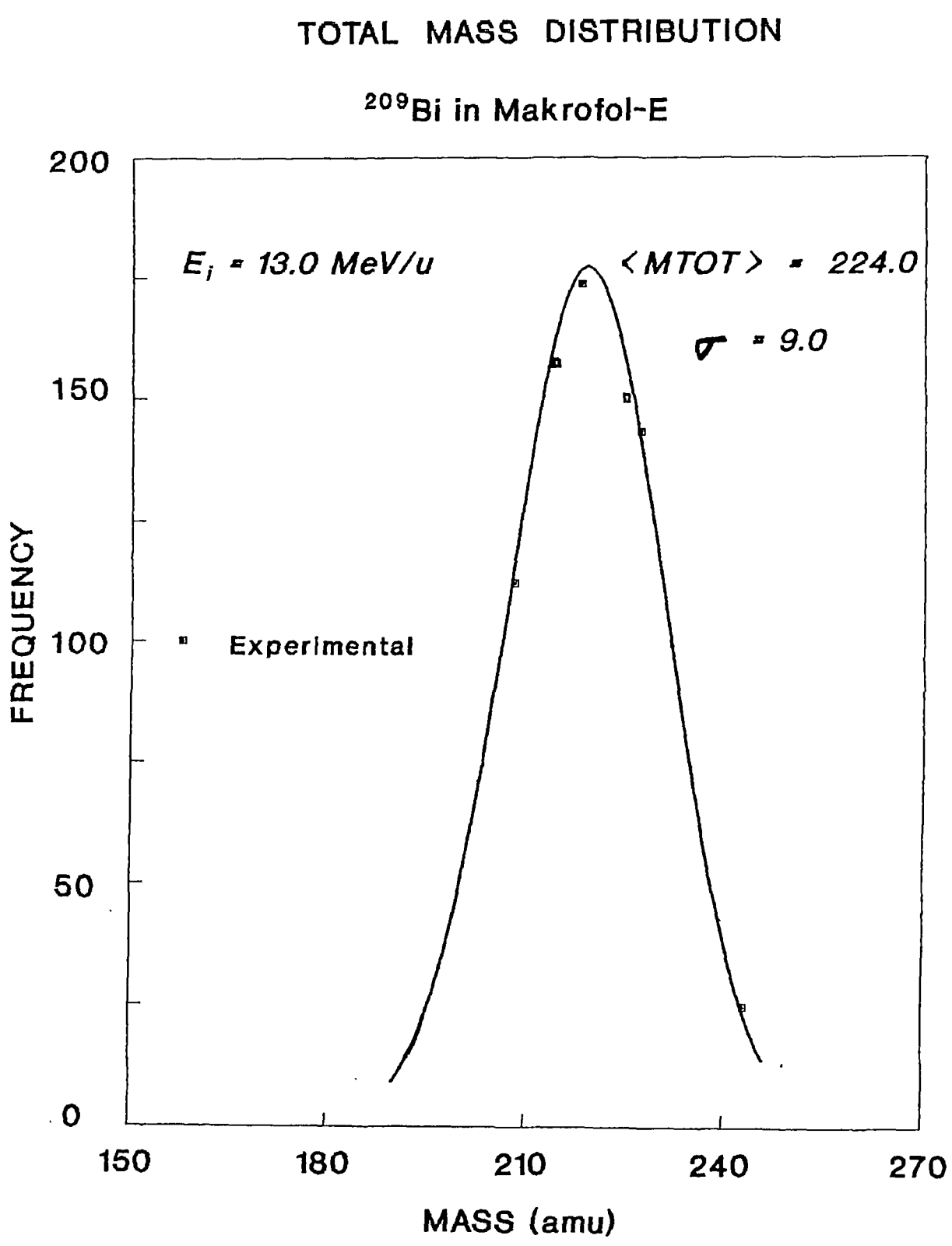

Fig. IV.17 Total mass of fragments distribution for 13.0 MeV/u ^{209}Bi in Makrofol-E.

Table IV.8

MOST PROBABLE VALUES OF TOTAL MASS OF FRAGMENTS FOR ^{238}U IN CR-39 AND MAKROFOL-E AT DIFFERENT ENERGIES

CR-39		MAKROFOL-E	
ENERGY (MeV/u)	MTOT*	ENERGY (MeV/u)	MTOT*
16.4	250 ± 10	17.2	249 ± 8
15.2	249 ± 9	16.0.	251 ± 9
14.0	252 ± 12	14.3	250 ± 10
13.0	250 ± 10	12.4	249 ± 11
11.3	250 ± 8		

* Corresponds to the most probable value.

Table IV.9

MOST PROBABLE VALUES OF TOTAL MASS OF FRAGMENTS FOR ^{209}Bi IN CR-39 AND MAKROFOL-E AT 13.0 MeV/u

CR-39		MAKROFOL-E	
ENERGY (MeV/u)	MTOT*	ENERGY (MeV/u)	MTOT*
13.0	225 ± 8	13.0	224 ± 9

* Corresponding to the most probable value

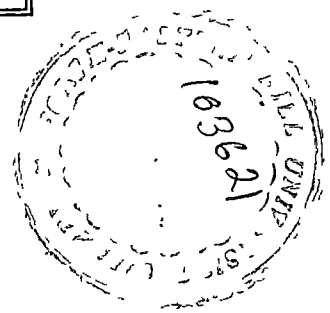

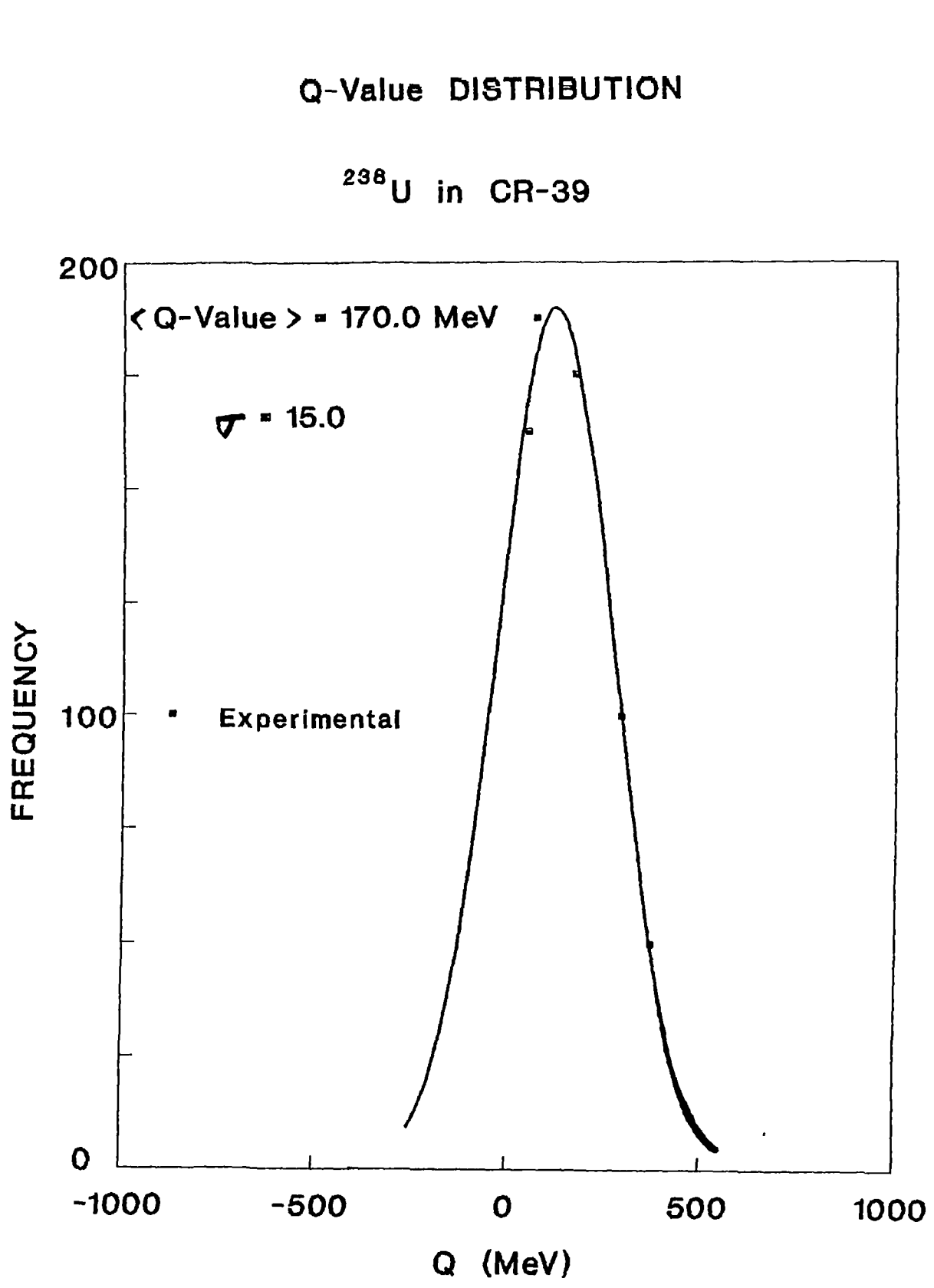

Fig. IV.18 Q-value distribution for 16.4 MeV/u ^{238}U in CR-39.

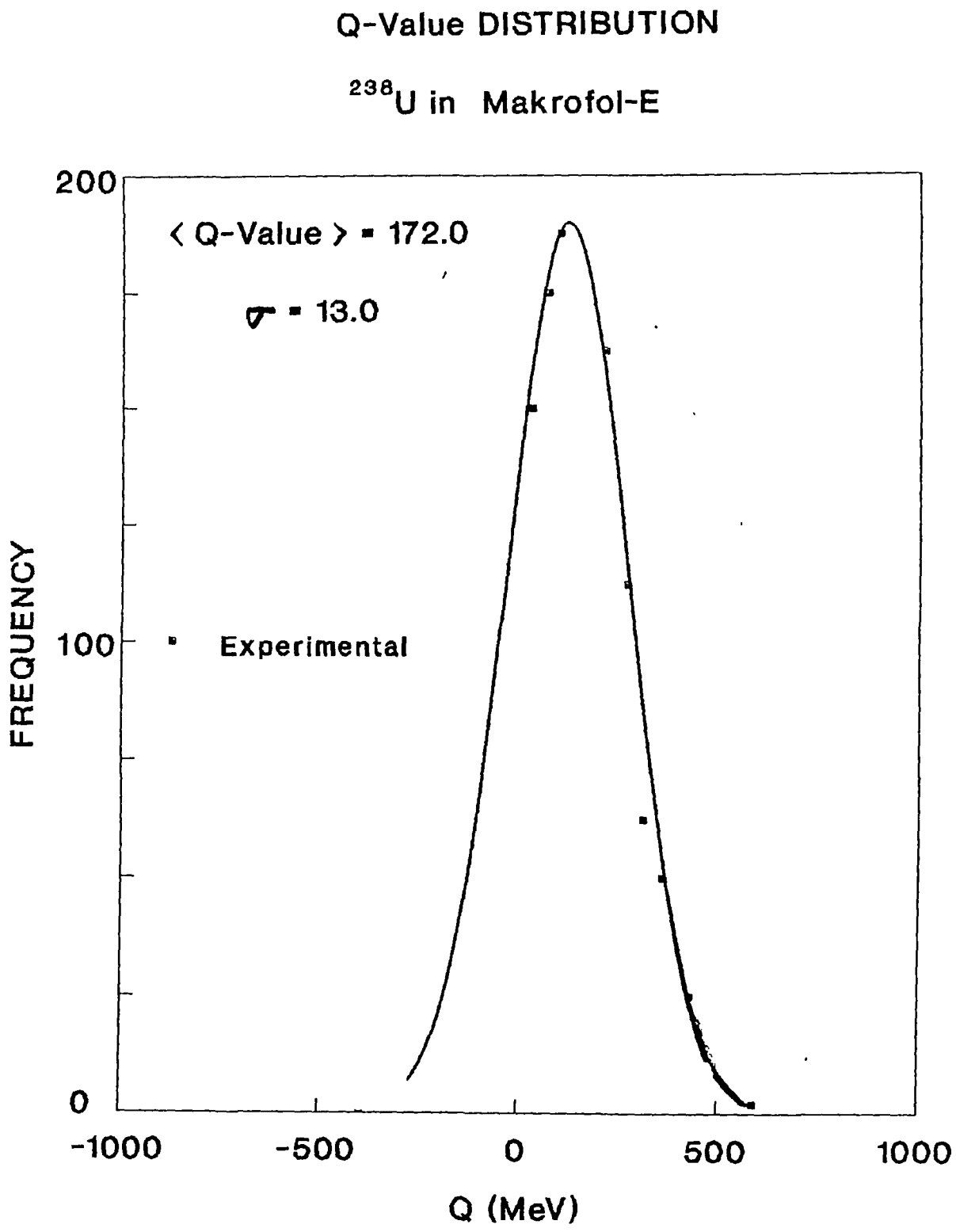

Fig. IV.19 Q-value distribution for 17.2 MeV/u ^{238}U in Makrofol-E

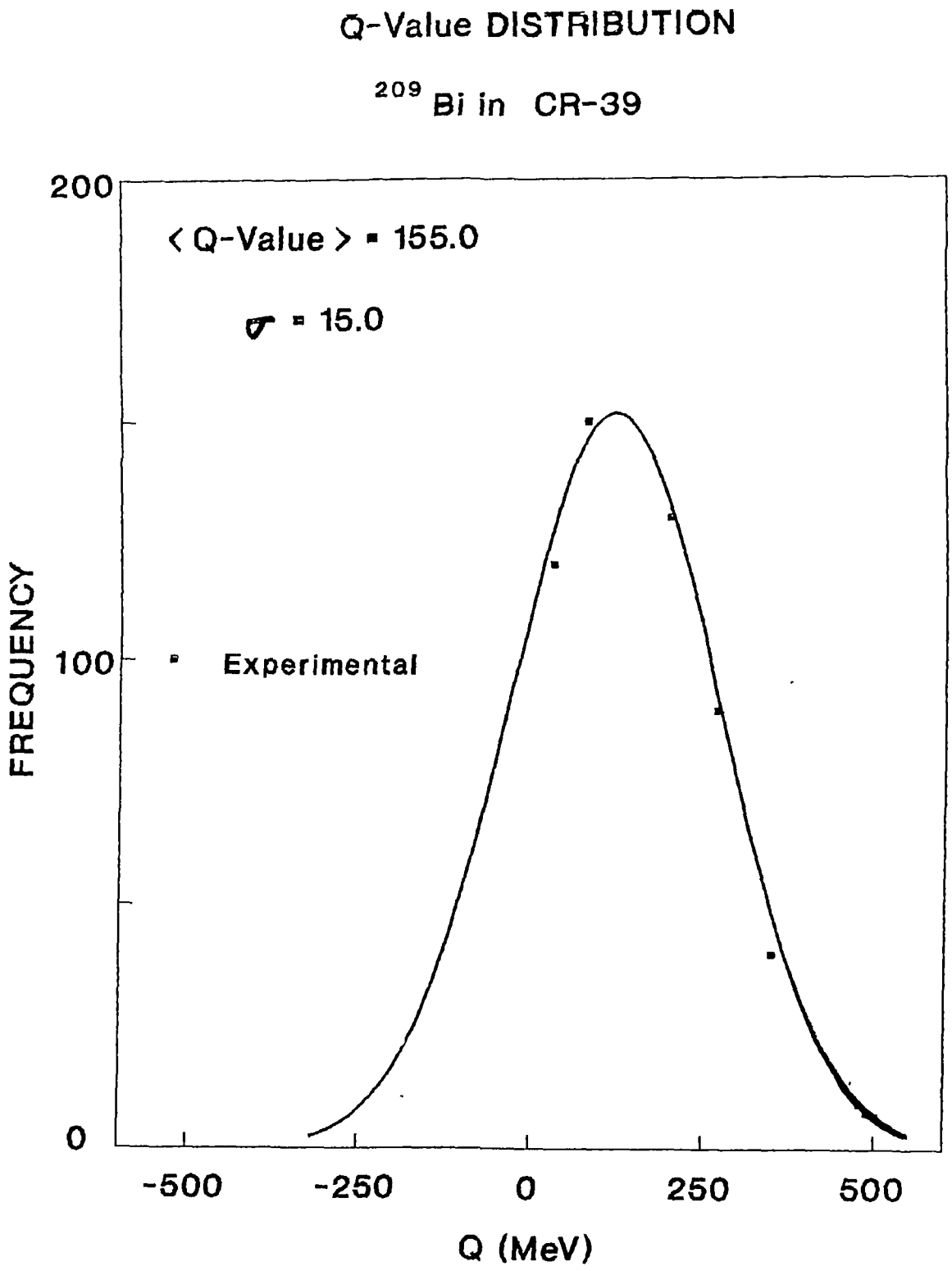

Fig. IV.20 Q-value distribution for 13.0 MeV/u ^{209}Bi in CR-39

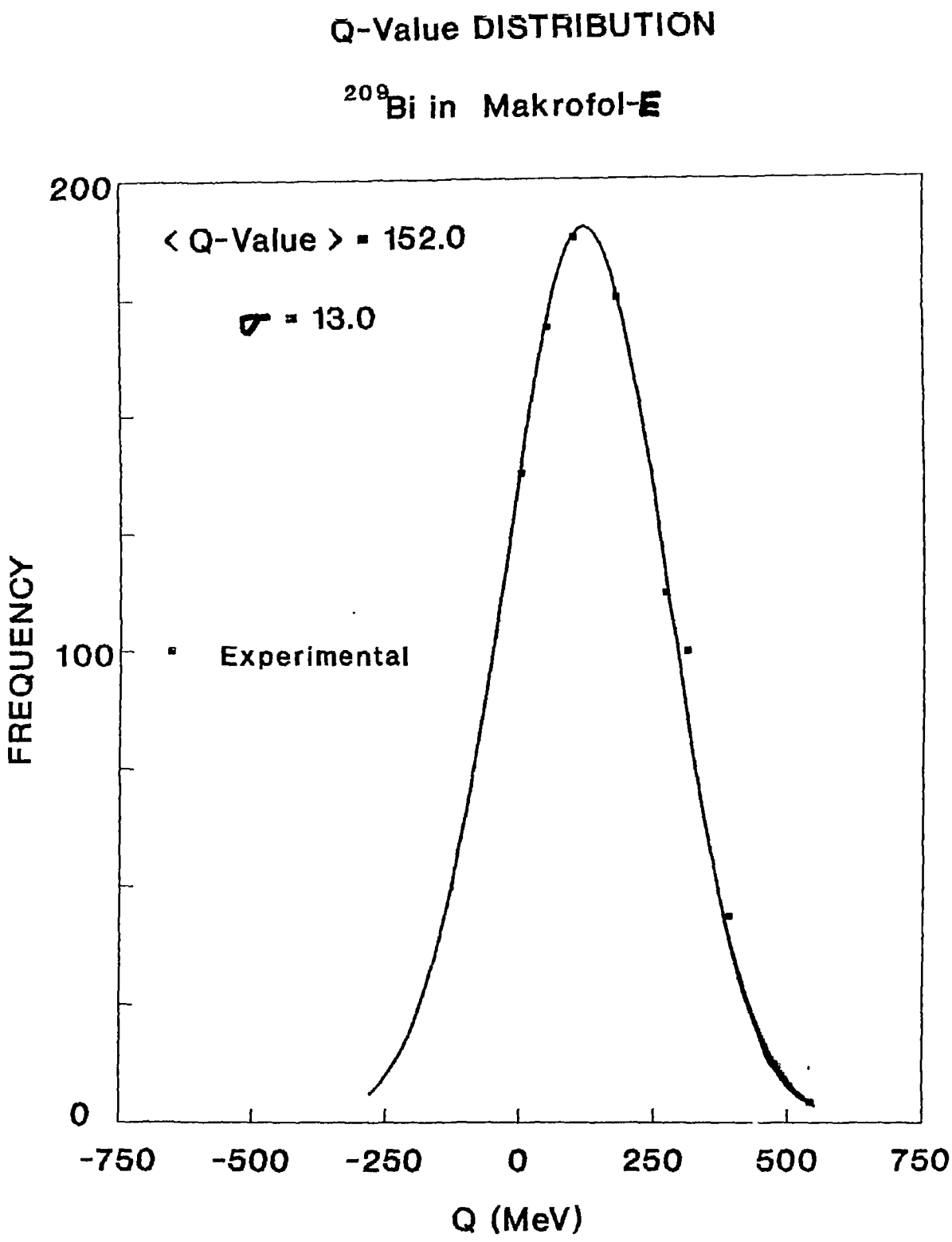

Fig. IV.21 Q-value distribution for 13.0 MeV/u ^{209}Bi in Makrofol-E

Table IV.10

MOST PROBABLE Q-VALUES FOR ^{238}U IN CR-39 AND MAKROFOL-E AT DIFFERENT ENERGIES

CR-39		MAKROFOL-E	
ENERGY (MeV/u)	Q-VALUE (MeV)	ENERGY (MeV/u)	Q-VALUE (MeV)
16.4	170 ± 15	17.2	172 ± 13
15.2	165 ± 10	16.0	182 ± 10
14.0	180 ± 15	14.3	170 ± 15
13.0	168 ± 20	12.4	168 ± 13
11.3	175 ± 15		

Table IV.11

MOST PROBABLE Q-VALUES FOR ^{209}Bi IN CR-39 AND MAKROFOL-E

CR-39		MAKROFOL-E	
ENERGY (MeV/u)	Q-VALUE (MeV)	ENERGY (MeV/u)	Q-VALUE (MeV)
13.0	155 ± 15	13.0	152 ± 13

From similar plots the most probable Q-Value in each case were found and tabulated in **Table IV.10 and Table IV.11**. The Q-Values for ^{238}U in CR-39 has been found to be within the range of 165 - 180 MeV with standard deviation ranging from 10 to 20 MeV. In the case of Makrofol-E variation is within 168 - 182 MeV with standard deviations of 10 - 15 MeV. For ^{209}Bi in CR-39 the Q-Value has been found to be 155 $\pm$ 15 MeV and in Makrofol-E 152 $\pm$ 13 MeV. The Q-Values for the mentioned systems are conforming well with the Viola systematics for binary fragmentation. Hence the first signature for the binary fragmentation of the projectile or the compound systems is detected. This also is an evidence for the formation of the excited compound nuclei. Hence it can be said that scission of the projectile or the compound systems are the reasons for the occurence of these fork like events.

IV.5 FRAGMENT MASS DISTRIBUTIONS

The masses of each fragment in the two exit channels were searched with the help of the 'BINARY SEARCH' algorithm in the program 'HIFISS'. A Plot of fragment mass distribution has been generated for ^{238}U in CR-39 and Makrofol-E as shown in **Fig. IV.22 and Fig. IV.23** respectively. Here fractional yield for each mass fragment has been plotted as a function of fragment masses. It is evident from these plots that scisssion of the projectile or the compound system did occur at the pre-fission point.

In the case of ^{209}Bi in CR-39 and Makrofol-E similar plots have been constructed and are shown in **Fig. IV. 24 and Fig. 25** respectively. Thus the idea of scission has further been supported by the results obtained from fragment mass distributions.

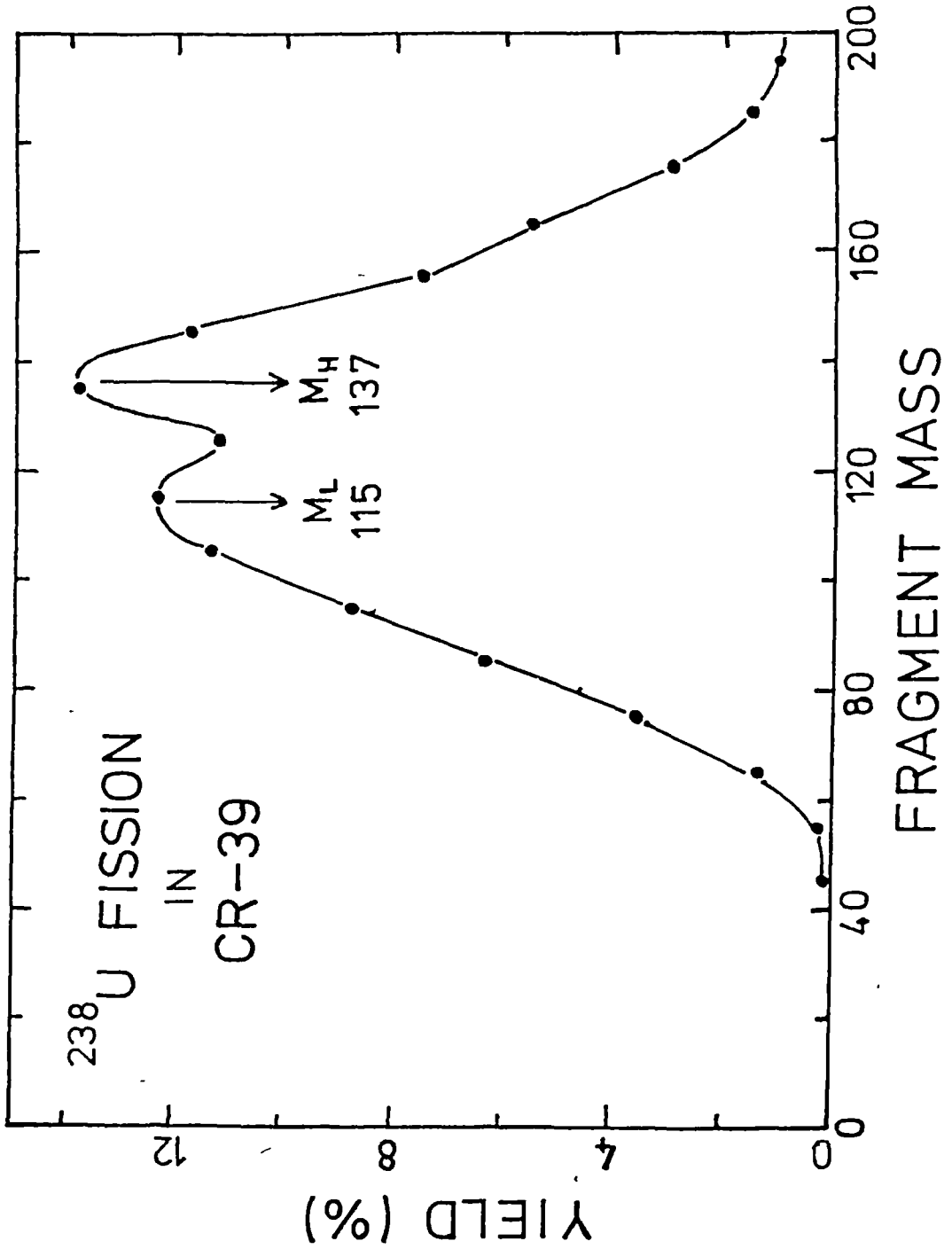

Fig. IV.22 Fragment mass distribution for ^{238}U in CR-39.

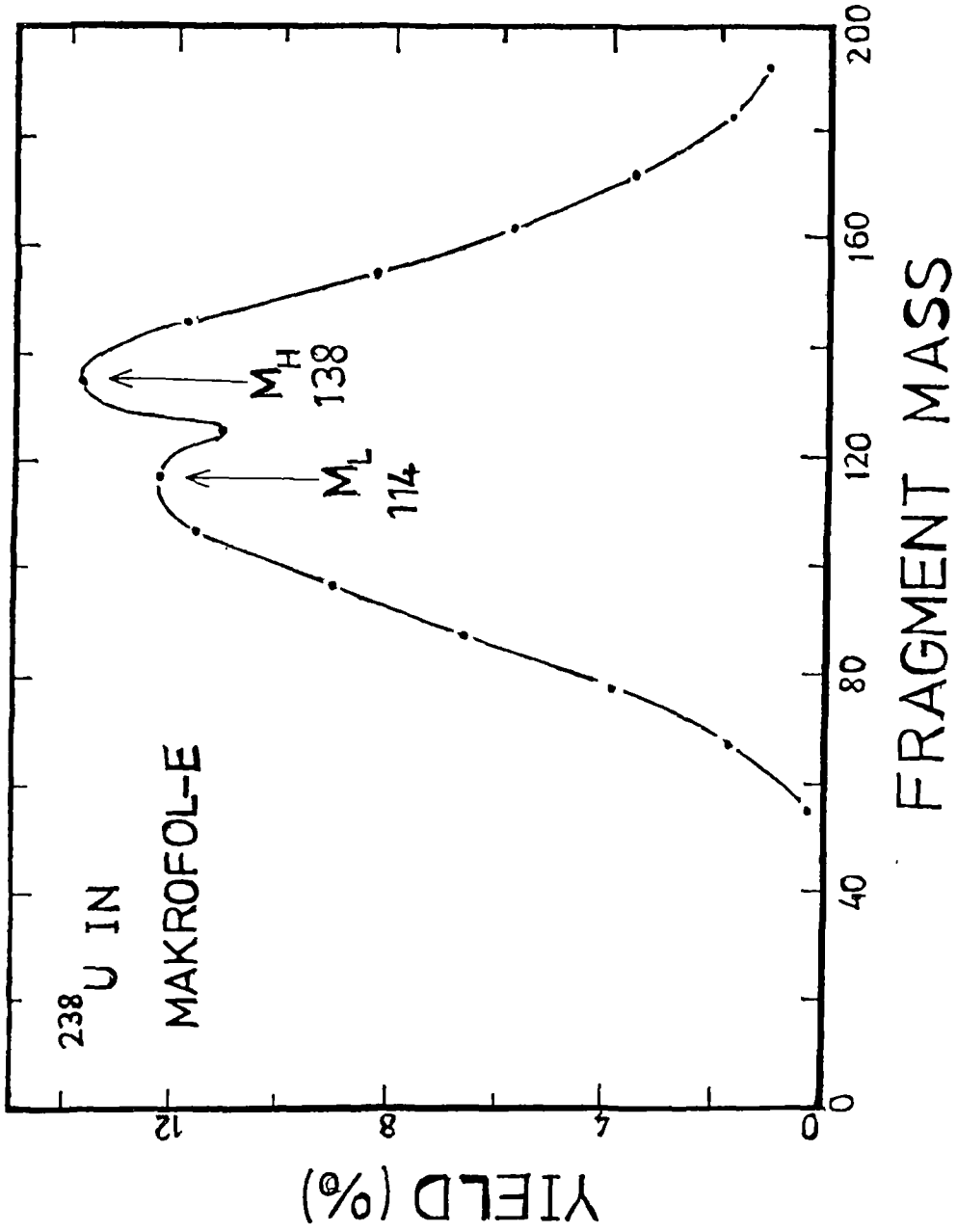

Fig. IV.23 Fragment mass distribution for ^{238}U in Makrofol-E.

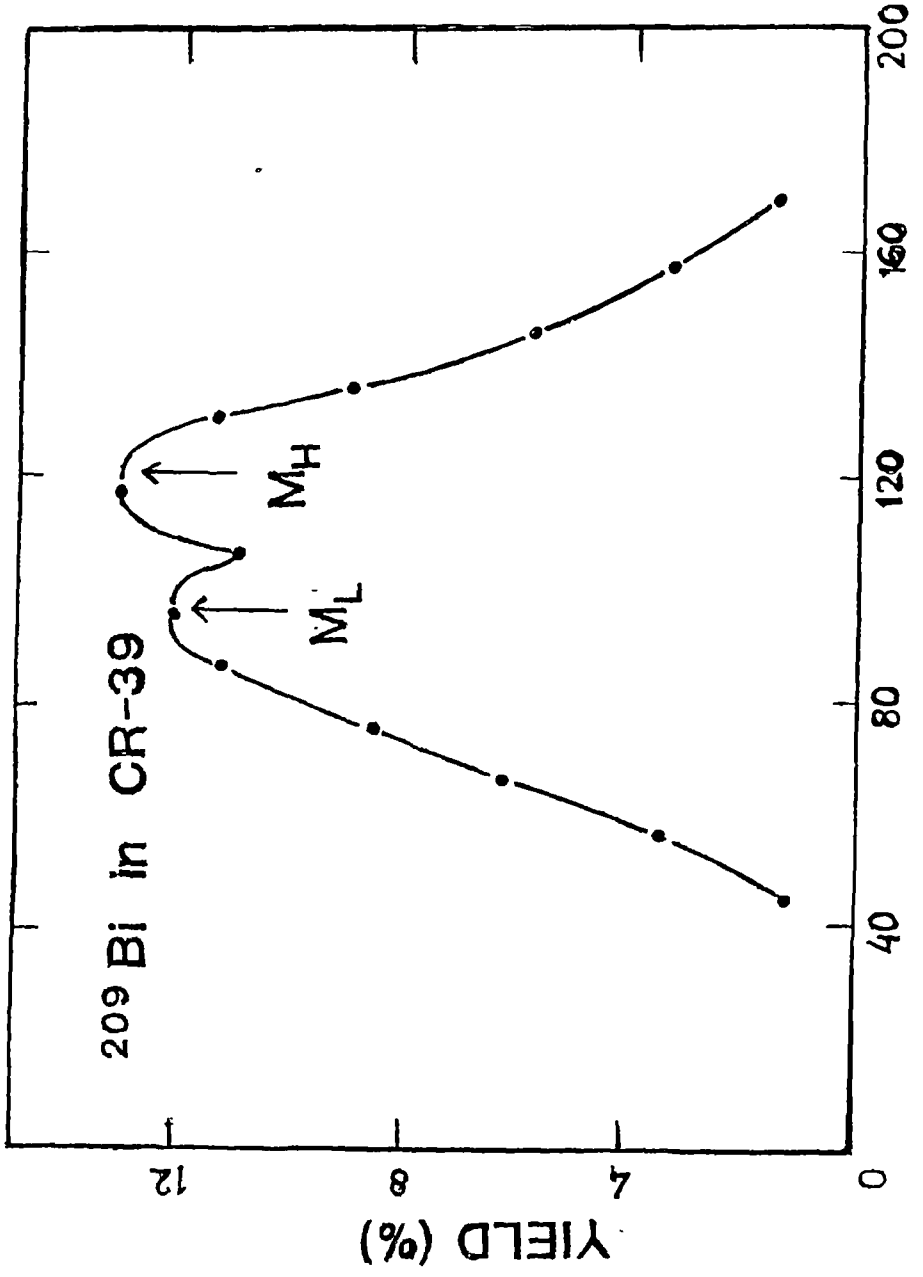

Fig. IV.24 Fragment mass distribution for ^{209}Bi in CR-39.

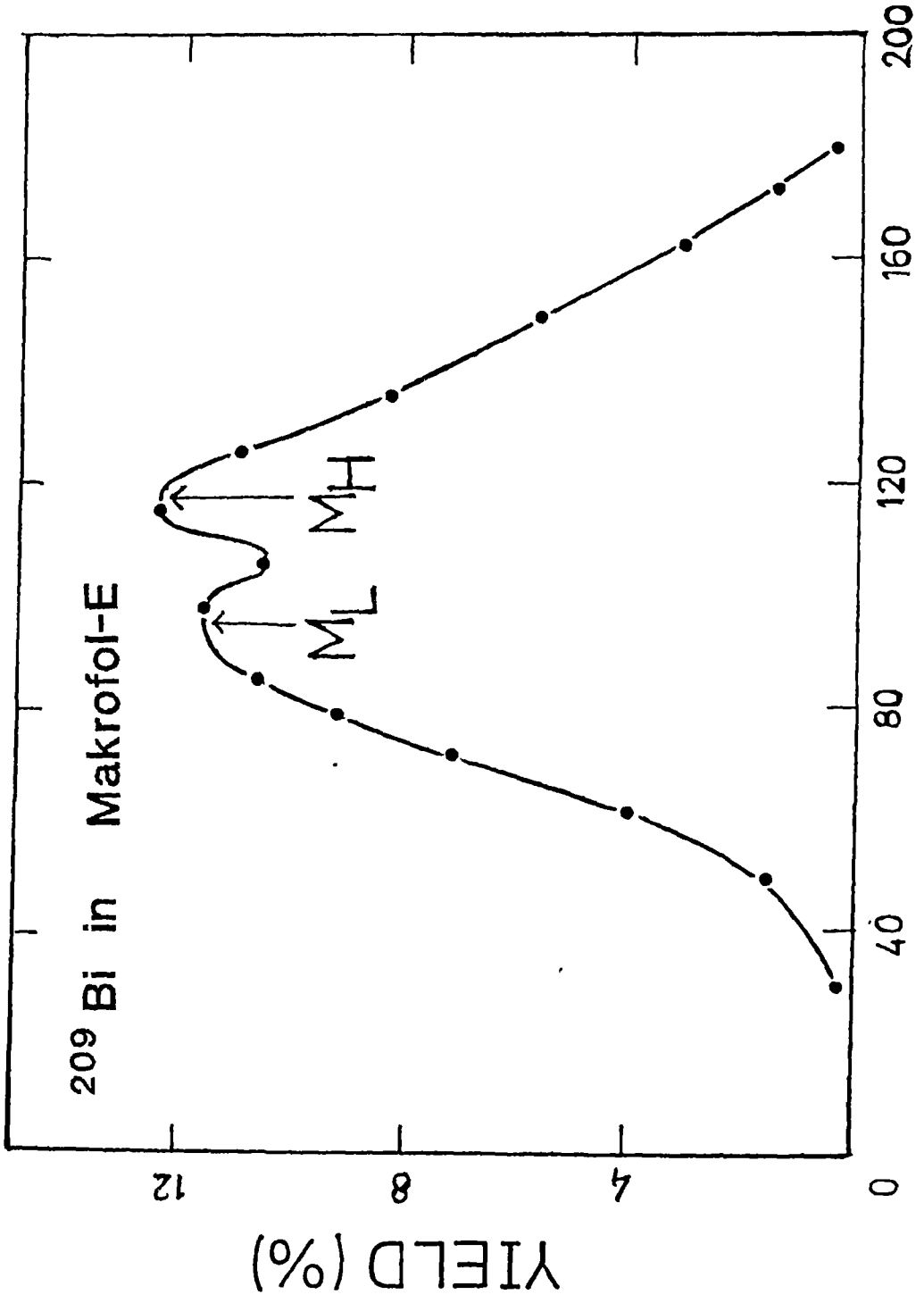

Fig. IV.25 Fragment mass distribution for ^{209}Bi in Makrofol-E.

IV.6 RELATIVE VELOCITY OF FRAGMENTS

As the search for different signatures of binary fragmentation of the projectile or the compound system has been undertaken, another important kinematic variable for these events which should indicate the processes involved for these events is the relative velocity of fragments with respect to each other. The relative velocity of fragments in binary fragmentation of the projectiles and the compound systems considered for the present study should be 2.4 cm/ns **[46, 48]**.

The relative velocity in each case is calculated by the program 'HIFISS'. These values are found to be randomly distributed and a best fitting could be achieved in the form of gaussians as shown in **Fig. IV.26 - Fig. IV.29**. From similar plots the most probable values of relative velocity of fragments are determined and are tabulated in **Table IV.12 and IV.13**. The value 2.4 ± 0.2 cm/ns is found to be the most probable relative velocity. This takes us one more step ahead in search of reasons for the occurence of binary fragmentation by random neck scission. Hence one more supporting evidence for the binary fragmentation of the projectile or the compound system responsible for creating the events has been found.

IV.7 TOTAL OPENING ANGLE IN LABORATORY SYSTEM

The total opening angle in the LABORATORY system is defined as the actual angle between the two prongs of an event i.e. $(\theta_A + \theta_B)$. Total opening angle can also be defined as the scattering angle between the fragments in the LABORATORY system. (**Fig. IV.30a, b and c**) are the plots of total opening as a function of pre-fission energy for ^{238}U in CR-39 for different initial energies of the projectile. For ^{238}U in Makrofol-E the plots are (**Fig. IV.31 a**

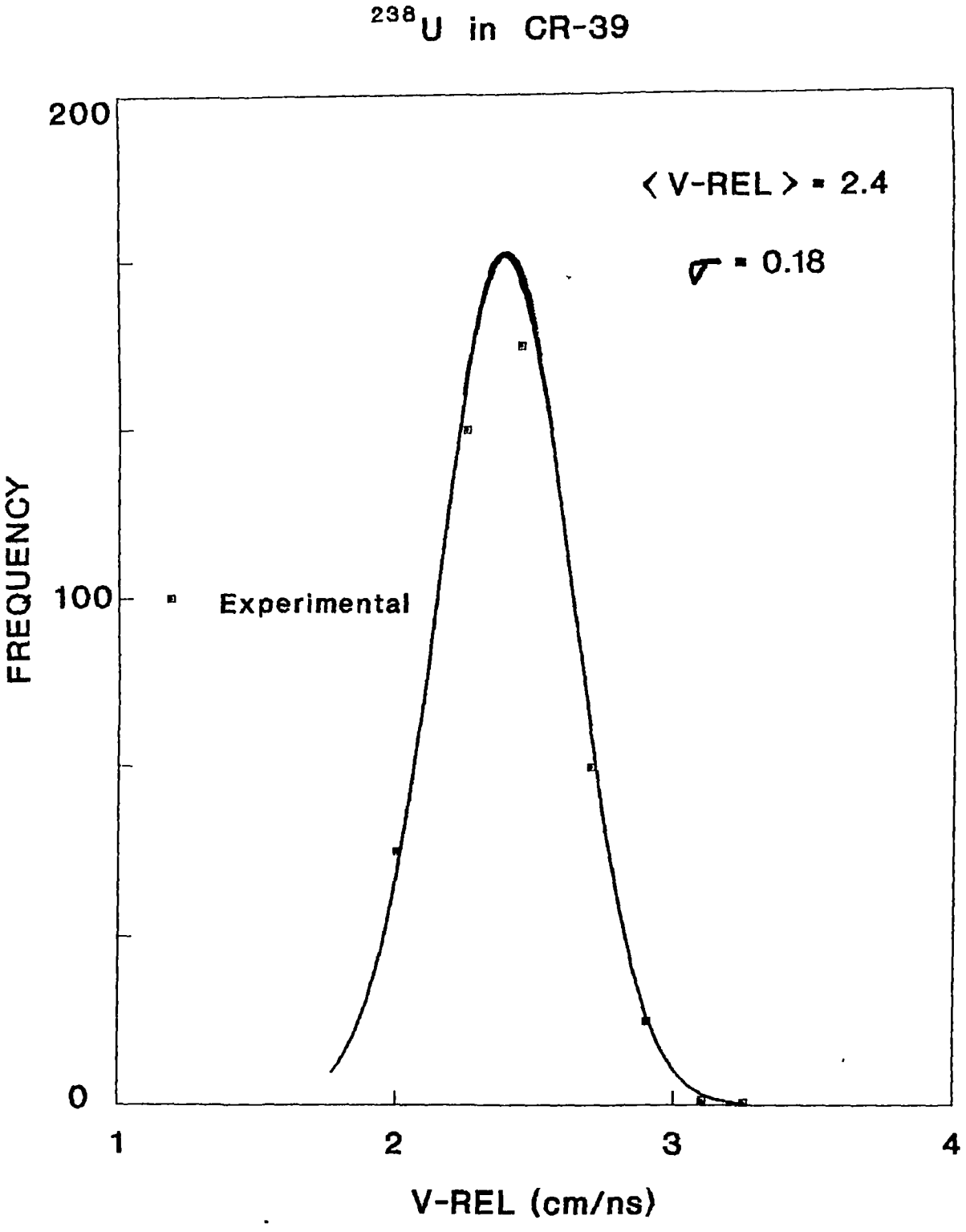

Fig. IV.26 Relative velocity distribution for 16.4 MeV/u ^{238}U in CR-39.

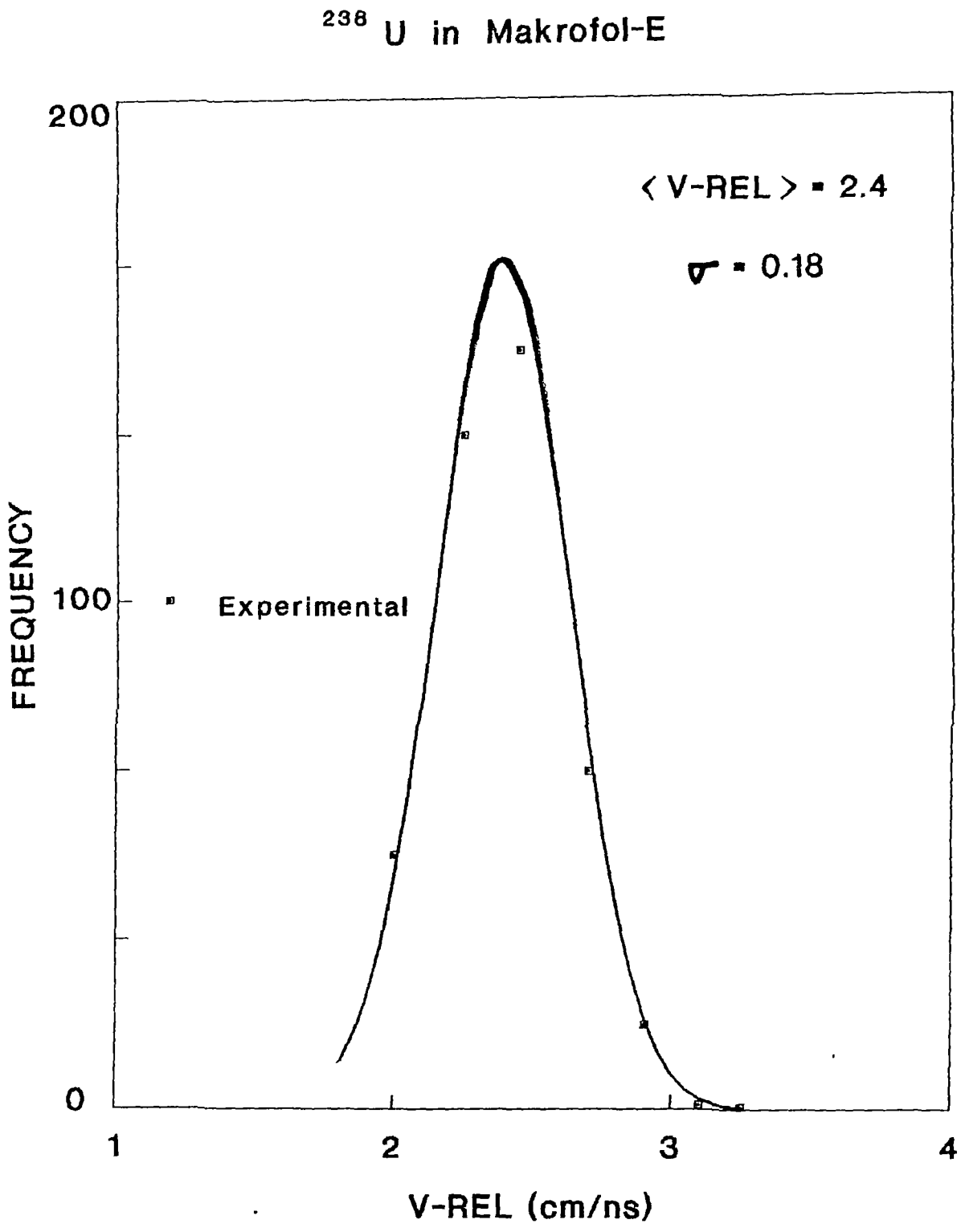

Fig. IV.27 Relative velocity distribution for 17.2 MeV/u ^{238}U in Makrofol-E.

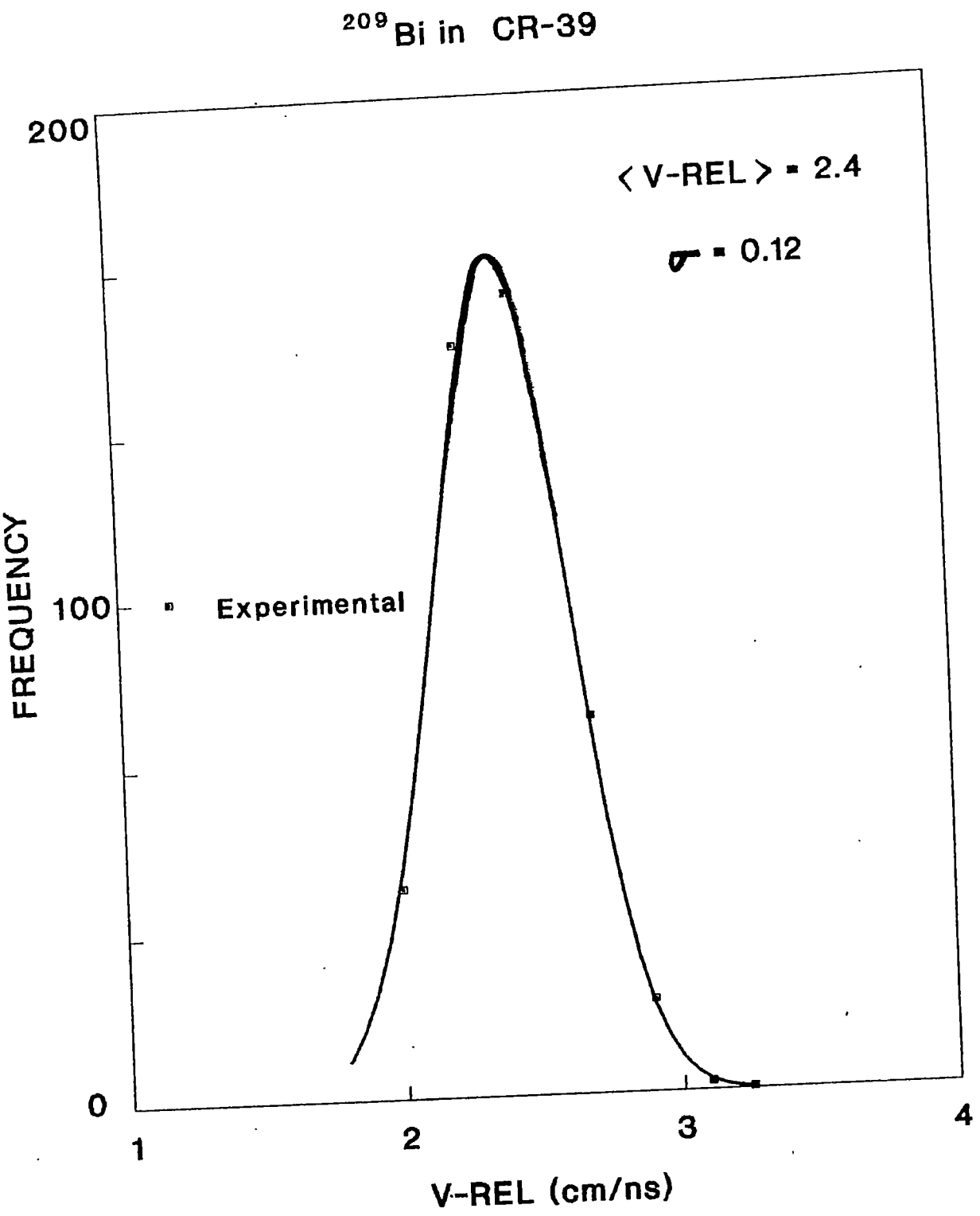

Fig. IV.28 Relative velocity distribution for 13.0 MeV/u ^{209}Bi in CR-39.

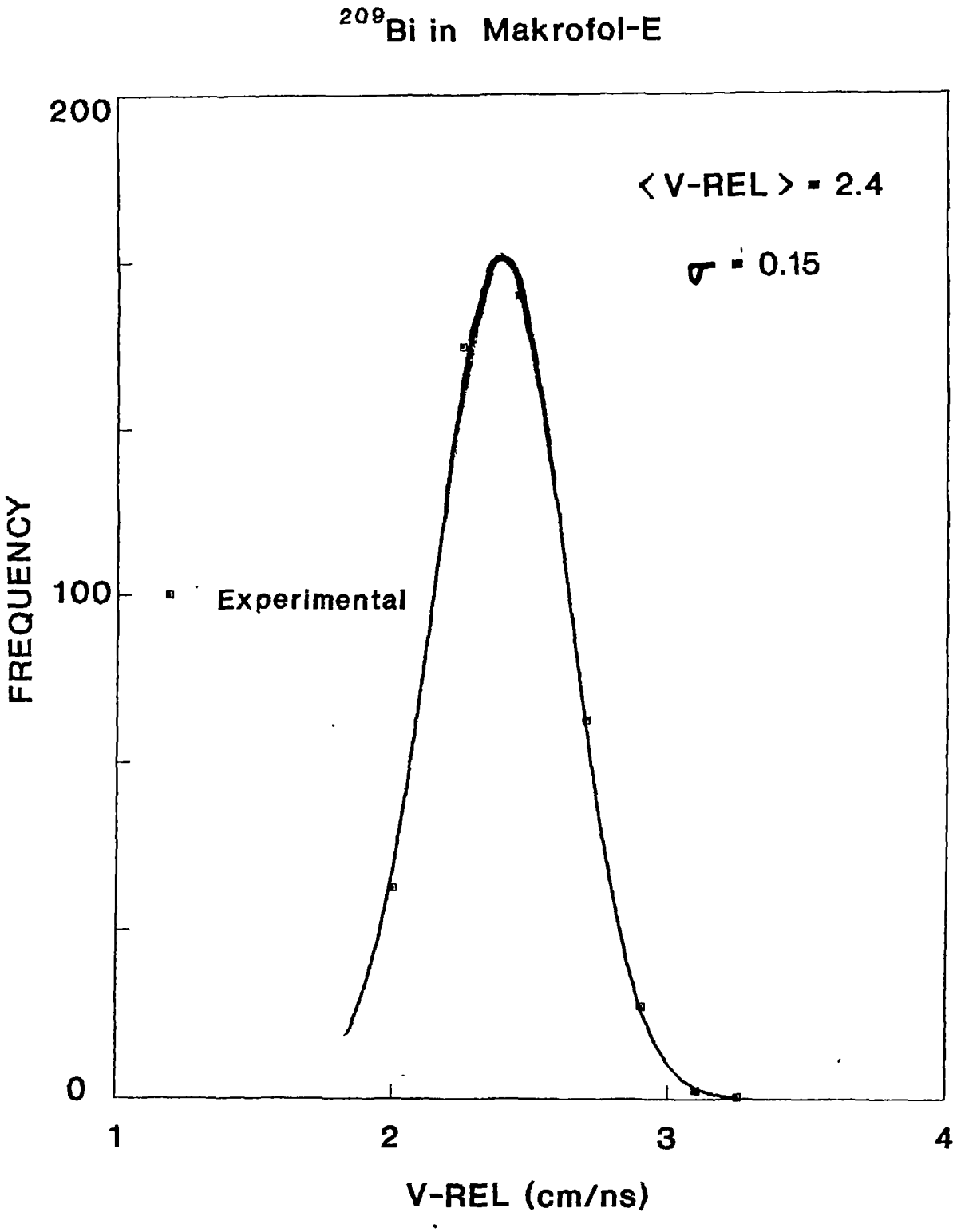

Fig. IV.29 Relative velocity distribution for 13.0 MeV/u ^{209}Bi in Makrofol-E.

Table IV.12

MOST PROBABLE VALUES OF RELATIVE VELOCITY FOR ^{238}U IN CR-39 AND MAKROFOL-E

	CR-39		MAKROFOL-E
ENERGY (MeV/u)	V-REL (cm/ns)	ENERGY (MeV/u)	V-REL (cm/ns)
16.4	2.4 ± 0.18	17.2	2.4 ± 0.18
15.2	2.4 ± 0.15	16.0	2.4 ± 0.15
14.0	2.4 ± 0.13	14.3	2.4 ± 0.13
13.0	2.4 ± 0.12	12.4	2.4 ± 0.12
11.3	2.4 ± 0.12		

Table IV.13

MOST PROBABLE RELATIVE VELOCITY FOR ^{209}Bi IN CR-39 AND MAKROFOL-E

	CR-39		MAKROFOL-E
ENERGY (MeV/u)	V-REL (cm/ns)	ENERGY (MeV/u)	V-REL (cm/ns)
13.0	2.4 ± 0.12	13.0	2.4 ± 0.15

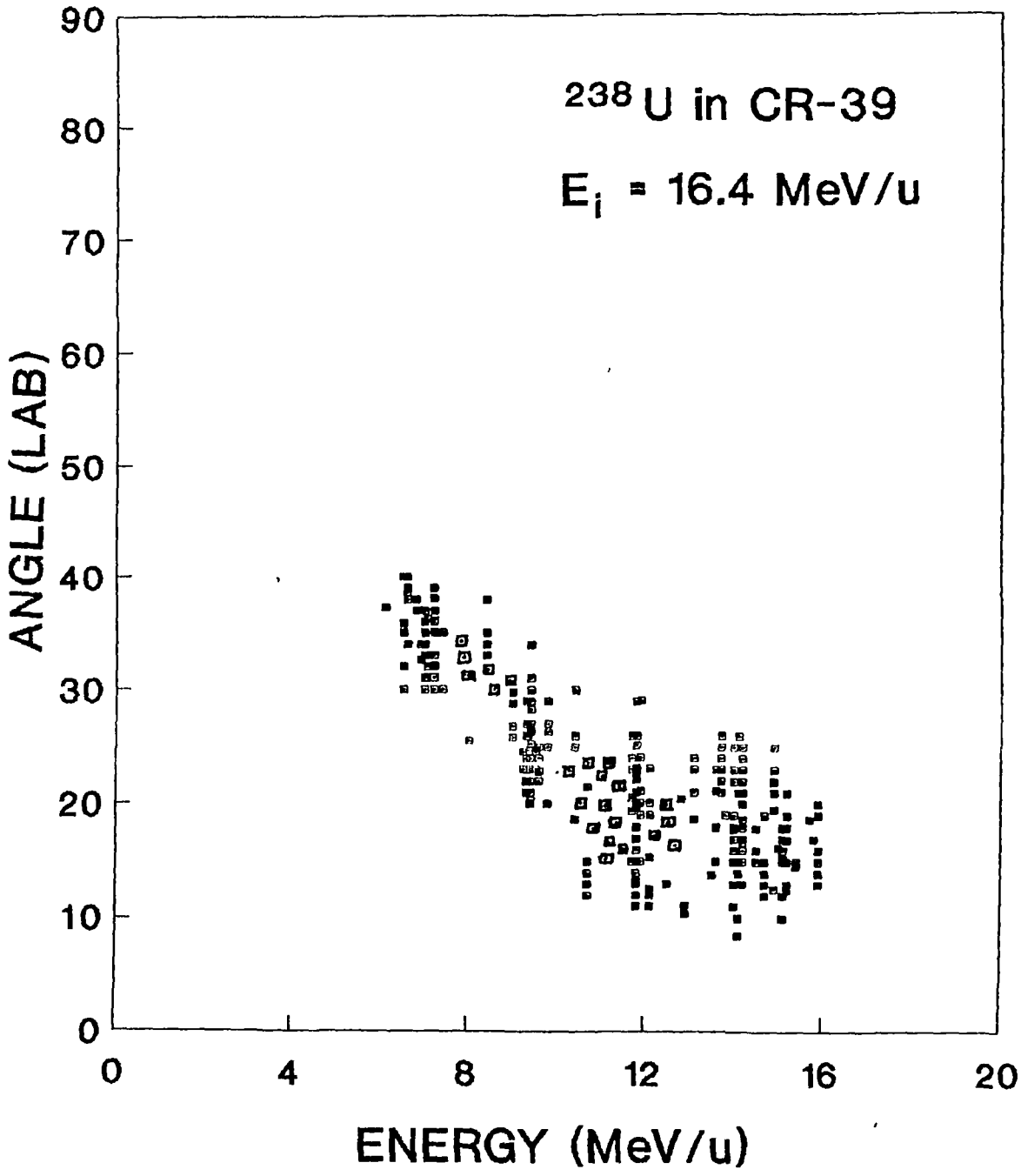

Fig. IV.30 (a) Plot of total opening angle in laboratory system at different pre-fission energy for ^{238}U of 16.4 MeV/u in CR-39.

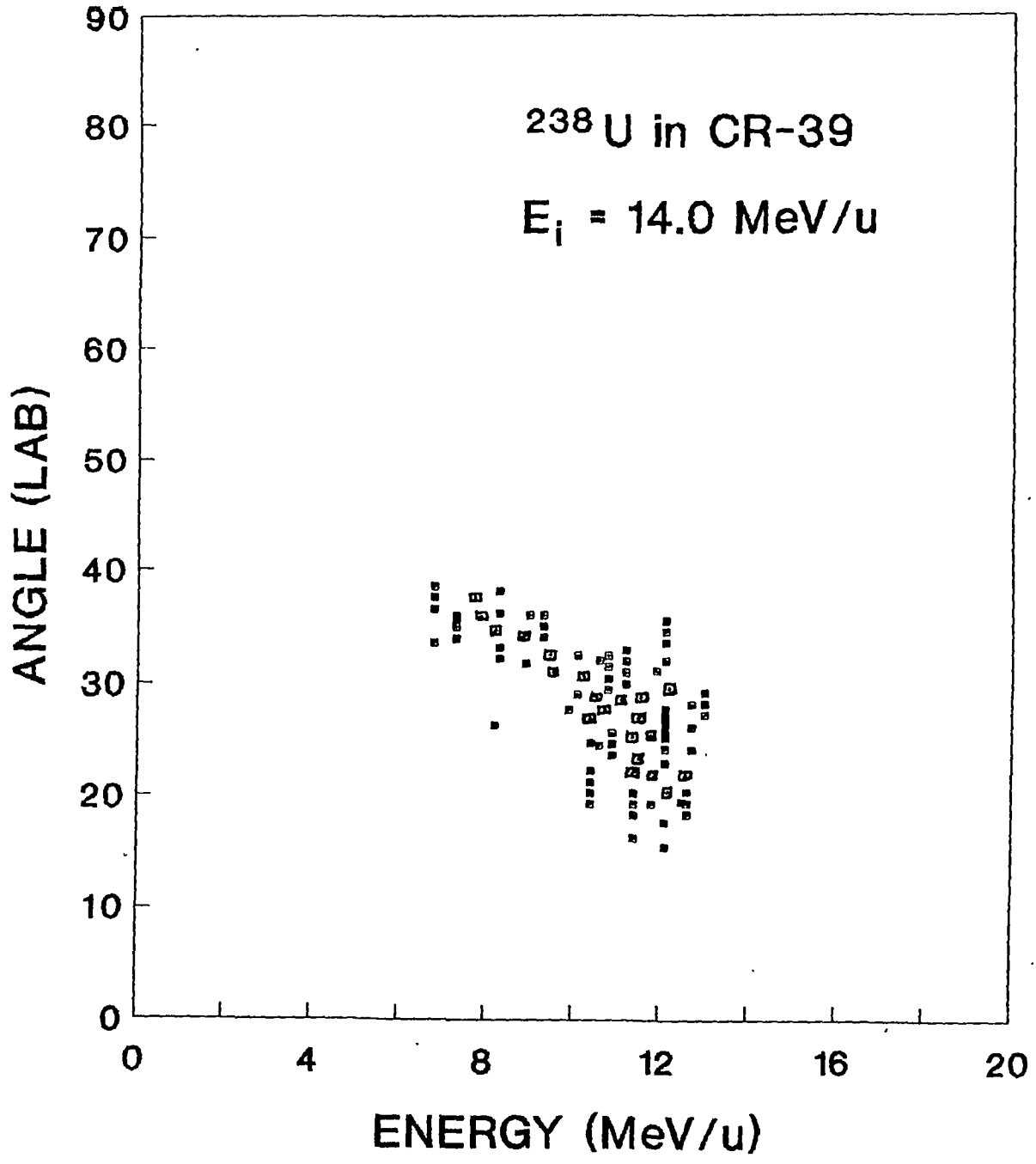

Fig. IV.30 (b) Plot of total opening angle in laboratory system at different pre-fission energy for ^{238}U of 14.0 MeV/u in CR-39.

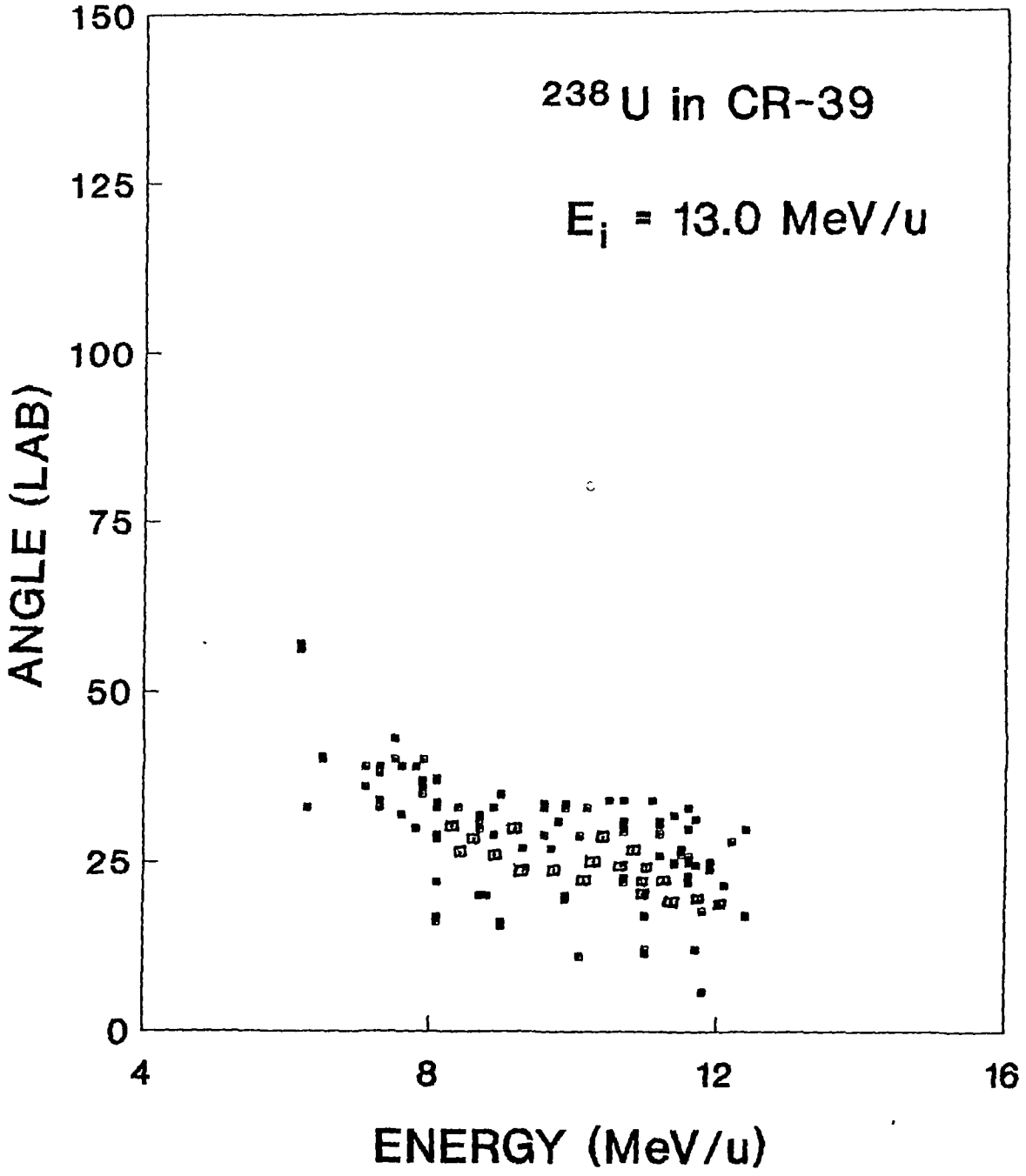

Fig. IV.30 (c) Plot of total opening angle in laboratory system at different pre-fission energy for ^{238}U of 13.0 MeV/u in CR-39.

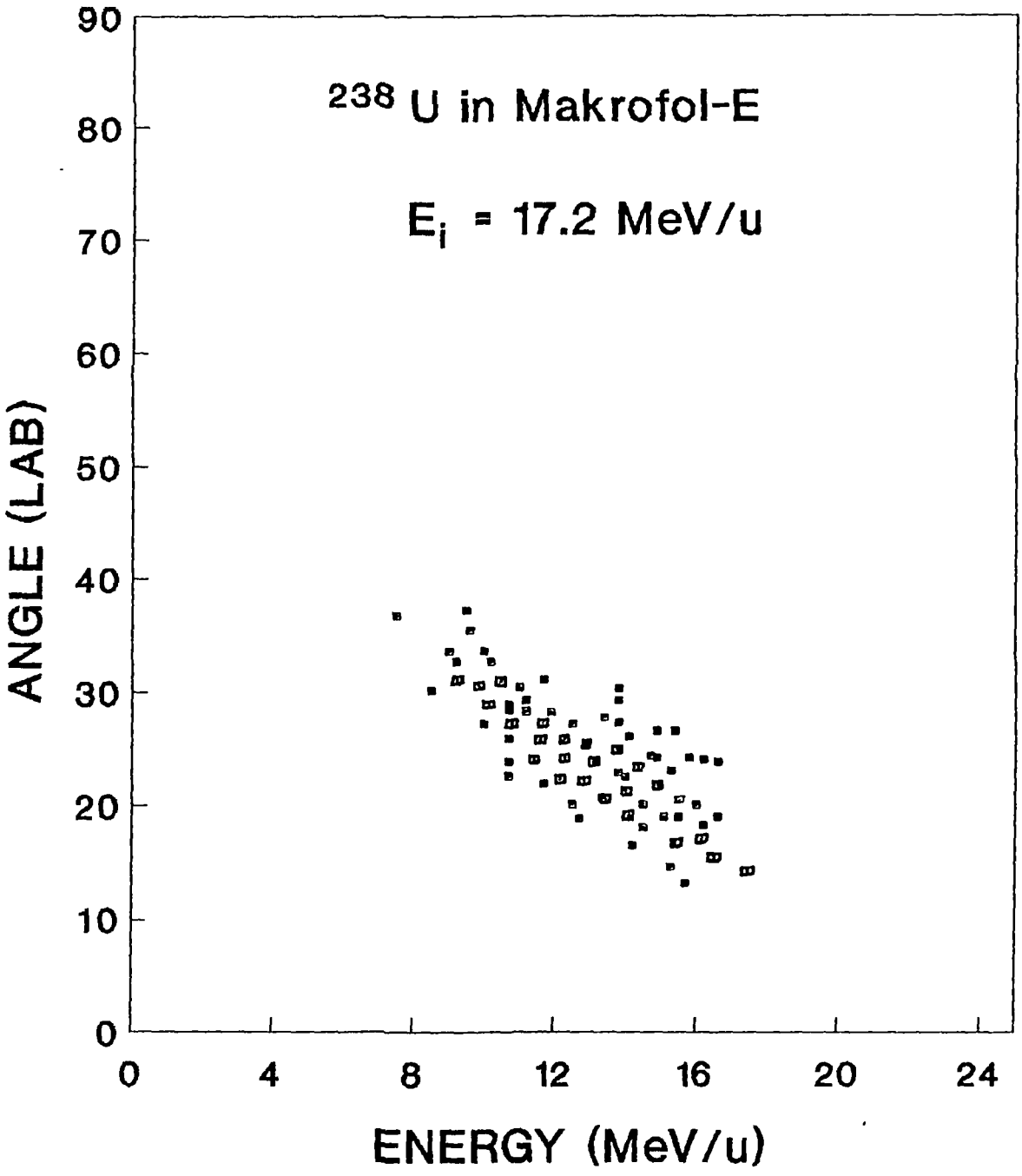

Fig. IV.31 (a) Total opening angle in laboratory system at different pre-fission energies for ^{238}U of 17.2 MeV/u in Makrofol-E.

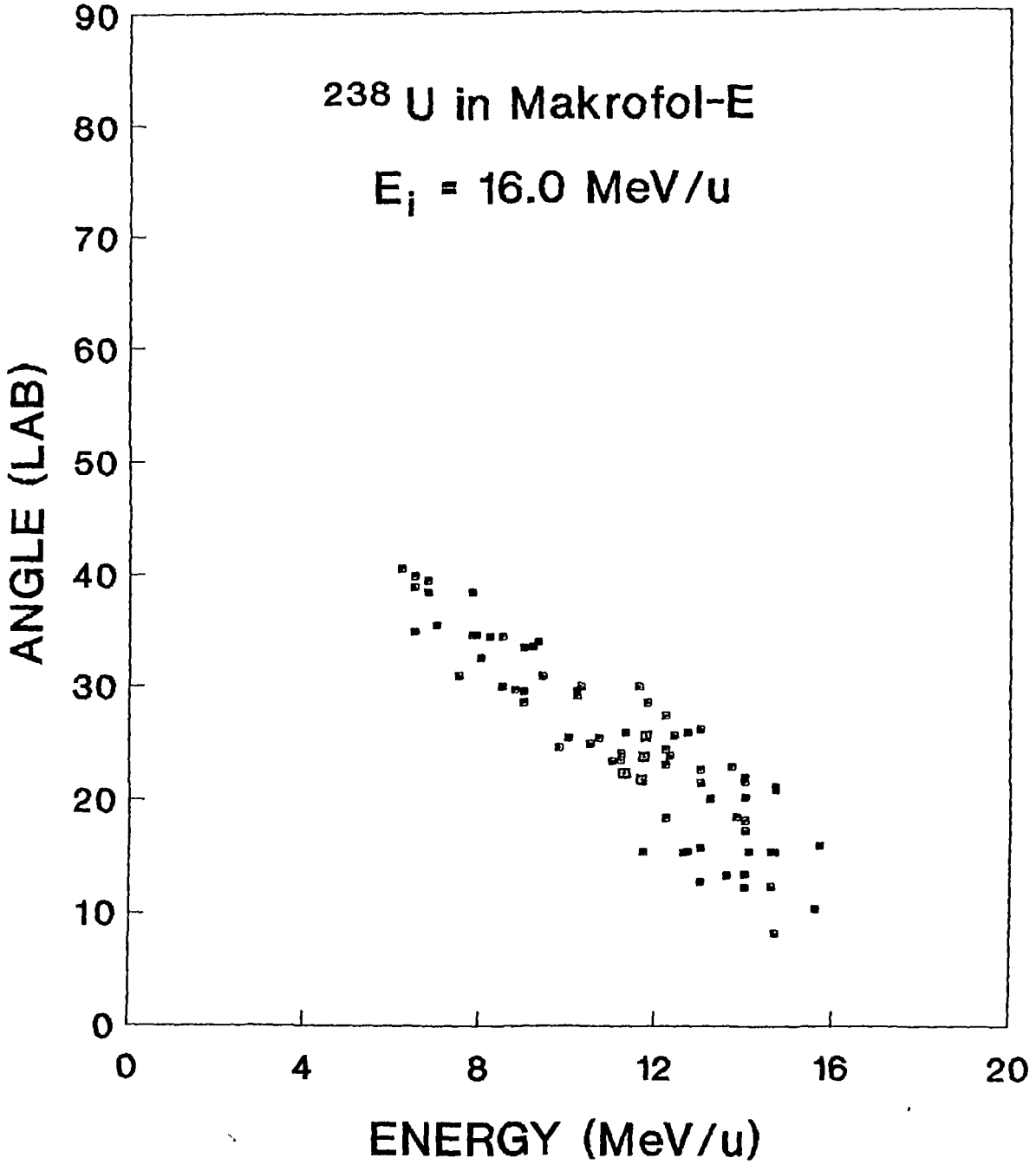

Fig. IV.31 (b) Total opening angle in laboratory system at different pre-fission energies for ^{238}U of 16.0 MeV/u in Makrofol-E.

and b). Similarly for 13.0 MeV/u ^{209}Bi in CR-39 and Makrofol-E the plots are given in **Fig. IV.32 and Fig. IV.33** respectively.

The significant observation from these plots is that the opening angle increases as the energy of the projectile decreases. Though it is a qualitative observation, it leads us to the conclusion that binary fragmentation or fission of the projectile or compound nuclei has taken place. Usually at low kinetic energy of a projectile or compound system, the repulsive forces of fragments at saddle point dominate over the forward momentum, which results in to large opening angle.

IV.8 TOTAL OPENING ANGLE IN CENTRE OF MASS SYSTEM

The values of total opening angle in the centre of mass system have been determined in each case and are illustrated in **Figs. IV.34 - IV.37** as a function of pre-fission energy. It is apparent from these plots that the opening angle in centre of mass system is independent of the pre-fission energy. This indicates that there exists a non-selective directional emission of fragments. Therefore it is concluded that fragments are isotropically emitted in the forward hemisphere proving the fact that fusion-fission is the cause for the occurence of these events.

IV.9 ANALYSIS OF THE THIRD PRONG

The fork like events with the third prong at the point of bifurcation were observed when ^{238}U projectiles at different pre-fission energies interact in CR-39. The creation of the third prongs may be due to the pre-fission emission of particles from the excited compound nuclei. However with ^{238}U

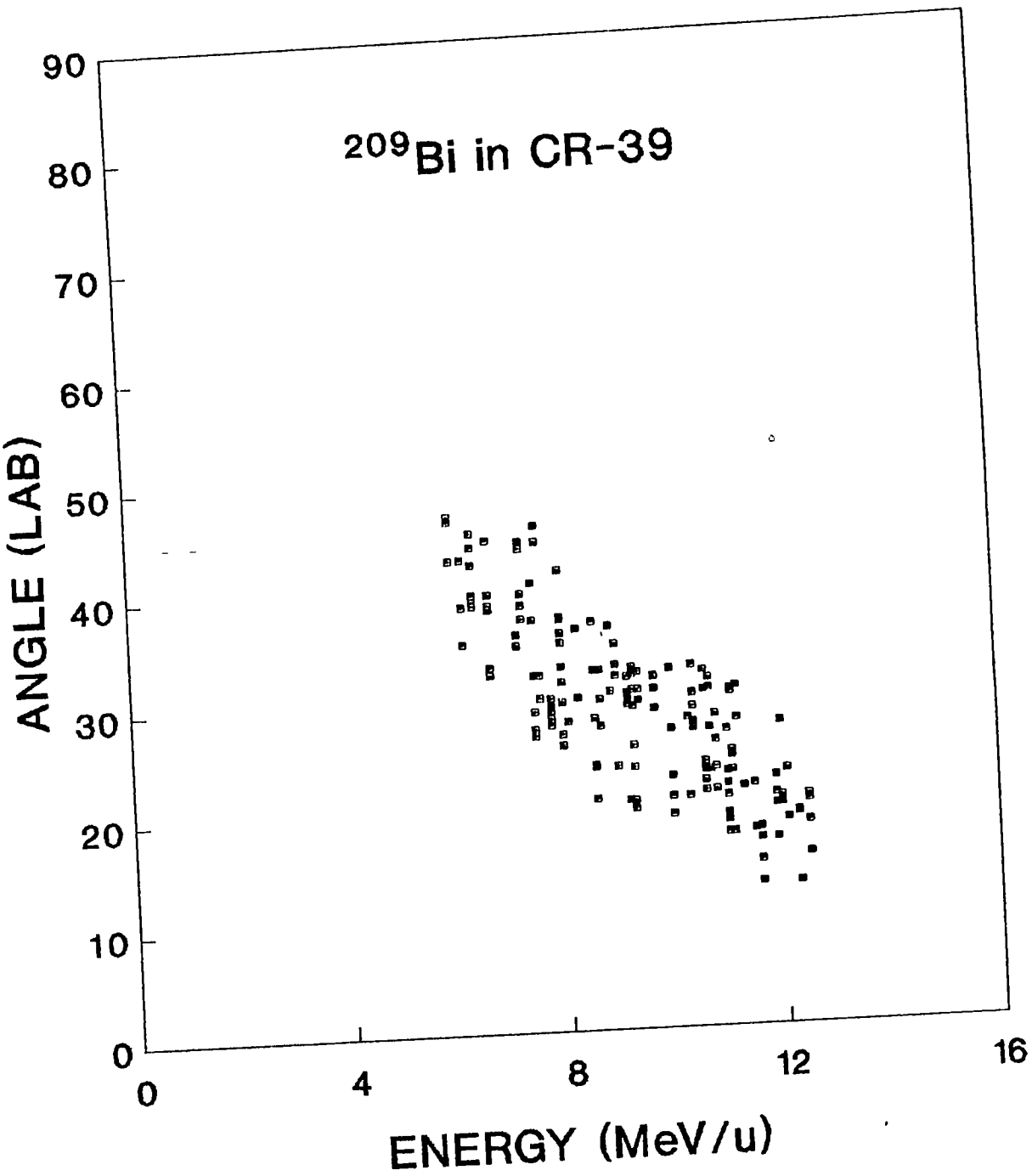

Fig. IV.32 Plot of total opening angle in laboratory system for 13.0 MeV/u ^{209}Bi in CR-39.

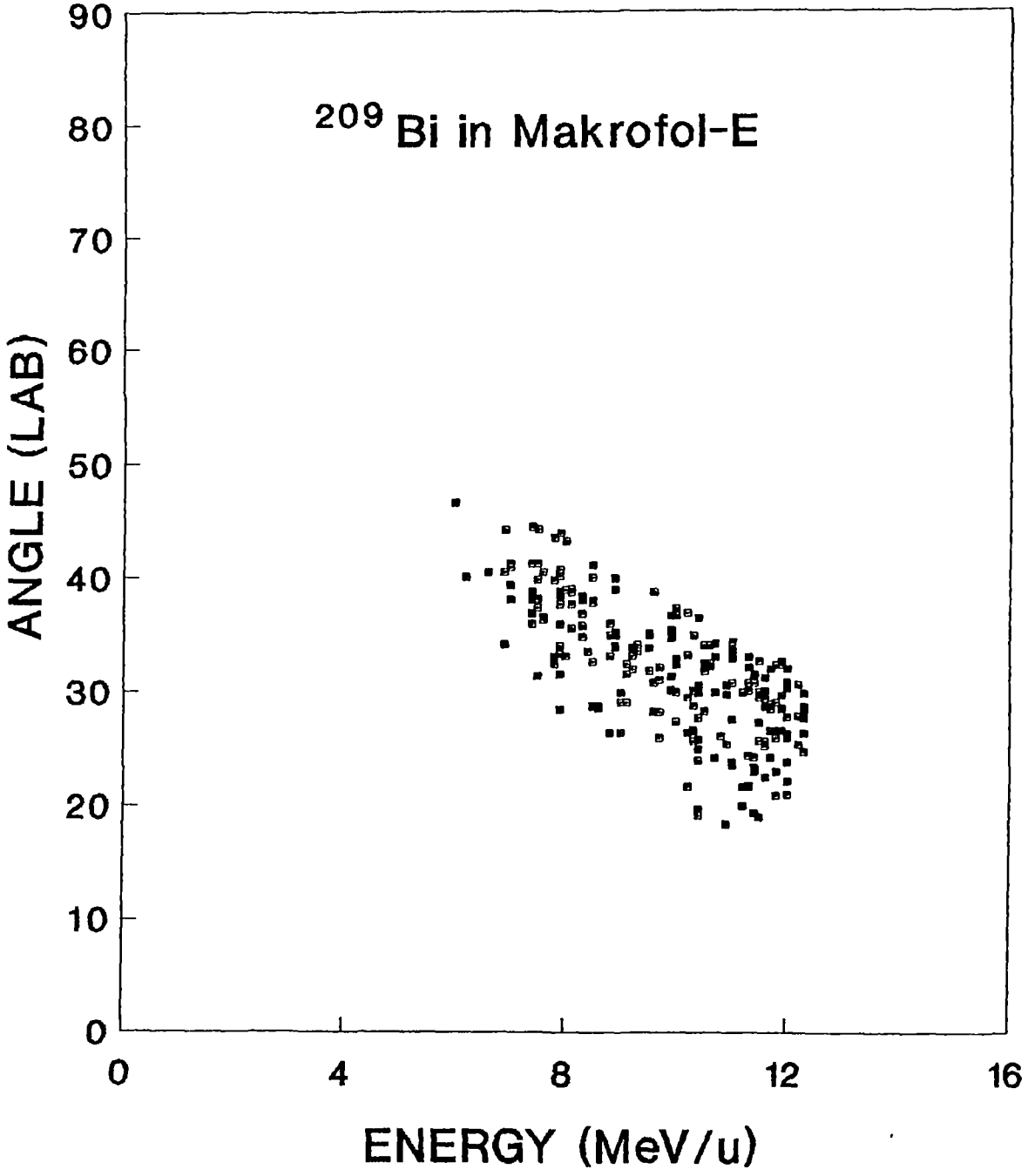

Fig. IV.33 Plot of total opening angle in laboratory system for 13.0 MeV/u ^{209}Bi in Makrofol-E.

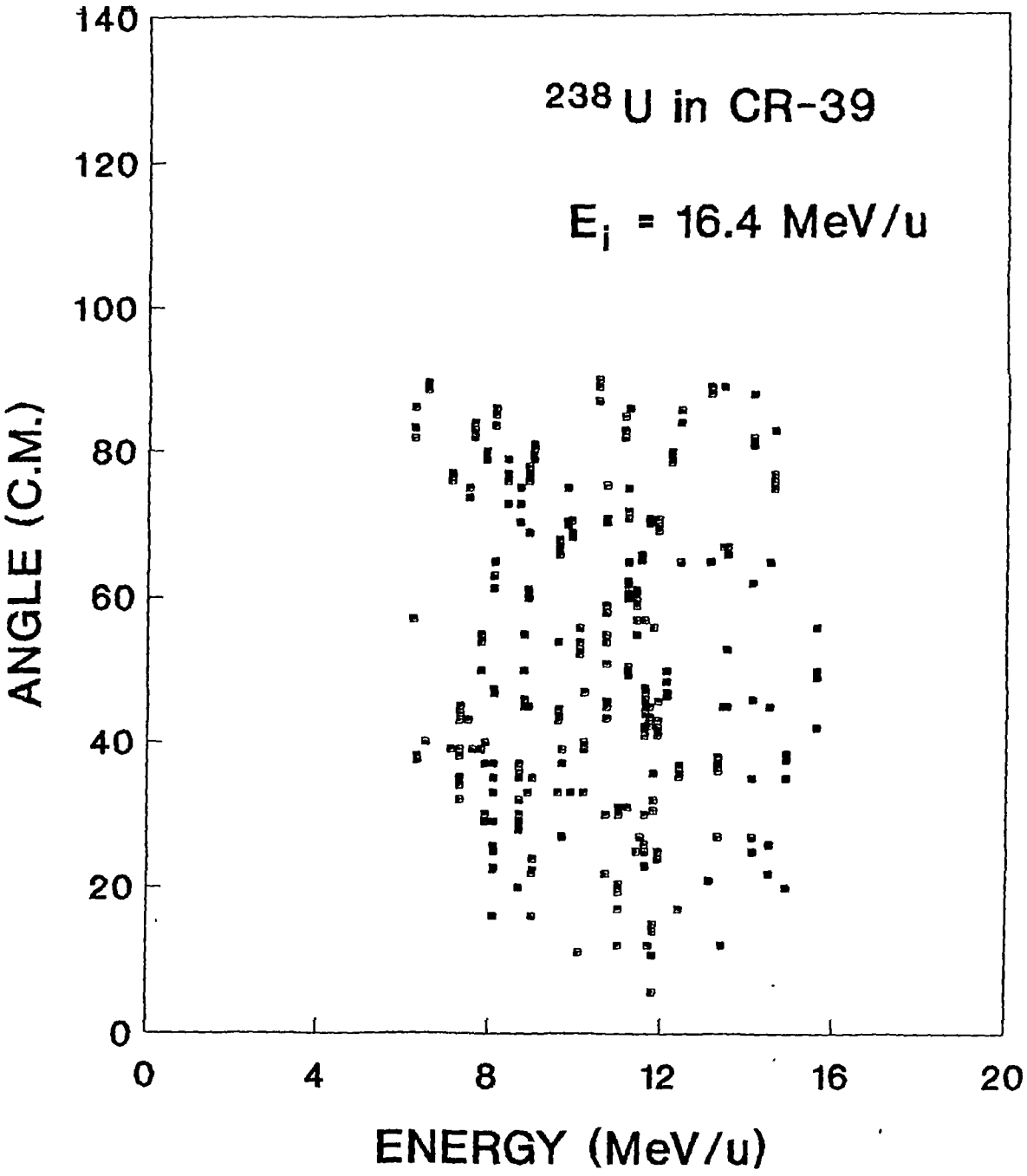

Fig. IV.34(a) Plot of total opening angle in centre of mass system for ^{238}U of 16.4 MeV/u in CR-39.

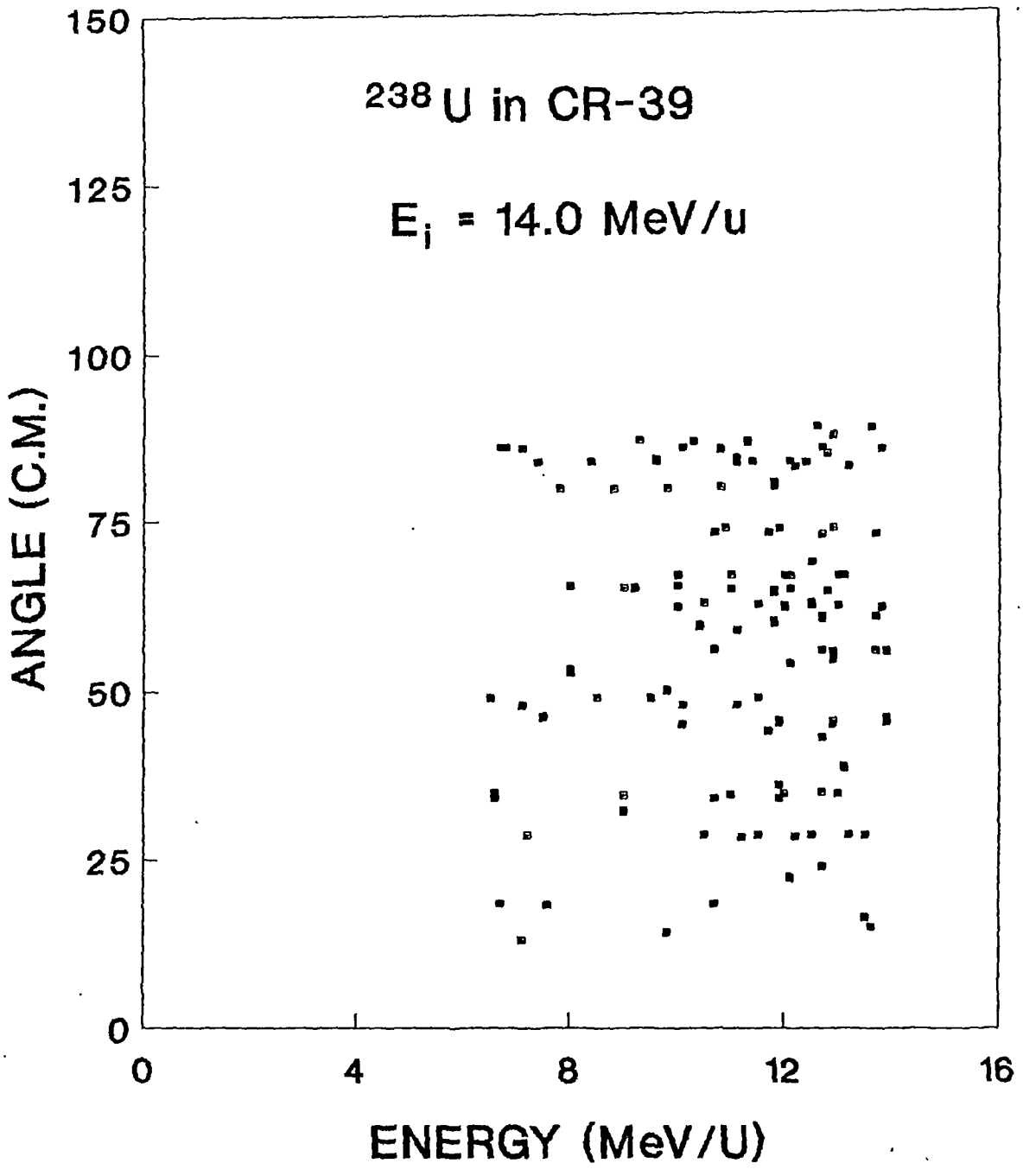

Fig. IV.34(b) Plot of total opening angle in centre of mass system for ^{238}U of 14.0 MeV/u in CR-39.

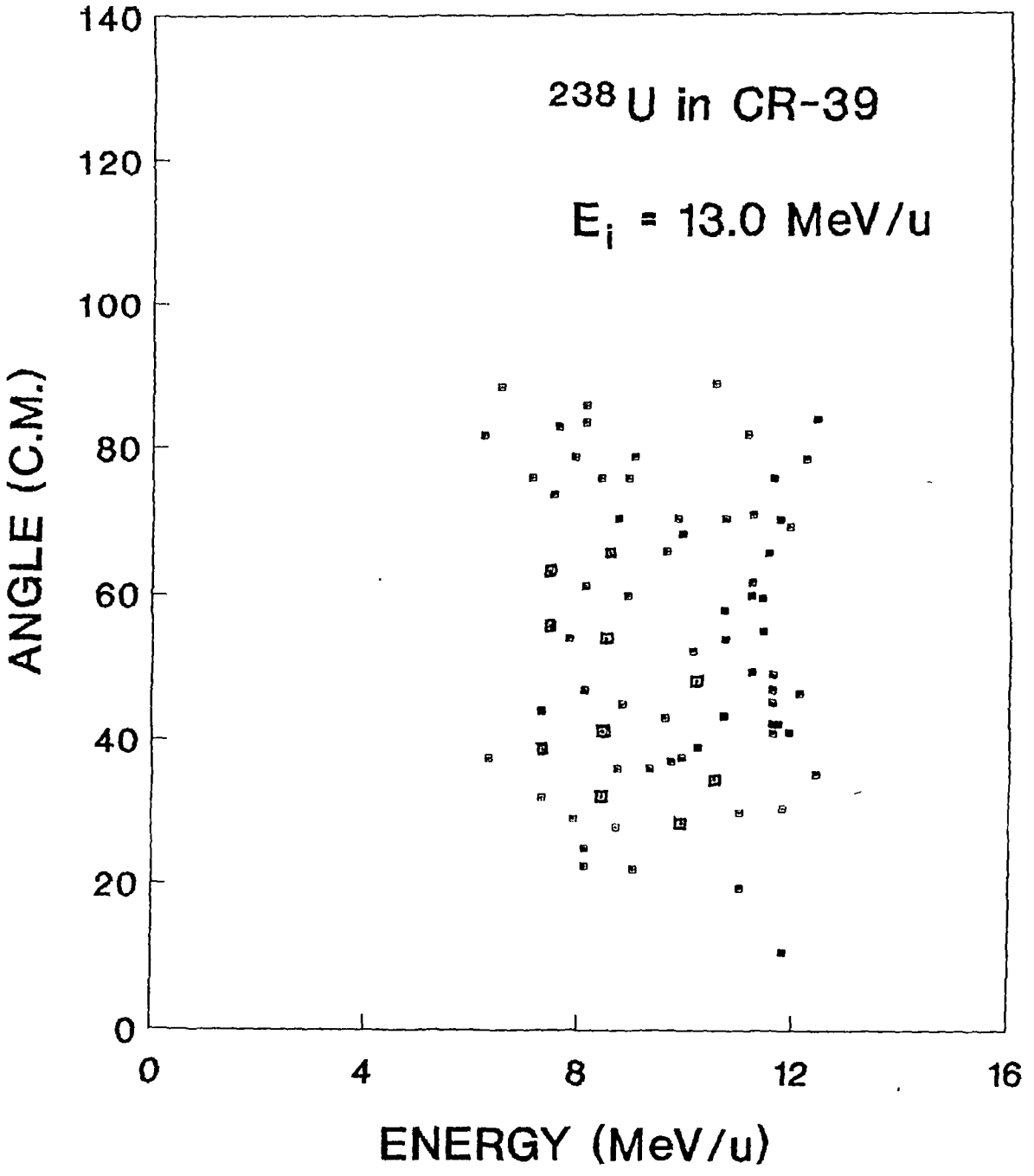

Fig. IV.34 (c) Plot of total opening angle in centre of mass system for ^{238}U of 13.0 MeV/u in CR-39.

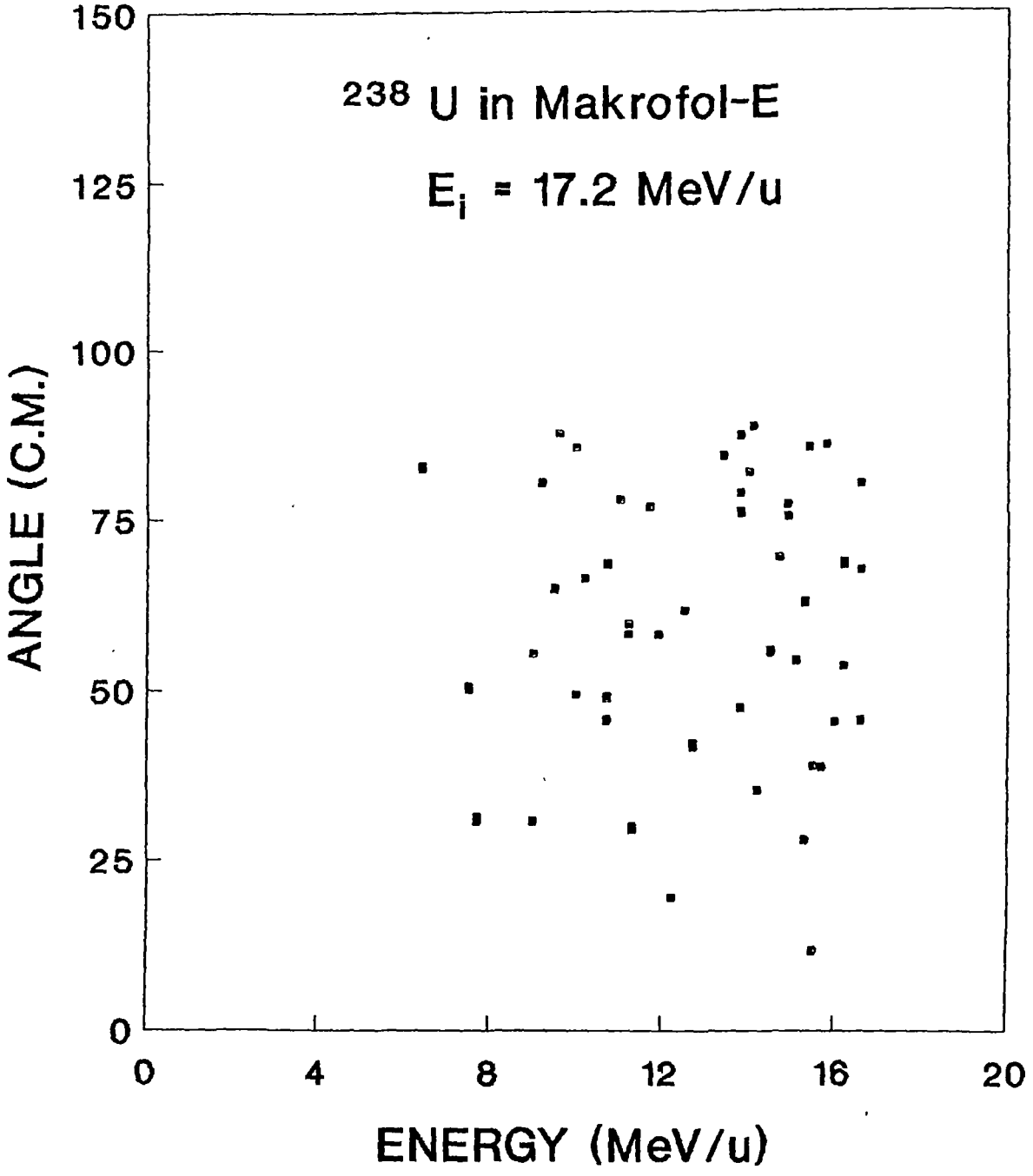

Fig. IV.35 (a) Plot of total opening angle in centre of mass system for ^{238}U of 17.2 MeV/u in Makrofol-E.

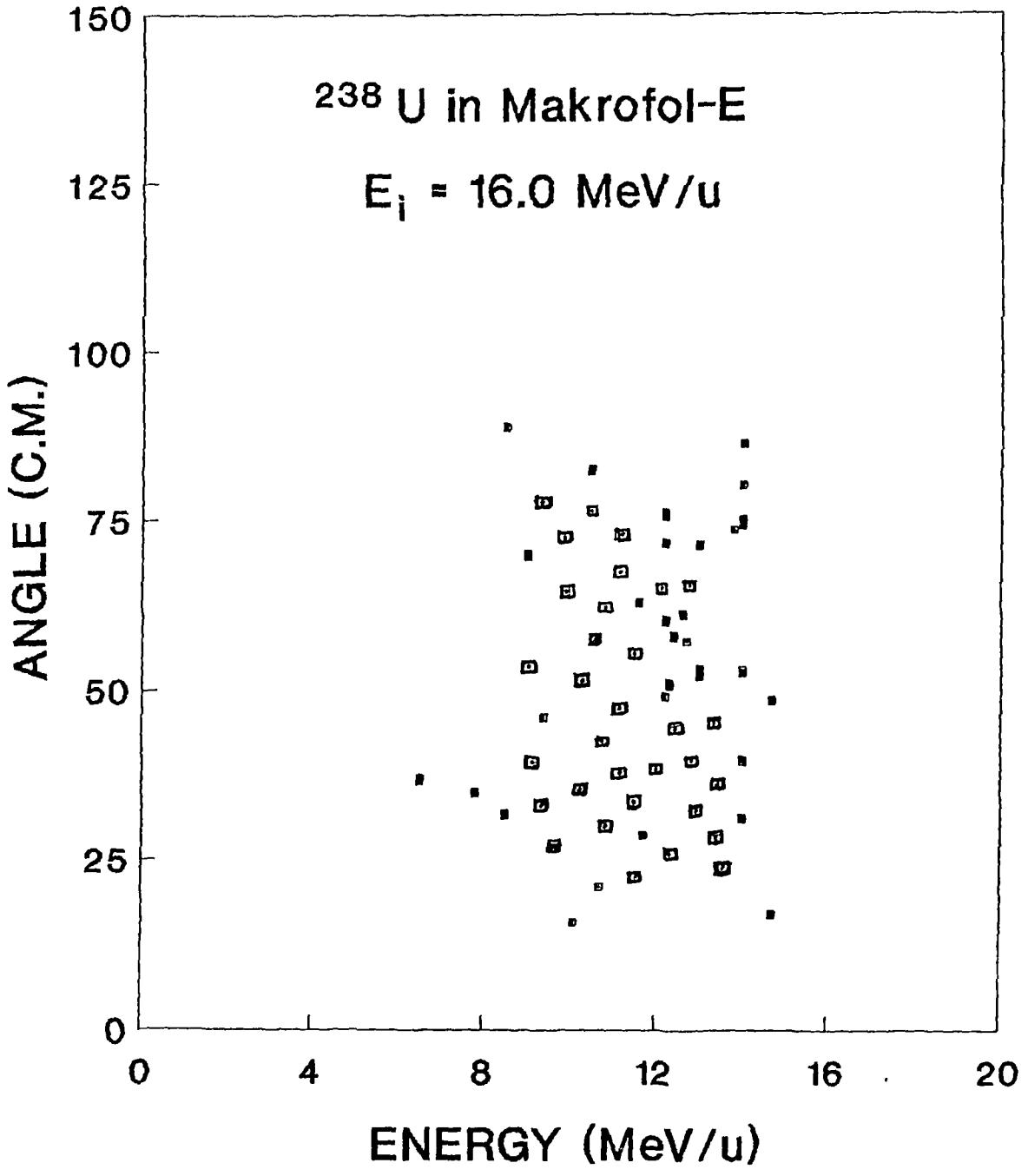

Fig. IV.35 (b) Plot of total opening angle in centre of mass system for ^{238}U of 16.0 MeV/u in Makrofol-E.

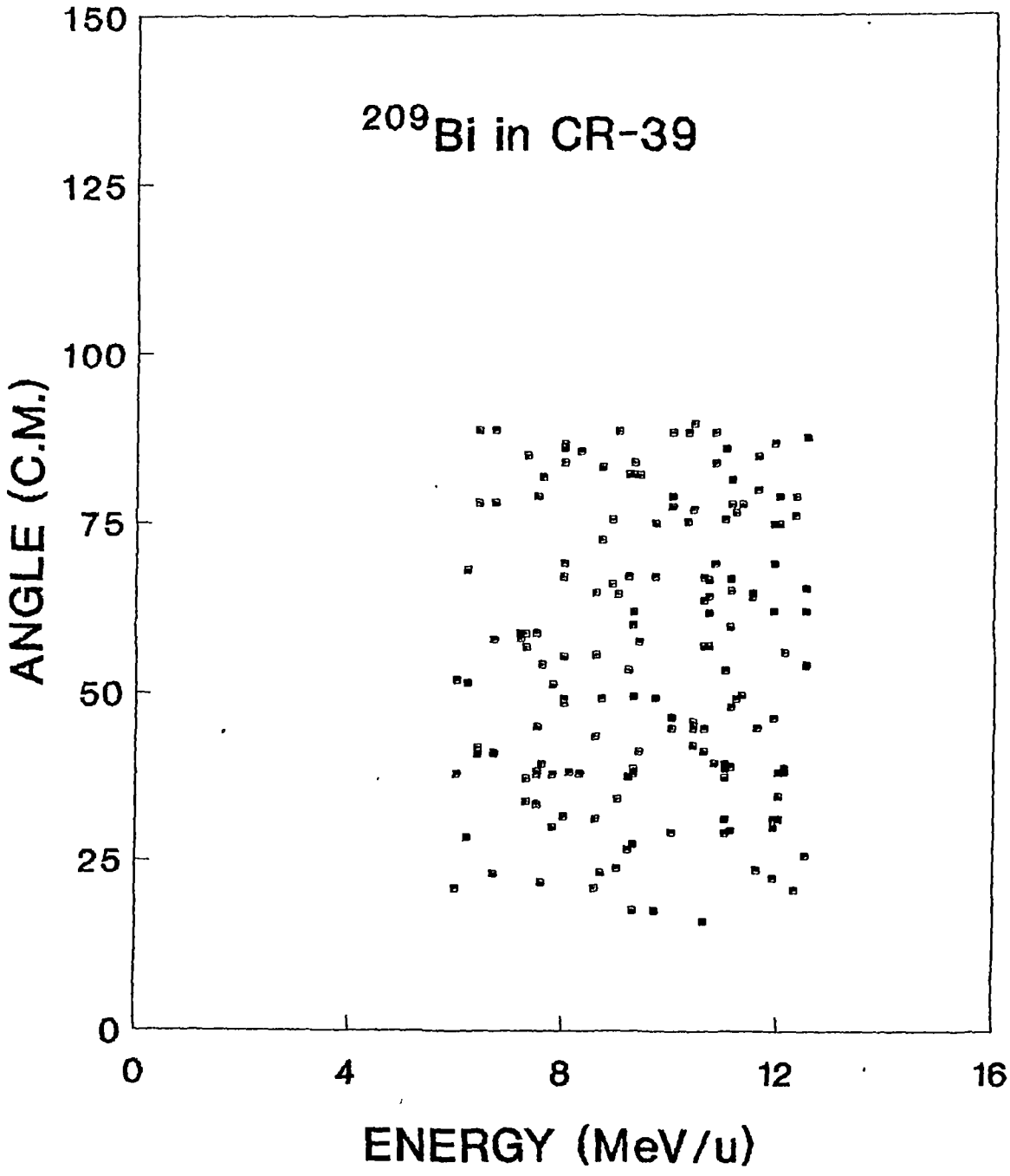

Fig. IV.36 Plot of total opening angle in centre of mass system for ^{209}Bi in CR-39.

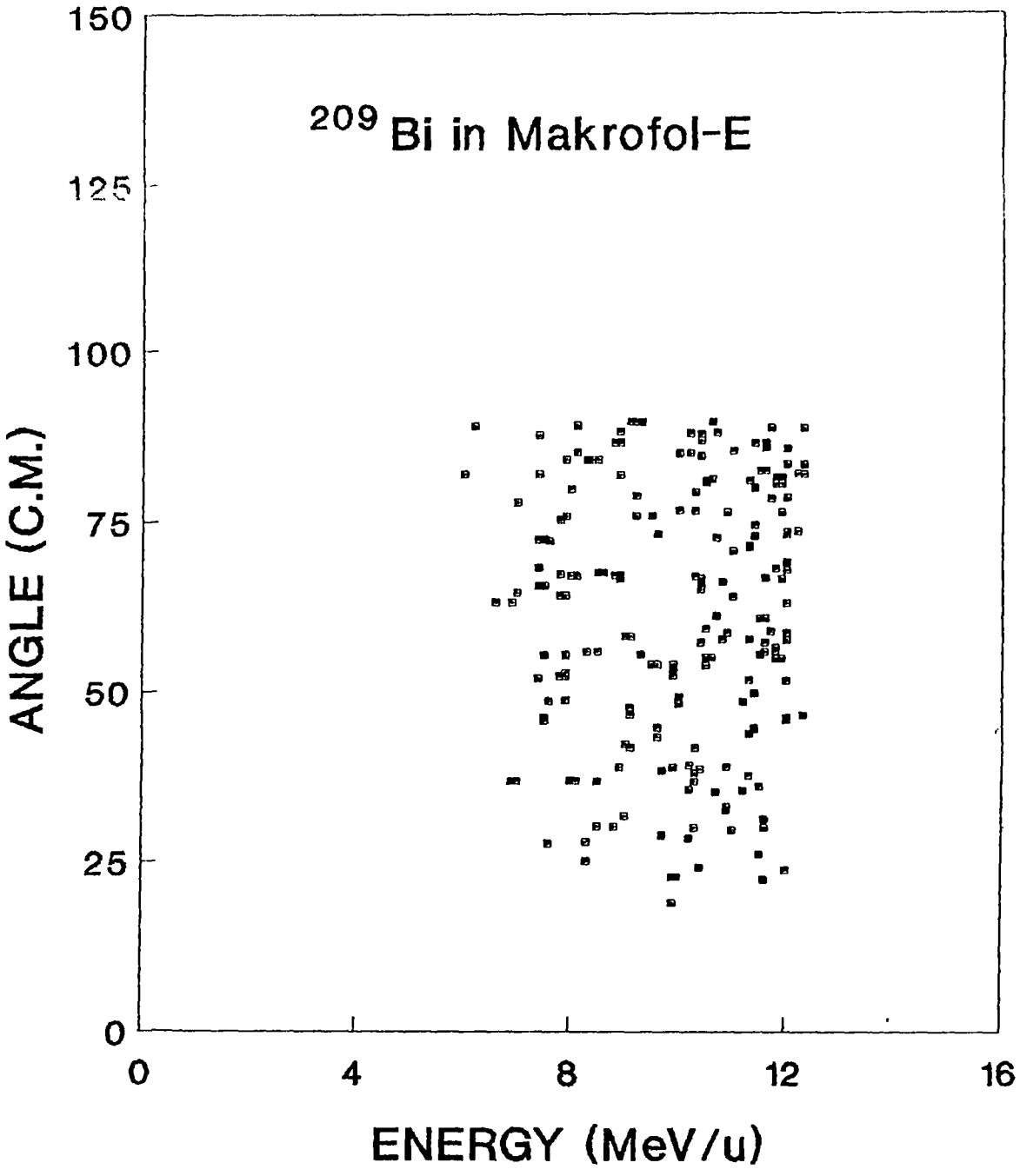

Fig. IV.37 Plot of total opening angle in centre of mass system for ^{209}Bi in Makrofol-E.

projectile in Makrofol-E such three pronged events were not observed probably due to the fact that the registration threshold of Makrofol-E is higher than the maximum energy deposition rate of the lighter particles (such as α particles). The assumption for the α-particle emission or evaporation from the compound nuclei is due to the following observation.

(i) In **Figs. IV.1 - IV.5** the resonance peaks are observed at 2.4 MeV/u apart in laboratory system. The 2.4 MeV/u in the laboratory system corresponds to 28 MeV in the centre of mass for ($^{238}U + ^{12}C$) as shown in **Fig. IV.38**. On the basis of binding energy per nucleon criteria this can be attributed to the emission of a cluster of 4 nucleons or multiples of 4 nucleons from the excited compound nuclei.

In CR-39 16 such events were found to be appropriate for measurement. Different parameters of the third prongs were measured and they have been analyzed in terms of their true lengths, emission angles with respect to beam direction in the forward or backward hemisphere. The different measured parameters for the third prong along with the derived parameters using the equations of chapter II (Section II. 6) for all the 16 events have been tabulated in **Table IV. 14. Fig. IV. 39** is a photomicrograph of the ninth event in **Table IV.14**.The measured length of the third prong is 13.44 μm and it lies in the third quadrant. The actual length of the third prong is 19.24 μm. It lies in the forward hemisphere and makes an angle of 338.5° with the beam direction.

From the distributions of these prongs, it has been observed that four out of sixteen such prongs were created by the emission of particles in the backward hemisphere. The evaporation of neutrons and charged particles like protons and α-particles from excited compound nuclei ($^{16}O + ^{23}U$ **[60, 61, 62]** and $^{12}C + ^{238}U$ **[63, 64]**) have already been reported on the basis of theoretical assumptions and experimental evidences. But as the nuclear track detectors

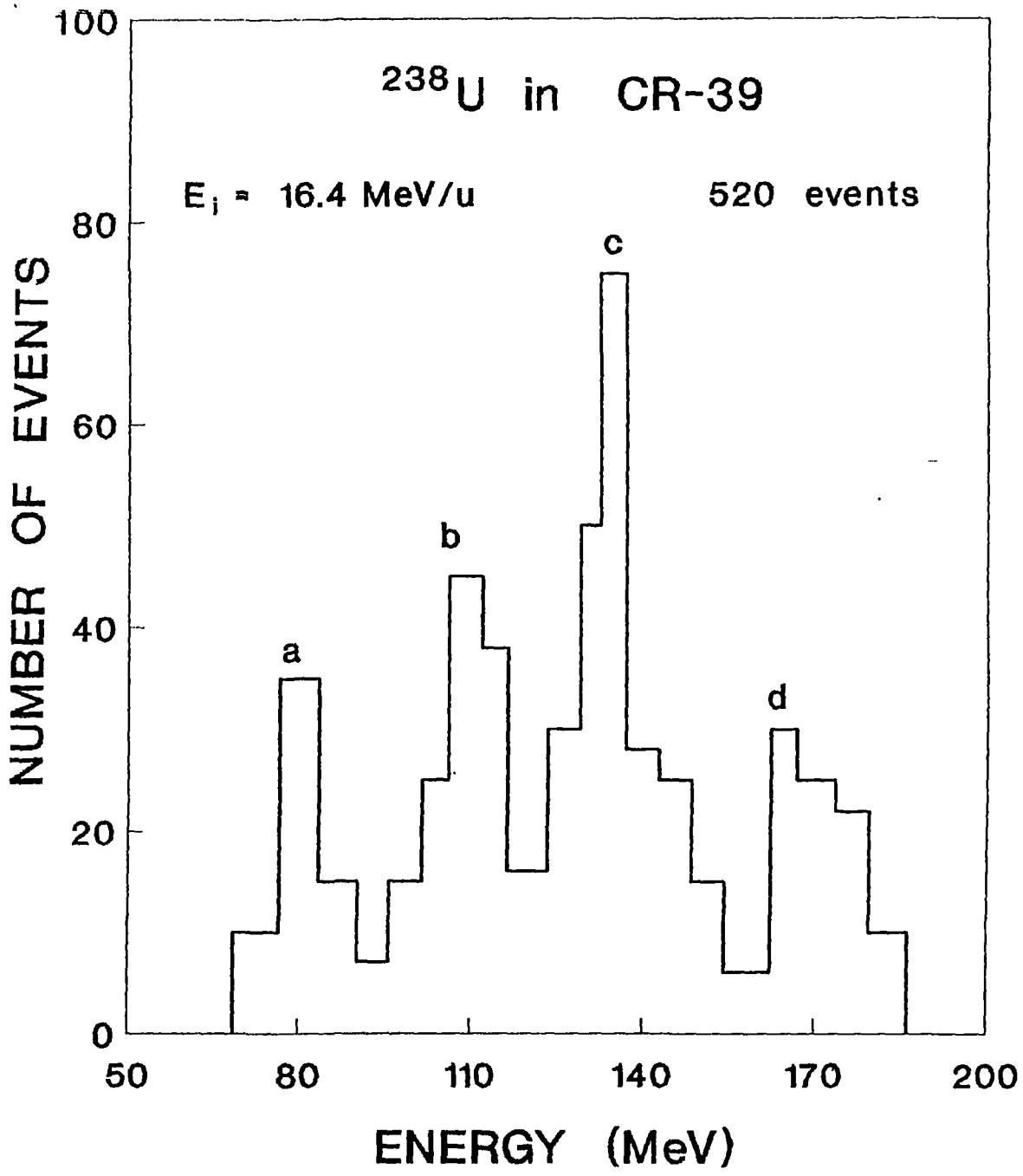

Fig. IV.38 Plot of number of events as a function of centre of mass energy (^{238}U +^{12}C) for ^{238}U of 16.4 MeV/u in CR -39.

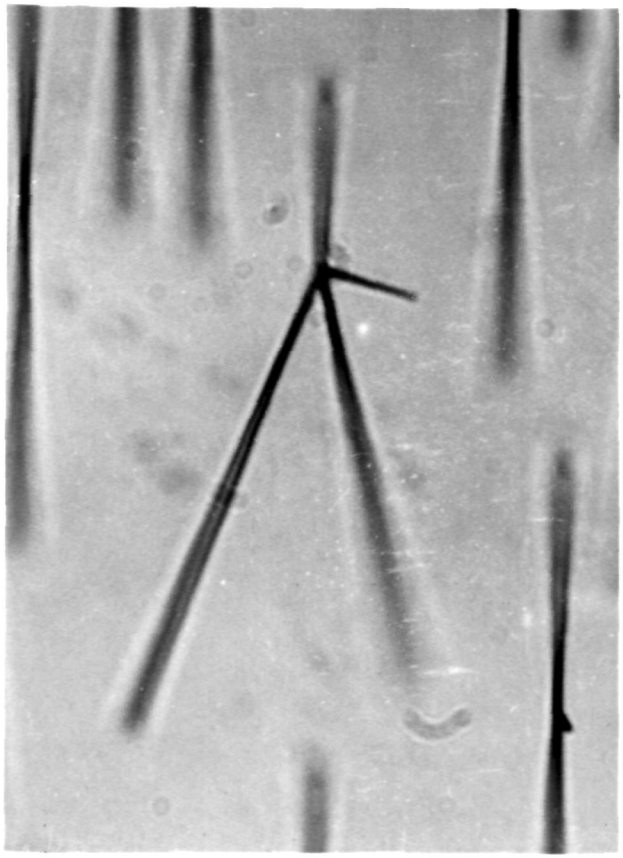

Fig. IV.39 A photomicrograph showing the ninth event of **Table IV.14**. The length (L_P) of the third prong is 19.24 μm. This prong is created by a particle emitted in the forward hemisphere at an angle (θ_P) of 338.5° with respect to the beam direction.

are insensitive to neutrons, charged particles like ^{4}He evaporated from the excited compound nuclei can be recorded. Fuchs et. al. **[65]** have reported that the α-particles emitted in the backward direction is entirely due to evaporation. Again Canto **[66]** have reported that the coulomb field of the outgoing fission fragments steers alphas in the perpendicular direction when particle emission and fission occur in the same time frame. The third prongs for the event nos. 12 and 14 in **Table IV. 14** are in the backward hemisphere. They were formed by the particles emitted at 96.2° and 90.7° with respect to the beam direction respectively. Even though the statistics of these prongs are less, but from the observations of the present study on these third prongs, it appears that the third prongs are due to the evaporation of charge particles from the excited compound nuclei formed by the interaction of the projectile ^{238}U with the nuclei of the atoms present in the detector matrix.

Table IV.14

VALUES OF MEASURED AND DERIVED PARAMETERS OF THE THIRD PRONGS FOR ^{238}U IN CR-39

No.	E_{pf} (MeV/u)	L_P (μm)	Φ_P in degrees	Z_P (μm)	Q_d	L_P (μm)	δ_P in degrees	Θ_P in degrees	DIRECTION (F,B)
1	11.4	4.48	25	0	III	4.48	0	45.0	F
2	13.1	4.48	20	0	III	4.48	0	45.0	F
3	13.5	29.12	10	42.36	IV	51.40	83.2	308.2	F
4	11.4	6.72	0	5.30	III/IV	8.50	90.0	315.0	F
5	15.2	13.44	0	15.90	III/IV	20.80	90.0	315.0	F
6	14.5	4.48	25	7.05	II	8.40	75.0	330.0	F
7	15.4	7.84	60	4.93	III	9.20	35.9	9.1	F
8	6.3	8.96	30	-7.77	III	11.86	60.0	105.0	B
9	9.8	13.44	30	13.77	III	19.24	66.5	338.5	F
10	9.8	5.60	30	10.23	IV	11.66	74.7	299.7	F
11	9.6	6.72	40	1.20	II	6.82	15.5	29.5	F
12	12.6	6.72	25	-3.53	III	7.59	51.2	96.2	B
13	8.2	4.48	30	-3.53	II	5.70	57.6	102.6	B
14	8.6	6.72	50	-3.29	III	8.55	45.7	90.7	B
15	10.8	13.44	15	15.88	II	20.80	77.6	327.6	F
16	9.2	17.92	15	10.60	IV	20.80	66.3	291.3	F

F : FORWARD; B : BACKWARD;

CHAPTER V

CONCLUSION AND FUTURE PERSPECTIVES

CHAPTER V

CONCLUSION AND FUTURE PERSPECTIVES

A simple technique has been developed in order to study the fission of heavy ions and associated particle emissions (evaporation) in Solid State Nuclear Track Detectors in 4π geometry. The technique consists of a geometrical approach followed by computational methods. The computational part is based on the logic of data structures and numerical methods. By this technique it has been possible to study individual events in terms of their different kinematical variables. Besides, few reasonable explanations for the occurence of these fork like events could be found.

The salient features on the analysis of the events are :

(i) Majority of the events (90% - 95%) were identified as fission events.

(ii) Existence of threshold value of energy for these events leads to the conclusion that these events are found due to the interaction of the projectiles with the nuclei of the atoms constituting the detector matrix.

(iii) Excitation function plots show resonances at intervals of 2.4 MeV/u in laboratory system or 28 MeV for $^{238}U + ^{12}C$ in the centre of mass system. Total cross-section is an increasing function of energy and hence these fork like events have been attributed to fusion-fission reactions.

(iv) Total mass of fragments support the formation of compound nuclei **[67 -70]** by the interaction of the projectiles with the nuclei of the atoms constituting the detector matrix.

(v) Q-Values of the reactions indicate the fission of these compound nuclei in the forward hemisphere.

(vi) The fragment mass distributions further support the fission of compound nuclei.

(vii) The most probable values of relative velocity of the fragments also signify the occurence of binary fragmentation (fission) of the compound nuclei.

(viii) The decreasing trend of total opening angle in laboratory system with increase in the energy of the projectile qualitatively indicate the fragmentation of the compound nuclei. Total opening angle in the centre of mass system is isotropic and hence the possibility of quasifission and incomplete fusion can be ruled out as in quasifission and incomplete fission the fragments are emitted in a directional manner **[71,72]**.

(ix) A systematic approach has been developed to study the third prongs observed in these events. The third prongs could be analyzed in terms of their actual track lengths, tilting angles and direction of existence in the forward or backward hemisphere. From the observations in the present study and the earlier reports it can be concluded that these third prongs are created by the

evaporated particles from the excited compound nuclei. The resonance peaks in the excitation function plots and the registration property of CR-39, these particles may be termed as α particles. Due to the poor statistics of these prongs, identification on the basis of residual range vs. track length has not been done.

An event with two evaporated particles was seen for 15.2 MeV/u ^{238}U in CR-39 (**Fig. V.1**). To the best of our knowledge this is the first evidence to show simultaneous evaporation of two particles from excited compound nuclei. Though a rare event but this definitely seems to be an evidence for more than one particle emission from the excited compound nuclei. It further supports the formation of excited compound nuclei and its scission which creates the fork like events and also the third prong due particle evaporation.

The present investigation has opened up a new field of study for the scission of heavy ions in nuclear track detectors. The systematic approach of geometric transformation can be applied in studying the multipronged events created in the 'SSNTD's during nuclear reactions. The program 'HIFISS' can be modified to study the multi-pronged events.

The systematic approach developed can now be utilized in the study of nuclear reactions in 4π geometry where the target itself can act as a detector. Inspite of the inherent measurement inaccuracies the technique is very simple, accurate and reliable. The effect of detector composition on the resonance peaks can be studied by using detectors of varying chemical compositions such as Mica, SR-86, ZnP-Glass, Cellulose Nitrate. As the systematic approach for the analysis of the evaporated particles have been developed, it can now be utilized for particle evaporation study with newer detector systems which can detect multi-particle evaporation with better efficiency.

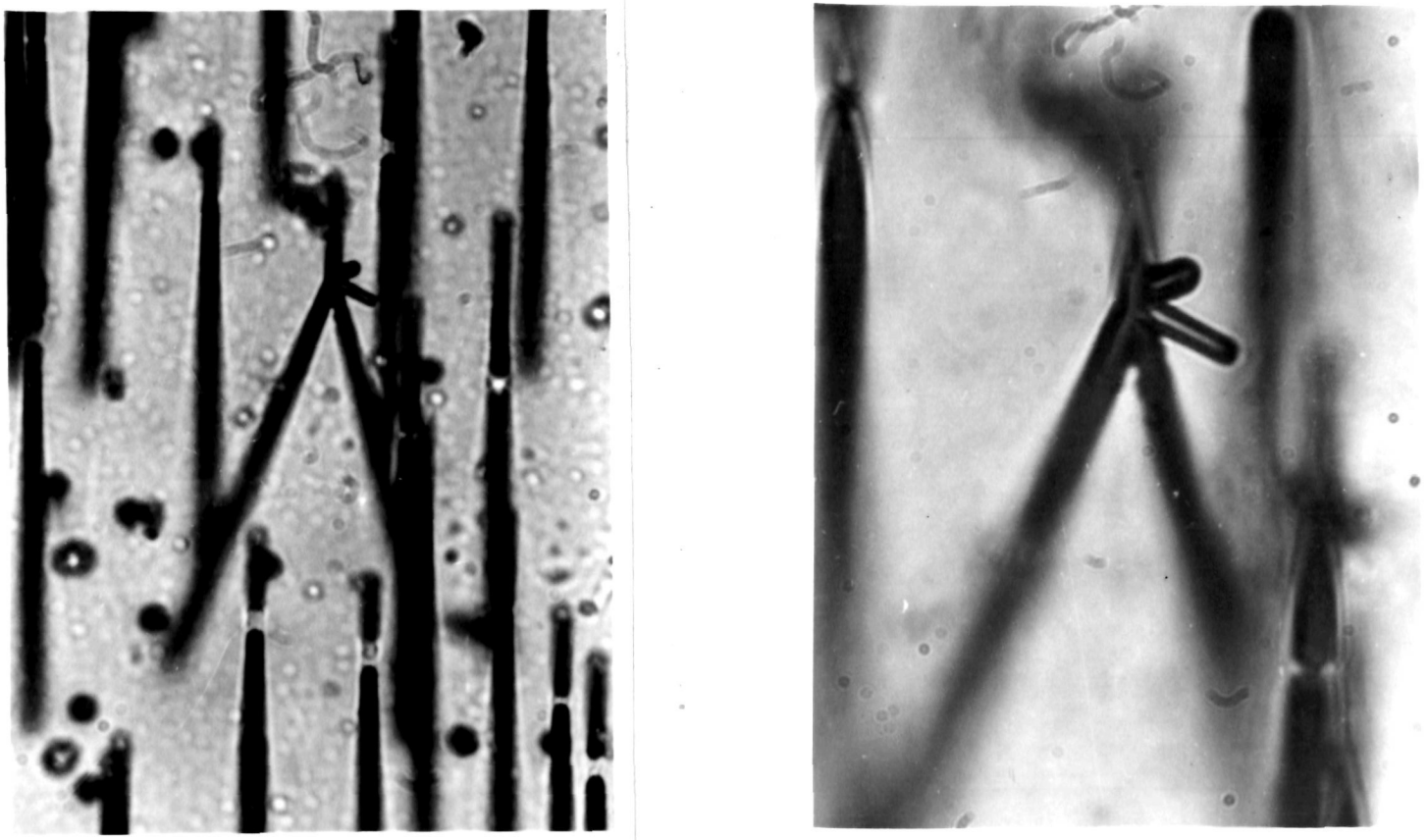

Fig. V.1 Two photomicrographs of the same event showing multiparticle emission in CR-39 irradiated to 15.2 MeV/u ^{238}U.

REFERENCES

1. R.L. Fleischer, P.B. Price and R.M. Walker,
"Solid State Track Detectors: Applications to Nuclear Science and Geophysics",
Ann. Rev. Nucl. Sci., **15** (1965) 1-28(and references therein).

2. P.B. Price and R.L. Fleischer,
"Identification of Energetic Heavy nuclei with Solid Dielectric Track Detectors : Application to Astrophysical and Planetary studies",
Ann. Rev.Nucl. Sci., **21** (1971) 295-334. (and references therein).

3. R.L. Fleischer, P.B. Price and R.M. Walker,
"Nuclear Tracks in Solids : Principles and applications", Univ. of California Press, California (USA) (1975).

4. R.L. Fleischer, P.B. Price, R.M. Walker and M. Maurette,
"Origins of Fossil Charged-Particle Tracks in Meteorites",
J. Geophys. Res., **72** (1967) 331-353.

5. R.L. Fleischer, H.R. Hart and G.M. Comstock,
"Very heavy solar cosmic rays: Energy spectrum and implications for lunar erosion",
Science, **171** (1971)1240-1242.

6. R.L. Fleischer, J.R.M. Viertil, P.B. Price and F.Aumento, "A Chronological test of ocean bottom spreading in the North Atlantic",
Rad. Effects, **11** (1971) 193-194.

7. R.L. Fleischer, R.M. Walker and L.S.B. Leakey,
"Fission track dating of a Mesolithic knife",
Nature, **205**(1965) 1138.

8. R.L. Fleischer, P.B. Price, E.M. Symes and D.S. Miller
"Fission track ages and track-annealing behaviour of some micas",
Science, **143** (1964) 349-351.

9. B.E. Fischer and R. Spohr,
"Production and use of Nuclear Tracks: Imprinting Structure on solids ",
Rev. Mod. Phys., **55** (1983) 907-948.

10. R. Beaujean, W. Enge, G. Siegmon, J. Krause and E. Fischer,
"Isotopic stack : Measurement of heavy cosmic rays",
Science, **225** (1984)194.

11. C.Trautmann, R. Spohr, J. Vetter, G. Eska and Y. Hirayoshi,
"Search for Superfluid Josephson effect",
Nucl. Tracks Radiat. Meas., **19** (1991) 967-990.

12. R. Spohr, " Ion tracks and microtechnology; Principles and applications", Vieweg Verlags, Braunschweig (Germany). (1990).

13. B.E. Fischer and R. Spohr,
"Heavy Ion Microlithography - a new tool to generate and investigate submicroscopic structures",
Nucl. Instrum. and Meth., **168** (1980) 241-246.

14. A.F. Hafez and G. Somogyi,
"Determination of radon and thoron permeability through some plastics by track technique",
Nucl. Tracks Radiat. Meas., **12**, (1986), 697-700.

15. R. Guillet, J. Vetter, B. Koutsouris, T. Benzard, M. Boynard,
"Individual Red blood cell (RBC) transit analysis through size micropores of oligopore filters: Application to RBC Subpopulations",
Nucl. Tracks Radiat. Meas., **19** (1991) 895-898.

16. P.A. Gottschalk, G. Grawert, P. Vater and R. Brandt,
"Two, three and four particle exit channels in the reaction (806 MeV) Kr+U",
Phys. Rev. C, **27** (1983) 2703-2719.

17. R. Brandt, P.A. Gottschalk and P. Vater,
"An application of SSNTD to nuclear physics: multipronged events in heavy ion reaction due to multiple sequential fission",
Nucl. Instrum. and Meth. , **173** (1980) 111-119.

18. R. Hagg, G. Fiedler, R. Ulbrich and G.Breitbach, P.A. Gottschalk,
"Fragment correlations in the reaction 9.03 MeV/u ^{238}U + ^{nat}U",
Z. Phys. A, **316** (1984) 183-193.

19. J. Ralarosy, M. Debeauvais, J.C. Adloff, M. Zamani, F. Fernandez, S. Jokic and Z. Todorovic,
"Interpretation of 3-pronged events for ^{238}U + Au reaction registered within CR-39 SSNTD,"
Nucl. Tracks Radiat. Meas., **19** (1991) 651-654.

20. C. Brechtmann and W. Heinrich,
"Fragmentation Crosssections of ^{28}Si at 4.5 GeV/nucleon",
Phys. Rev. C, **7** (1989) 2222-2226.

21. A. Hoffmann, C. Brechtmann, W. Heinrich,
"Search for projectile fragments with fractional charge in relativistic heavy ion collisions",
Phys. Lett. B, **200** (1988) 583-586.

22. C. Brechtmann and W. Heinrich,
"Fragmentation Cross section of ^{32}S at 0.7, 1.2 and 200 GeV/nucleon",
Z. Phys. A, **331** (1988) 463-472.

23. A. Murakami,
"A new method for particle identification on light nuclear charged particles by means of a solid-state track detector",
Nucl. Instrum. and Meth., **111** (1973) 567-579.

24. J. Charvat and F. Spurny,
"The (D-D) fusion reaction products identification using the CR-39 track detectors ",
Nucl. Tracks Radiat. Meas., **19** (1991) 585-589.

25. M. Calicchio et. al.,
"The track-etch detector of the MACRO experiment",
Nucl. Tracks Radiat. Meas., **15** (1988) 331-336.

26. L. Patrizi et. al.,
"Improvements in the CR-39 polymer for the MACRO experiment at GRAN SASSO laboratory",
Nucl. Tracks Radiat. Meas., **19** (1991) 641-646.

27. J.P. Unik, E.P. Horwitz, K.L. Wolf, I. Ahmad, S. Fried, D. Cohen, P.R. Fields, C.A.A. Bloomquist, D.J. Henderson,
"Production of actinides and the search for super-heavy elements using secondary reactions induced by GeV protons",
Nucl. Phys. A, **191** (1972) 233-244.

28. P.B. Price, J.D. Stevenson, S.W. Barwick and H.L. Ravn,
"Discovery of Radioactive decay of ^{222}Ra and ^{224}Ra by ^{14}C emission",
Phys. Rev. Lett., **54** (1985) 297-299.

29. S.W. Barwick, P.B. Price and J.D. Stevenson,
"Radioactive decay of ^{232}U by ^{24}Na emission",
Phys. Rev. C, **31** (1985) 1984-1986.

30. M.H.Salamon, P.B. Price, M. Tincknell, Shi-Lun Guo and G. Tarle,
"Charge resolution of Plastic track detectors used to identify relativistic nuclei",
Nucl. Instrum. and Meth., **B6** (1985) 504-512.

31. S. Ghosh, Atul Saxena and K.K. Dwivedi,
"Range and energy-loss of 16.34 MeV/u ^{238}U in Kapton Polyamide",
Rad. Eff. Def. in solids, **112** (1989) 149-153.

32. K.K. Dwivedi,
"Range and energy-loss measurement of heavy ions by a nuclear track technique",
Nucl. Tracks Radiat. Meas., **19** (1991) 71-76 (and references therein).

33. S. Ghosh, J.Raju, P.P. Choubey and K.K. Dwivedi,
"Characterisation of overhead projector transparency as nuclear track detector",
Nucl. Tracks Radiat. Meas., **19** (1991) 77-78.

34. J. Raju, K.K. Dwivedi and M. Fujii,
"Response of a new track detector (SR-90) to alpha and fission fragments", Presented in Eighth National Symposium on Solid State Nuclear Track Detectors, Oct. 27-29,1993, AMU, Aligarh, India.

35. J. Raju, S. Ghosh, A. Saxena and K.K. Dwivedi,
"Response of 350 Mev ^{90}Zr ions of Polycarbonate detectors",
Nucl. Instrum. and Meth., **51** (1990) 168-172.

36. J. Raju, S. Ghosh, A. Saxena and K.K. Dwivedi,
"Calibration of CR-39 and ZnP-Glass detector with 350 MeV ^{90}Zr ions",
Meas. Sci. Technol., **1** (1990) 903-907.

37. J. Raju and K.K. Dwivedi,
"V_T (Track etch rate): reflection of total energy-loss rate (dE/dx) for ^{238}U in CR-39",
Nucl. Tracks Radiat. Meas., 000 (1993) 000, (In press).

38. K.K. Dwivedi and G. Fiedler,
"Detection of evaporated α-particle during the passage of 3.89 GeV ^{238}U in CR-39 detector",
Nucl. Tracks Radiat. Meas., **15** (1988), 353-356.

39. J. Raju and K.K. Dwivedi,
"Computer based analysis of Nuclear Track Data: I and II",
Proceedings of the 7th National Conference on Particle Tracks in Solids, Jodhpur, India, (1991), 200-216.

40. Phillip R. Bevington,
"Data reduction and error analysis for physical sciences",
Mcgraw-Hill Book Company, London (U K), (1969).

41. Jeffrey K. Johnson,
"Numerical methods in Chemistry", Marcel and Dekker Inc.,
New York (USA), 1980).

42. James J. Cooper,
"Introduction to Pascal for Scientists",
Wiley-Intersciences Publications, New York (USA),(1973).

43. James J. McGregor, Allan H. Watt,
"Pascal for Science and engineering",
Galgotia Publications Pvt. Ltd., New Delhi (India),(1989).

44. Steven C. Chapra and Raymond P. Canale,
"Numerical Methods for engineers with personal computer applications",
Mcgraw-Hill Book company, London (U K), (1985).

45. H. Horowitz and S. Sahni,
"Fundamentals of data structures in Pascal",
Galgotia Publications, New-Delhi (India),(1983).

46. V.E. Viola,
Nucl. Data Sect. A, **1**(1966) 391.

47. V.E. Viola,
"Systematics of fission fragment total kinetic energy release",
Phys. Rev. C, **31** (1985) 1550-1551.

48. R. Vandenbosch and J.R. Huizenga,
"Nuclear Fission",
Academic Press, New York (USA), (1973).

49. A. Waheed, G. Moschini, H.A. Khan, R. Cherubini,
L. Lembo and A.M.I. Haque.
"Registration of low energy protons in CR-39 for use in fast neutron dosimetry",
Nucl. Tracks Radiat. Meas., **15** (1988) 129-133.

50. H.A. Khan, R. Brandt, N. Khan and K. Jamil,
"Track registration and development characteristics of CR-39 plastic track detector",
Nucl. Tracks, **7** (1983) 129-133.

51. B. Dörschel, A. Guhr, M. Mansy, P. Schmidt and G. Strenbel,
"Proton detection properties of CR-39 made in GDR",
Nucl. Tracks Radiat. Meas., **19** (1991) 155-159.

52. H. Dreschel, C. Brechtman, W. Heinrich, J. Dreute and E.V. Benton,
"Search for anomalous fragments produced in collisions with heavy target nuclei and in Z = 1 peripheral interactions",
Phys. Rev. Lett., **55** (1985) 1258-1264.

53. C. Brechtman and W. Heinrich,
"Fragmentation Cross sections of ^{16}O at 60 and 200 GeV/Nucleon",
Z. Phys. A, **330** (1988) 407-416.

54. C. Brechtman and W.Heinrich,
"Measurement of elemental fragmentation cross section for relativistic heavy ions using CR-39 plastic nuclear track detectors",
Nucl. Instrum. and Meth., **29** (1978) 675-679.

55. B.G. Cartwright, E.K. Shirk and P.B. Price,
"A nuclear Track recording polymer of Unique sensitivity and resolution ",
Nucl. Instrum. and Meth., **153** (1978) 475-460.

56. M. Sohrabi and E. Khajeian,
"Some electrochemical etching studies on the registration of alpha particle tracks in polycarbonate",
Nucl. Instrum. and Meth., **185** (1981) 407-413.

57. M.F. Cesar and M.A.R. Franco,
"Some studies on the registration of particles on Makrofol-E",
Nucl. Tracks Radiat. Meas., **12** (1986) 193-196.

58. G. Somogyi, I. Hunyadi, E. Koltay and L. Zolnai,
"On the detection of low-energy ^{4}He, ^{12}C, ^{14}N, ^{16}O ions in PC foils and its use in nuclear reaction measurement",
Nucl. Instrum. and Meth., **147** (1977) 287-295.

59. Dr. Jhannes Heidenhain,
"Operating Instruction Manual", VRZ 210, CERTO COUNTER, Postfach 1260, D-8225, Traunruet, Germany (1985).

60. H. Homeyer, U. Jahnke, G. Ingold, M. Bürgel, H. Fuchs and D. Hilscher,
"Two different sources of fast forward-emitted α- particles in Heavy - ion reaction"
Z. Phys. A, **314** (1983) 143-147.

61. John M. Alexander, Daniel Guerreau and L,C. Vaz,
"Evaporation barriers for ^{4}He indicate very long extended forms for many emitting nuclei",
Z. Phys. A, **305** (1982) 313-318, (and references there in).

62. A. Iwamoto and R. Herrmann,
"Evaporation of charged particles from highly deformed nuclei",
Z. Phys. A, **338** (1991) 303-307.

63. T. Sikkeland, J. Maly amd D.F. Lebeck,
"Evaporation of 3 to 8 neutrons in reactions between ^{12}C and various Uranium nuclides",
Phys. Rev., **169** (1968) 1000-1006.

64. T. Sikkeland, Stanley Thompson and A. Ghiorso,
"Reactions of Uranium -238 with Carbon Ions",
Phys. Rev., **112** (1958) 543-547.

65. H. Fuchs, M. Bürgel, H. Homeyer, G. Ingold, U. Jahnke and G. Thoma,
"Production of fast α-particles in $^{20}Ne + {}^{197}Au$collision studied by counting the simultaneous emitted neutrons",
Phys. Rev. C, **31** (1985) 465-472.

66. L.F. Canto, R. Donangelo and L.F. Oliveria,
"Fission mechanism of 0.2 TeV Uranium beams",
Phys. Rev. C, **35** (1985) 2175-2183.

67. J. Toke, R. Bock, DAI Guang-xi, A. Gobbi, S. Gralla, K.D. Hilderbrand, J. Kuzminski, W.F.J. Müller, A. Olmi, W. Reisdorf,
"Compound nucleus fission and quasi-fission in reactions of ^{238}U with ^{16}O and ^{77}Al",
Phys. Lett., **142** (1984) 258-262.

68. J.J. Hogan, D.J. Parker, J. Asher,
"Fission following complete or incomplete fusion of 135 MeV ^{16}O and ^{238}U",
Z. Phys. A, **33** (1991) 325-337.

69. W. Bohne, H. Morgenstern, K. Grabisch, T. Nakagawa and S. Proschitzki,
"Critical excitation energy in fission evaporation reactions",
Phys. Rev. C, **41** (1990) R5-R8.

70. V.E. Viola Jr. B.B. Back, K.L. Wolf, T.C. Awes, C.K. Gelbke and H. Breuer,
"Linear momentum transfer in non-relativistic nucleus- nucleus collisions",
Phys. Rev. C, **26** (1982) 178-188.

71. B.B. Back, R.R. Betts, K. Cassidy, B.G. Glagola, J.E. Gindler, L.E. Glendenin and B.D. Wilkins,
"Experimental signature of quasifission reactions",
Phys. Rev. Lett., **50** (1983), 818-821.

72. A. Gavron, P. Eskola, A.J. Sierk, J. Boissevain, H.C. Britt, K. Eskola, M.M. Fowler, H. Ohm, J.B. Wilhelmy, S. Wald, R.L. Ferguson,
"New evaluation of fission fragment angular distribution in heavy-ion reactions",
Phys. Rev. Lett., **52** (1984) 589-592.

APPENDIX A

COMPUTER CODE 'TRANSCORD'

The computer program **'TRANSCORD'(TRANSformation of Co-ORDinate)** has been developed to carry out the first step of analysis in the study of heavy ion fission in SSNTDs. The code has been developed in high level language 'FORTRAN'. It has two subroutines 'PXY' and 'ACTCAL'. This program is used to calculate the actual values of different parameters of the events from the projected (measured) parameters. The equations used are the ones described in chapter II. The source code occupies small memory space (< 10 kB). Two output files can be generated by this program. One to record all the parameters of the events in detail, while the other to be used as an input file for the program 'HIFISS' i.e. the second step of analysis. The listing of the program 'TRANSCORD' is given here.

```
      PROGRAM  TRANSCORD
C     ************************************************************
C     PROGRAM  TO COMPUTE THE VALUES OF REAL PARAMETERS
C     OF THE EVENTS  FROM  THE  MEASURED  PARAMETERS
C     ************************************************************
      COMMON     D(50,50),K1,L1
      DIMENSION  TLU(200),TL1(200),TL2(200),PHI1(200),PHI2(200)
      DIMENSION  THET1(200),THET2(200),THET3(200)
      DIMENSION  ZA(200),ZB(200),ZM(200)
      DIMENSION  Y(200),Z(200),A(36)
      REAL       ELAB,LU1,T1,T2,THE1,THE2,Z1,Z2,ZFAC,MFAC,REF
      CHARACTER  HEAD3
      INTEGER    NEVENT,J,P,TEMP
 1000 WRITE(*,1)
    1 FORMAT(1H,'INCIDENT ANGLE, Magfn.& Z FACTOR, Refractive
      Index')
      READ(*,*)ALPHA,MFAC,ZFAC,REF
      ALPHA=ALPHA*0.017453293
      WRITE(*,2)
    2 FORMAT(1H,'$ NUMBER OF EVENTS ? ')
      READ(*,*)NEVENT
      WRITE(*,3)
    3 FORMAT(1H,'Name of the Input DATA FILE containing TL,phi,z'/)
C
C   **   INPUT  DATA  FILE  CONTAINS  THE  MEASURED  PARAMETERS  **
C
      OPEN(9,FILE='            ')
      WRITE(*,4)
    4 FORMAT(1H$,'INPUT TLU,TL1,PHI1,TL2,PHI2,ZA,ZB'/)
      DO 5 J=1,NEVENT
      READ(9,*)TLU(J),TL1(J),PHI1(J),TL2(J),PHI2(J),ZA(J),ZB(J)
    5 CONTINUE
      DO 6 J=1,NEVENT
      WRITE(*,*)TLU(J),TL1(J),PHI1(J),TL2(J),PHI2(J),ZA(J),ZB(J)
    6 CONTINUE
C
C     ************************************************************
C     Using the  coefficients from the polynom fit
C     program 'TRAPOL2' calculate the value of pre-fission energy;
C     X  is  constant  throughout  &  input Y
C     ************************************************************
C
      WRITE (*,10)
   10 FORMAT(1H$,'Name of the input file having coeff.:')
      OPEN (10,FILE='      ',STATUS='OLD')
C
      WRITE (*,20)
   20 FORMAT (1H$,'Input the mass of the ion ,format free: ')
      READ(*,*) AMASS
C
      WRITE (*,30)
   30 FORMAT(1H$,'Outpput data file ie. the input for HIFISS:')
      OPEN (12,FILE='      ',STATUS='NEW')
C
      WRITE(*,35)
   35 FORMAT(1H$,'Output file having the parameters in detail')
      OPEN(11,FILE='           ',STATUS='NEW')
C
      WRITE(11,19)
   19 FORMAT(1H$,' No.  LU     ELAB     LA     THETAA   LB  THETAB
     1 DELTAA  DELTAB   ALPHAA   ALPHA   ALPHAB   BETA'/)
```

```
C
      WRITE (*,40)
   40 FORMAT(1H$,'DEG.OF POLYN. IN X-DIR. AND Y-DIR.: K,L:')
      READ (*,41) K,L
   41 FORMAT(2I2)
      WRITE(*,40)
      WRITE(*,41) K,L
C
      K1=K+1
      L1=L+1
      P=K1*L1
      TEMP=K1
C
      DO 51 I = 1,P
      READ (10,50) A(I)
   50 FORMAT(E16.7)
   51 CONTINUE
      WRITE(*,60)
   60 FORMAT(1H$,'The values of coefficients are :')
C
C     CONVERTS THE COEFFICIENT MATRIX IN TO REQUIRED FORM
C     concept of memory mapping ; convesion of one type
C     of  data  structure to the other type
C
      DO 150 I=1,K1
      M=I
      DO 150 J=1,L1
      D(I,J)=A(M)
      M=M+TEMP
      WRITE(*,70) D(I,J)
   70 FORMAT(E16.7)
  150 CONTINUE
C
      DO 200 I=1,NEVENT
      TLU(I)=(TLU(I)*FAC/COS(ALPHA))
  200 Z(I)=PXY(AMASS,TLU(I))
C
C
      DO 250 J=1,NEVENT
      T1=TL1(J)*FAC
      T2=TL2(J)*FAC
      PHI1(J)=180.0-PHI1(J)
      PHI2(J)=PHI2(J)-180.0
      ZA(J)=ZA(J)*REF
      ZB(J)=ZB(J)*REF
      WRITE(*,*) PHI1(J),PHI2(J),T1,T2
      THE1=PHI1(J)*0.017453293
      THE2=PHI2(J)*0.017453293
      Z1=ZA(J)
      Z2=ZB(J)
      ELAB=Z(J)
      LU1=TLU(J)
      CALL ACTCAL (J,LU1,T1,THE1,T2,THE2,Z1,Z2,ALPHA,ELAB,NEVENT)
  250 CONTINUE
C
      CLOSE(9)
      CLOSE(10)
      CLOSE(11)
      CLOSE(12)
      WRITE(*,80)
   80 FORMAT(1H$,'Resume Calculation (Y/N) ? ')
```

```
      READ(*,90) HEAD3
 90   FORMAT (A1)
      IF (HEAD3.EQ.'Y') GOTO 1000
      STOP
      END
C
C
      FUNCTION PXY(AMASS,X)
C
C     PXY calculates the value of polynom in the way shown
C
C            P(X,Y)= A(1,1) +A(1,2)Y +.....+A(1,L+1)Y^L
C                  +A(2,1)X+A(2,2)XY+.....          .
C                     .                             .
C                     .                             .
C                     .                  +A(K+1,L+1)X^K*Y^L
C
C      (K=K1-1, L=L1-1)
C
      COMMON     D(50,50),K1,L1
      DIMENSION  U(20),V(20)
C
      DO 1 I=1,K1
 1    U(I)=E(AMASS,I-1)
      DO 2 I=1,L1
 2    V(I)=E(X,I-1)
C
      PXY=0.
      DO 3 I=1,K1
      DO 3 J=1,L1
 3    PXY= PXY+D(I,J)*U(I)*V(J)
C
      RETURN
      END
C
C
      FUNCTION E(X,N)
C
      E=1.0
      IF(N.EQ.0) RETURN
C
      DO 2 I=1,N
 2    E=E*X
      RETURN
      END
C
      SUBROUTINE ACTCAL(J,LU1,T1,PHI1,T2,PHI2,Z1,Z2,ALPHA,
     1 ELAB,NEVENT)
C  **  CALCULATION OF  REAL PARAMETERS     **
      REAL   LU1,A1,A2,A3,B1,B2,B3,TL1,TL2,THE1,THE2,ZA,ZB
      REAL   DELTAA,DELTAB,THETA1,THETA2,C1,C2,D1,D2
      REAL   ALPHAA,ALPHAB,A,BETA,LA,LB,LR1,LR2
      RAD=0.017452393
      TL1=T1
      TL2=T2
      THE1=PHI1
      THE2=PHI2
      ZA=Z1
      ZB=Z2
      A=ALPHA
C
```

```
      A1=TL1*COS(THE1)*TAN(A)
      A2=ZA
      A3=TL1*SIN(THE1)/COS(A)
      DELTAA=ATAN((A1-A2)/A3)
C     WRITE(*,*) A1,A2,A3,DELTAA
C
      B1=TL2*COS(THE2)*TAN(A)
      B2=ZB
      B3=TL2*SIN(THE2)/COS(A)
      DELTAB=ATAN((B1-B2)/B3)
C
      ALPHAA=ATAN(ZA/TL1)
      ALPHAB=ATAN(ZB/TL2)
C
      C1=TL1*SIN(THE1)*SIN(ALPHAA)
      C2=ZA*COS(ABS(DELTAA))
      THETA1=(ASIN(C1/C2))/RAD
C
      D1=TL2*SIN(THE2)*SIN(ALPHAB)
      D2=ZB*COS(ABS(DELTAB))
      THETA2=(ASIN(D1/D2))/RAD
C
      LA=ZA/SIN(ALPHAA)
      LB=ZB/SIN(ALPHAB)
C
      DELTAA=DELTAA/RAD
      DELTAB=DELTAB/RAD
      ALPHAA=ALPHAA/RAD
      ALPHAB=ALPHAB/RAD
      BETA=180-(ABS(ABS(DELTAA)-ABS(DELTAB)))
      A=A/RAD
C
      A1=TL1*SIN(THE1)
      A2=SIN(THETA1)*COS(DELTAA)
      LR1=A1/A2
C
      A1=TL2*SIN(THE2)
      A2=SIN(THETA2)*COS(DELTAB)
      LR2=A1/A2
C
C
C   **  STORING ALL  THE OUTPUT  VALUES  IN  DETAIL **
C
      WRITE(11,20)J,LU1,ELAB,LA,THETA1,LB,THETA2,DELTAA,DELTAB,
     X ALPHAA,A,ALPHAB,BETA
 20   FORMAT(1H,I3,2X,F6.2,F8.2,2X,10F8.2)
C
C   **  STORING  ONLY THE  OUTPUT VALUES REQUIRED  AS AN INPUT FOR
C       'HIFISS'     **
C
      WRITE(12,30)LA,THETA1,LB,THETA2,ELAB
 30   FORMAT(1X,4F7.2,F10.2)
      RETURN
      END
```

APPENDIX B

COMPUTER CODE 'HIFISS'

The application program 'HIFISS' **(Heavy ion FISSion)** has been developed in order to carry out the second step of analysis in the study of heavy ion fission in SSNTDs. The source code once again has been developed in 'FORTRAN', which occupies a memeory space of < 25 kB. The subroutines and functions used in the program are explained in **Fig. II.12**. The first step in the computation is the determination of masses in the two exit channels of scission by applying the logic of 'BINARY SEARCH' in the dynamic mode. Then it computes the other kinematic variables of an event. The listing of the source code **'HIFISS'** is given here.

```
C
      PROGRAM HIFISS
C     ************************************************************
      PROGRAM FOR THE ANALYSIS  OF TWO PRONGED EVENTS IN TERMS
                 OF  DIFFERENT  KINEMATIC  VARIABLES
      ************************************************************
C     HIFISS.FOR
      DIMENSION    NCNTRL(10),NPRINT(10),NERROR(10)
      DIMENSION    A0(5),A1(5),A2(5),XIN(500,6),C(15),AC(15)
      DIMENSION    VV(100),RR(100),E1(3),E2(3),A(10)
      DIMENSION    PIN(3),VE1(3),VE2(3),VE12(3),RES(3)
C
      REAL         MP,MT,M1,M2,M12,MTOT,V12,EF1,EF2
      INTEGER      IEV,NDIM,NX,L
      CHARACTER*25 HEAD,HEAD1,HEAD2
C
      COMMON       /PROVAR/NCNTRL,NPRINT,NERROR,IER
      COMMON       /INTPOL/VV,RR,IQDIM
      COMMON       /RANGE/R1,R2,R3,R4,R5
      COMMON       /VELCOF/C,FA
      COMMON       /FITCOF/A0,A1,A2
      COMMON       /PRINT/IP1,IP2,IP3,IP4,IP5,IP6,IP7,IMASS
C
      DATA         RAD/0.017453293/,ZH15/32767.0/
C
      WRITE (*,1)
  1   FORMAT (1H,10X,'PROGRAM HIFISS', 26X,/)
C
C   *  FEED THE VALUES  *
      WRITE(*,2)
  2   FORMAT(1H,'  NUMBER  OF  EVENTS & SAMPLE NUMBER:' )
      READ(*,110)NDIM,HEAD2
 110  FORMAT(I5,A25)
      WRITE(*,3)
  3   FORMAT(1X,' MASS OF THE PROJECTILE :')
      READ(*,*)MP
      WRITE (*,201)
C
C  *   ONLY FOR SIMULATION   *
C
 201  FORMAT(1X,'IS THE FISSION SYMMETRIC ?  Y/N ')
      READ(*,202)HEAD1
 202  FORMAT(A25)
      WRITE(*,202)HEAD1
      IF (HEAD1.EQ.'N') GO TO 203
      GO TO 205
 203  WRITE(*,204)
 204  FORMAT(1H$,'INPUT M1 M2')
      READ(*,*)M1,M2
      WRITE(*,*)M1,M2
 205  WRITE(*,4)
  4   FORMAT(1X,'Number  of Elements  in the  Media')
      READ(*,*)NX
      WRITE(*,5)
  5   FORMAT(1X,'Masses  of  the Elements in the Media')
      READ(*,*)(A(I),I=1,NX)
      MX=NX+1
      MT=0.0
      DM=0.0
      MTOT=MP+MT-DM
      WRITE (*,6) MP,MT,DM,MTOT
  6   FORMAT (1H,10X,'ELAB IS VARIABLE (MeV)'/1H,10X
     ,'MP=',F6.1,'AMU',5X,'MT=',F6.1,'AMU',5X,'DM=',F6.1
```

```
     ,'AMU',5X,'MTOT=',F6.1,'AMU')
C
      WRITE(*,7)
  7   FORMAT(/,1X,'INPUT THE FILE HAVING COEFF MASS & VEL
      RELATED',/)
      OPEN (14,FILE='            ',STATUS='OLD')
      READ(14,8)(AC(I),I=1,15)
  8   FORMAT(E16.7)
      L=1
      DO 100 J=1,5
      A0(J)=AC(L)
      A1(J)=AC(L+1)
      A2(J)=AC(L+2)
      L=L+3
 100  CONTINUE
      WRITE(*,9)
   9  FORMAT(1X,'IP7=1/0 Pin=0 IF 1; IMASS=1/0 1 IF Mass cons')
      READ(*,10)IP7,IMASS
  10  FORMAT(2I3)
      WRITE(*,10)IP7,IMASS
C
      WRITE (*,11)
  11  FORMAT (1X,'NAME OF THE MATERIAL: ')
      READ (*,12) HEAD
  12  FORMAT (A25)
      WRITE (*,13)
  13  FORMAT (1H,'Name of the Output file? Unit 8',/)
      WRITE (8,801)
  801 FORMAT (1H,10X,'PROGRAM  H I F I S S',/)
C
      WRITE (8,802) MP,HEAD,HEAD2
  802 FORMAT(//,10X,'FISSION OF ',F7.2,'-X IN
     1',A25,'SAMPLE:'A25,//)
      WRITE (8,803) NDIM
  803 FORMAT (1H,10X,' NUMBER OF EVENTS: ',I5//)
      WRITE (*,101)
  101 FORMAT (1H,'Name of the Output file WITH Q VALUES? Unit 10',/)
      OPEN(10,FILE='            ',STATUS='NEW')
C
C  *   MASS CALCULATION LOOP   *
C
      WRITE(8,804)
  804 FORMAT(1H,1X,'EVENTNO.',1X,'EI(MeV/u)',4X,'M1',6X,'E1'
     ,6X,'M2',
     1,6X,'E2',6X,'MTOT',4X,'ETOT',4X,'Q-VALUE',3X,'V-REL.',2X
     1,'ASSY.PARA.',2X,'ETA12',3X,'SCAT-ANG(CM)')
C
      WRITE(8,805)
  805 FORMAT (1H, 1X,'------',3X,'-------',6X,'----',3X,'----'
     1,4X,'-----',2X,'------',4X,'-----',3X,'------',3X,'-------',3X
     1,'------',3X,'------',4X,'------',3X,'------------',)
C
C
      WRITE(*,14)
  14  FORMAT(1H,'Name the input file containing data; unit 9 ')
      OPEN(9,FILE='            ')
C
      WRITE (10,102)
  102 FORMAT (1H,10X,'PROGRAM  H I F I S S',/)
C
      WRITE (10,103) MP,HEAD
  103 FORMAT(//,10X,' FISSION OF  ',F7.2,'-X IN  ',A25//)
      WRITE (10,104) NDIM
```

```
  104  FORMAT (1H,10X,' NUMBER OF EVENTS: ',I5//)
       WRITE(10,105)
  105  FORMAT(1H,1X,'EVENT NO.',1X,'EI(MeV/u)',4X,'M1',6X,'M2'
     1,6X,'MTOT',4X,'ETOT',4X,'Q-VALUE',3X,'V-REL.',2X
     1,'Q12      ',2X,'Q12EMP',3X,'ETA12',3X,'SCAT-ANG(CM)')
       WRITE(10,106)
  106  FORMAT (1H, 1X,'------',3X,'-------',6X,'----',3X,'----'
     1,4X,'-----',2X,'------',4X,'-----',3X,'------',3X,'-------',3X
     1,'------',3X,'------',3X,'------------',)
C
C
       READ (9,901)((XIN(IEV,J),J=1,5),IEV=1,NDIM)
 901   FORMAT(1X,4F7.2,F10.2)
C
       DO 8000 L=1,MX
        DO 200 K=1,15
         C(K)=0.0
 200    CONTINUE
       DO 7000 IEV=1,NDIM
       IER=0
       R1=XIN(IEV,1)
       R2=XIN(IEV,3)
       CALL COEFF (R1,1,A0,A1,A2)
       CALL COEFF (R2,2,A0,A1,A2)
       WRITE (*,15) IEV
  15   FORMAT (//,1H,10X,'EVENT NR.',I5)
       WRITE(*,16)
  16   FORMAT (1H,10X,'--------------',/)
       IF (HEAD1.EQ.'N') GOTO 210
       M1=MTOT/2.0
       M2=MTOT/2.0
 210   ELAB=XIN(IEV,5)
       R1=XIN(IEV,1)
       R2=XIN(IEV,3)
       V1=VELF(M1,R1,0.0)
       V2=VELF(M2,R2,0.0)
       PHI1=0.0
       PHI2=180.0*RAD
       THET1=XIN(IEV,2)*RAD
       THET2=XIN(IEV,4)*RAD
C
C
       CALL CARTES(1.0,THET1,PHI1,E1)
       CALL CARTES(1.0,THET2,PHI2,E2)
       DO 7100 I=1,3
       VE1(I)=V1*E1(I)
 7100  VE2(I)=V2*E2(I)
C
 7150  P=SQRT(2.0*103.5*MTOT*ELAB)
 7200  PIN(1)=0.0
       PIN(2)=0.0
        PIN(3)=P
C
       CALL MASS(ELAB,PIN,VE1,VE2,THET1,THET2,MTOT,ET1,ET2
     1 ,ETOT,QVAL,Q12,Q12EMP,RES,VE12,V12,M1,M2,M12,ETA,C12)
C
C
       CALL ANGL12(VE12,PIN,PP12)
       IF (PP12.GT.90.0)  PP12=180.0-PP12
C
C*     WRITE RESULTS TO OUTPUT FILE OR OUTPUT TABLE  *
C
       EI=ELAB/MP
```

```
      ETA12=(THET1+THET2)/RAD
C
C     CHI IS THE ASSYMETRY PARAMETER
C
      CHI=ABS(M1-M2)/M12
C
      WRITE(8,873)IEV,EI,M1,ET1,M2,ET2,M12,ETOT,QVAL
     1,V12,CHI,ETA12,PP12
  873 FORMAT(1H,2X,I3,6X,F5.1,6X,F5.1,2X,F7.2,2X,F5.1
     1,2X,F7.2,2X,F6.1
     1,3X,F6.1,3X,F6.1,2X,F6.4,3X,F6.3,6X,F5.1,4X,F5.1)
C
      WRITE(10,107)IEV,EI,M1,M2,M12,ETOT,QVAL,V12,Q12
     1,Q12EMP,ETA12,PP12
  107 FORMAT (1H,2X,I3,6X,F5.1,6X,F5.1,2X,F5.1,2X,F6.1
     1,3X,F7.2,3X,F6.1,2X,F6.4,3X,F6.1,3X,F6.1,5X,F5.1
     1,4X,F5.1)
C
 7000 CONTINUE
      MT=A(L)
      MTOT=MP+MT
 8000 CONTINUE
C
      CLOSE(8)
      CLOSE(9)
      CLOSE(10)
      CLOSE(11)
      CLOSE(14)
C
      STOP
      END
C
C
C
C
      SUBROUTINE CARTES (R,THET,PHI,V)
C *   EVALUATION OF  CARTESIAN CO-ORDINATES  *
C
      DIMENSION V(3)
      V(1)=R*SIN(THET)*COS(PHI)
      V(2)=R*SIN(THET)*SIN(PHI)
      V(3)=R*COS(THET)
      RETURN
      END
C
C
C
C
      SUBROUTINE SKALAR (V1,V2,C)
C
C  *  COMPUTES THE SKALAR PRODUCT OF THE TWO VECTORS  *
C
      DIMENSION V1(3),V2(3)
      C=0.0
      DO 1 I=1,3
    1 C=C+V1(I)*V2(I)
      RETURN
      END
C
C
C
```

```
      SUBROUTINE MASS(ELAB,PIN,VE1,VE2,THET1,THET2,MTOT,ET1,ET2
     1, ETOT,QVAL,Q12,Q12EMP,RES,VE12,V12,M1,M2,M12,ETA,C12)
C *     EVALUATION OF MASSES   *
C *     LOGIC:  BINARY TREE SEARCH IN A DYNAMIC MODE *
      REAL M1,M2,M12,MTOT,XMTOT,V12,ET1,ET2
      DIMENSION RES(3),VE1(3),VE2(3),PIN(3),VE12(3)
      DIMENSION A0(5),A1(5),A2(5),C(15)
      COMMON    /PRINT/IP1,IP2,IP3,IP4,IP5,IP6,IP7,IMASS
      COMMON    /FCTV2/R,PSCTG1,PSCTG2
      COMMON    /FCTVV2/RR,XMTOT
      COMMON    /RANGE/R1,R2,R3,R4,R5
      COMMON    /FITCOF/A0,A1,A2
      COMMON    /VELCOF/FA,C
      EXTERNAL  FV1,FV2
      IP2=1
      XMTOT=MTOT
      X10=XMTOT-10.0
      CALL SKALAR (VE1,VE1,V1)
      CALL SKALAR (VE2,VE2,V2)
      RAD=0.017453293
      V1=SQRT(V1)
      V2=SQRT(V2)
      P=PIN(3)
      CTG1=COS(THET1)/SIN(THET1)
      CTG2=COS(THET2)/SIN(THET2)
      SIN1=SIN(THET1)
      SIN2=SIN(THET2)
      CTG=CTG1+CTG2
      IF (IP7.GT.0) GOTO 12
      GO TO 2
 2    M1=P/(103.5*V1*SIN1*CTG)
      M2=P/(103.5*V2*SIN2*CTG)
      C12=M1/M2
      C21=1.0/C12
      IF (IMASS.GT.0) M1=XMTOT/(1.0+C21)
      IF (IMASS.GT.0) M2=XMTOT/(1.0+C12)
      GO TO 3
 12   R=R1
      PSCTG1=P/(103.5*SIN1*CTG)
      CALL RTME(M1,F,FV1,10.0,X10,1.E-6,1000,IER)
      IF (IER.NE.0) GO TO 999
      IF (IP2.NE.0) WRITE(*,*) M1,F,IER
      R=R2
      PSCTG2=P/(103.5*SIN2*CTG)
      CALL RTNE(M2,F,FV2,10.0,X10,1.E-6,1000,IER)
      IF (IER.NE.0) GO TO 999
      IF (IP2.NE.0) WRITE(*,*) M2,F,IER
      C12=M1/M2
      C21=1.0/C12
      IF (IMASS.GT.0) M1=XMTOT/(1.0+C21)
      IF (IMASS.GT.0) M2=XMTOT/(1.0+C12)
 30   V1=VELF1(M1)
      V2=VELF2(M2)
      VE1(3)=V1*CTG1*SIN1
      VE2(3)=V2*CTG2*SIN2
      VE1(2)=0.
      VE2(2)=0.
      VE1(1)=V1*SIN1
      VE2(1)=-V2*SIN2
      GO TO 3
 999  WRITE (*,9999)
9999  FORMAT (1H,'  ROOT  IN  MASS  IS  NOT  FOUND !!!')
      M1=-100.0
```

```
      M2=-100.0
      GOTO 3
    3 M12=M1+M2
      ETA=(M1-M2)/M12
      C12=M1/M2
      IF (C12.LT.1.0) C12=1.0/C12
      ET1=0.5*103.5*M1*V1**2
      ET2=0.5*103.5*M2*V2**2
      ETOT=0.5*103.5*(M1*V1**2+M2*V2**2)
      QVAL=ETOT-ELAB
      DO 10 I=1,3
      RES(I)=(103.5*(M1*VE1(I)+M2*VE2(I)))-PIN(I)
   10 VE12(I)=VE1(I)-VE2(I)
      CALL SKALAR(VE12,VE12,X)
      V12=SQRT(X)
      Q12EMP=0.019814*ABS(M12)**1.66666667
      Q12=0.5*103.5*M1*M2/M12*V12**2
      RETURN
      END
C
C
C
      SUBROUTINE COEFF(R,K,A0,A1,A2)
C *   COMPUTATION OF VELOCITY FROM MASS AND TRACK LENGTH *
C
      DIMENSION A0(5),A1(5),A2(5),C(15)
      COMMON   /PRINT/IP1,IP2,IP3,IP4,IP5,IP6,IP7,IMASS
      COMMON   /VELCOF/C,FA
      IP3=1
      K1=(K-1)*3
      DO 2 I=1,5
      I1=I-1
      C(1+K1)=C(1+K1)+A0(I)*R**I1
      C(2+K1)=C(2+K1)+A1(I)*R**I1
      C(3+K1)=C(3+K1)+A2(I)*R**I1
  2   CONTINUE
      RETURN
      END
C
C
      SUBROUTINE RTNE (X,F,FV1,XLI,XRI,EPS,IEND,IER)
C   * PURPOSE : Iterations to find the masses of the fragments
C     by conserving momentum
C   * LOGIC :  Root of Non-linear EQUATIONs
      COMMON/PRINT/IP1,IP2,IP3,IP4,IP5,IP6,IP7,IMASS
      EXTERNAL FV1
      IP6=1
      IER=0
      XL=0.0
      XR=0.0
      X=0.0
      TOL=0.0
      FL=0.0
      FR=0.0
      F=0.0
      XM=0.0
      FM=0.0
      DX=0.0
      A=0.0
      XL=XLI
      XR=XRI
      X=XL
      TOL=X
```

```
      F=FV1(TOL)
      IF (F) 1,16,1
 1    FL=F
      X=XR
      TOL=X
      F=FV1(TOL)
      IF (F) 2,16,2
 2    FR=F
      IF (SIGN(1.,FL)+SIGN(1.,FR)) 25,3,25
 3    I=0
      TOLF=100.0*EPS
 4    I=I+1
      DO 13 K=1,IEND
      X=0.5*(XL+XR)
      TOL=X
      F=FV1(TOL)
      IF (F) 5,16,5
 5    IF (SIGN(1.,F)+SIGN(1.,FR)) 7,6,7
 6    TOL=XL
      XL=XR
      XR=TOL
      TOL=FL
      FL=FR
      FR=TOL
 7    TOL=F-FL
      A=F*TOL
      A=A+A
      IF (A-FR*(FR-FL))8,9,9
 8    IF (I-IEND) 17,17,9
 9    XR=X
      FR=F
      TOL=EPS
      A=ABS(XR)
      IF(A-1.0)11,11,10
10    TOL=TOL*A
11    IF (ABS(XR-XL)-TOL) 12,12,13
12    IF(ABS(FR-FL)-TOLF) 14,14,13
13    CONTINUE
      IER=1
14    IF(ABS(FR)-ABS(FL)) 16,16,15
15    X=XL
      F=FL
16    RETURN
17    A=FR-F
      DX=(X-XL)*FL*(1.0+F*(A-TOL)/(A*(FR-FL)))/TOL
      XM=X
      FM=F
      X=XL-DX
      TOL=X
      F=FV1(TOL)
      IF(F) 18,16,18
18    TOL=EPS
      A=ABS(X)
      IF(A-1.0) 20,20,19
19    TOL=TOL*A
20    IF(ABS(DX)-TOL) 21,21,22
21    IF (ABS(F)-TOLF) 16,16,22
22    IF (SIGN(1.,F)+SIGN(1.,FL)) 24,23,24
23    XR=X
      FR=F
      GOTO 4
24    XL=X
      FL=F
```

```
      XR=XM
      FR=FM
      GOTO 4
   25 IER=2
  100 FORMAT (1H,'RTMI,1',2E12.3)
  101 FORMAT (1H,'RTMI,2',2E12.3)
  102 FORMAT (1H,'RTMI,3',2E12.3)
  103 FORMAT (1H,'RTMI,4',2E12.3)
      RETURN
      END
C
C
C
      FUNCTION  FV1(A)
C *   Computation of momentum for fragment 'A' *
      EXTERNAL  VELF1
      DIMENSION C(15)
      COMMON    /FCTV2/R,PSCTG1,PSCTG2
      COMMON    /VELCOF/C,FA
      FA=1.0
      FV1=(A*(FA*(C(1)+A*(C(2)+A*C(3)))))-PSCTG1
      RETURN
      END
C
C
C
C
C
C
C
      FUNCTION  FV2(A)
C *   Computation of momentum for fragment 'B'*
      EXTERNAL  VELF2
      DIMENSION C(15)
      COMMON    /FCTV2/R,PSCTG1,PSCTG2
      COMMON    /VELCOF/C,FA
      FA=1.0
      FV2=(A*(FA*(C(4)+A*(C(5)+A*C(6)))))-PSCTG2
      RETURN
      END
C
C
C
       FUNCTION VELF1(A)
       DIMENSION C(15)
       COMMON    /VELCOF/C,FA
       FA=1.0
       VELF1=FA*(C(1)+A*(C(2)+A*C(3)))
       RETURN
       END
C
C
       FUNCTION VELF2(A)
       DIMENSION C(15)
       COMMON     /VELCOF/C,FA
       FA=1.0
       VELF2=FA*(C(4)+A*(C(5)+A*C(6)))
       RETURN
       END
C
C
```

```
      SUBROUTINE  ANGL12(X1,X2,P12)
C *   Computes the centre of mass scattering angle *
      DIMENSION X1(3),X2(3)
      REAL M1,M2
      RAD = 57.2957795
      R1=SQRT(X1(1)**2+X1(2)**2+X1(3)**2)
      R2=SQRT(X2(1)**2+X2(2)**2+X2(3)**2)
      IF ((R1.LT.1.E-7).OR.(R2.LT.1.E-7))  GOTO 1
      GO TO 2
 1    P12=0.0
      RETURN
 2    X12=(X1(1)*X2(1)+X1(2)*X2(2)+X1(3)*X2(3))/(R1*R2)
      IF (ABS(X12).LE.1.E-7) GOTO 4
      IF (ABS(X12-1.0).LE.1.E-7) GOTO 5
      IF (ABS(X12+1.0).LE.1.E-7) GOTO 6
      P12=(ACOS((X1(1)*X2(1)+X1(2)*X2(2)+X1(3)*X2(3))/(R1*R2)))*RAD
      RETURN
 4    P12=90.0
      RETURN
 5    P12=0.0
      RETURN
 6    P12=180.0
      RETURN
      END
C
C
C
      FUNCTION VELF(XMASS,REI,ELOSS)
      INTEGER SIGN
      R=REI
      X=XMASS
      XMTOT=238.0
      Z=X/2.587
      E=30.0
      RE=F1(X,E)
      IF (R.GT.RE) GO TO 200
      DELTE=0.5*E
      SIGN=-1
      DO 100 I=1,12
      E=E+DELTE*SIGN
      RE=F1(X,E)
      IF (ABS(RE-R).LT.0.1) GOTO 300
      SIGN=1
      IF (RE.GT.R) SIGN=-1
100   DELTE=0.5*DELTE
      GO TO 300
 200  RALT=F1(X,E-1.0)
      RDIFF=RE-RALT
      DELTE=(R-RE)/RDIFF
      E=E+DELTE
      IF (E.LE.0.) GO TO 400
 300  VELF=0.1389*SQRT(E)
      RETURN
 400  VELF=1.0
      RETURN
      END
C
C
      FUNCTION F1(X,Y)
      DIMENSION A(15)
      COMMON D(5,5)
      INTEGER  I,J,M,TEMP
      OPEN(11,FILE='UCR.COF')
```

```
      K1=3
      L1=4
      M=K1*L1
      TEMP=K1
      READ(11,20)(A(I),I=1,M)
 20   FORMAT(E16.7)
      DO 150 I=1,K1
        M=I
          DO 150 J=1,L1
             D(I,J)=A(M)
              M=M+TEMP
 150          CONTINUE
      F1=PXY2(X,Y,K1,L1)
C      CLOSE(11)
      RETURN
      END
C
C
```

```
      FUNCTION PXY2(X,Y,K1,L1)
      DIMENSION U(20),V(20)
      COMMON D(5,5)
C
      DO 1 I=1,K1
 1    U(I)=E(X,I-1)
      DO 2 I=1,L1
 2    V(I)=E(Y,I-1)
      XY=0.0
      DO 3 I=1,K1
      DO 3 J=1,L1
      XY=XY+D(I,J)*U(I)*V(J)
  3   CONTINUE
      PXY2=XY
      RETURN
      END
C
C
      FUNCTION E(X,N)
      E=1.0
      IF (N.EQ.0) RETURN
      DO 2 I=1,N
  2   E=E*X
      RETURN
      END
```

LIST OF PUBLICATIONS

1. J. Raju, S. Ghosh, A. Saxena and K.K. Dwivedi.
"Calibration of CR-39 and ZnP-Glass Detectors with 350 MeV ^{90}Zr ions",
Meas. Sci. and Technol., **1** (1990) 903-907.

2. J. Raju, S. Ghosh, A. Saxena and K.K. Dwivedi.
"Response to 350 MeV ^{90}Zr ions of Polycarbonate Detectors",
Nucl. Instrum. Meth. in Phys. Res., **B51** (1990) 168-172.

3. J. Raju and K.K. Dwivedi.
"Computer based analysis of Nuclear Track Data: Part I",
Proc. of 7th National Symposium on Particle Tracks in Solids, Defence Lab., Jodhpur, India (1992), (**BEST PAPER AWARDED**).

4. J. Raju and K.K. Dwivedi.
"Computer based analysis of Nuclear Track Data: Part II",
Proc. of 7th National Symposium on Particle Tracks in Solids, Defence Lab., Jodhpur, India (1992), (**BEST PAPER AWARDED**).

5. K.K. Dwivedi, S. Ghosh and J. Raju.
"Measurement of Traget Thickness by Nuclear Track Technique",
Nucl. Tracks Radiat. Meas., **19** (1991) 597.

6. S. Ghosh, J. Raju, P.P. Choubey and K.K. Dwivedi.
"Characterisation of Overhead Projector Transperancy as Heavy Ion Detector",
Nucl. Tracks Radiat. Meas., **19** (1991) 77.

7. A. Bhattacharya, A. Saxena, J. Raju, S.Ghosh and K.K. Dwivedi.
"Investigations on Fission Fragment Tracks in ZnP-Glass and SR-86 Detectors",
Nucl. Tracks Radiat. Meas., **19** (1991) 577.

8. S. Ghosh, J.Raju and K.K. Dwivedi.
"Track lengths of ^{132}Xe in CR-39 detector",
Rad. Eff. and Def. in Solids, **25** (1994) 000.

9. A. Bhattacharya, J. Raju, A. Saxena and K.K. Dwivedi.
"Investigations on ^{252}Cf fission fragment tracks in polycarbonate detectors",
Proc. of 7th National Symposium on Particle tracks in Solids, Defence Lab., Jodhpur, India (1992).

10. J. Raju and K.K. Dwivedi,
"V_T(Track etch rate): reflection of total energy-loss rate (dE/dx) for ^{238}U in CR-39",
Nucl. Tracks Radiat. Meas., **000** (1993) 000.

11. J. Raju and K.K. Dwivedi,
"Fusion-Fission of ^{209}Bi and ^{238}U in Different Solid State Nuclear Track Detectors",
Nucl. Tracks Radiat. Meas., **000** (1993) 000, (in press).

12. K.K. Dwivedi, J. Raju, P. Vater and R. Brandt,
"Studies on Fission of Heavy ions and evaporation of alpha particles using Nuclear Track Detectors",
Nucl. Tracks Radiat. Meas., **000** (1993) 000, (in press).

13. K.K. Dwivedi, S. Ghosh and J. Raju,
"Registration Threshold for Tracks of ^{40}Ar in Muscovite Mica",
Nucl. Tracks Radiat. Meas., **000** (1993) 000, (in press).

14. M. Dey, J. Raju, S. Ghosh and K.K. Dwivedi,
"Development and Characterisation of Polycarbonate Microfilters",
Nucl. Tracks Radiat. Meas., **000** (1993) 000, (in press).